



Faculty of Science and Technology

MASTER'S THESIS

Study program/specialization:

Mechanical and Structural Engineering and
Materials Science / Mechanical Systems

Spring semester, 2018

Open access

Author:

Jonas Olsvik Rydland

(Signature author)

Faculty supervisor: Professor Dimitrios G. Pavlou

Supervisor(s): Kristen Rege (UiS)

Thesis title:

Design of loading devices for mixed-mode fatigue crack propagation testing

Credits (ECTS): 30

Key word:

Mixed-mode fatigue, CTS specimen, loading
device, crack growth rate, crack propagation
life, 5754-H22 aluminum alloy, crack
monitoring, finite element analysis.

Pages: 69

+ enclosure: 19

Stavanger, 14.06.2018

Date/year

Abstract

Traditional fatigue crack propagation tests are performed in mode I, i.e. with a cyclic load applied perpendicularly to the initial crack. However, fatigue cracks in real components are often subjected to mixed-mode loading. It is therefore important to obtain experimental data also for mixed-mode fatigue crack propagation.

In this thesis, a loading device suitable for mixed-mode I and II fatigue crack propagation tests of a compact tension shear (CTS) specimen has been designed and constructed. Computations of fatigue crack propagation life and maximum applied load to a CTS specimen in order to follow linear elastic fracture mechanics was performed. Based on these loadings a finite element analysis was conducted using ANSYS Workbench 17 in order to establish the maximum von Mises Stress and displacement occurring in the loading device during fatigue testing. The obtained results were then used to choose a suitable material for the loading device based on information gained from available S-N curves and relevant standards.

Suitable test specimens were prepared, and the produced loading device was used for experimental investigation of three CTS specimens of the 5754 aluminum alloy furnished in the H22 temper. The fatigue crack propagation tests were performed using a servo-hydraulic MTS fatigue testing machine. Tests were conducted for both pure mode I loading and mixed-mode I and II loading for a loading angle of 60 degrees. Further, fatigue crack growth rates and direction of crack growth was measured.

A photo camera was used in order to monitor the crack growth during the fatigue tests. Necessary preparations were done, namely finding a suitable tripod for camera mounting and trying different surface coatings in order for improved visibility of the crack. A total of three different coating methods was tried. Finally, a procedure for performing mixed-mode I and II fatigue propagation tests using the designed loading device was prepared.

Based on results from conducted fatigue tests, the designed loading device was found well suited for mixed-mode fatigue crack propagation testing.

Table of Contents

| | |
|---|-------------|
| Abstract | III |
| Table of Contents | IV |
| List of Abbreviations..... | VI |
| List of Symbols | VII |
| Acknowledgements | VIII |
| 1 Introduction..... | 1 |
| 1.1 Background..... | 1 |
| 1.2 Scope | 2 |
| 2 Theory | 4 |
| 2.1 Fatigue Strength | 4 |
| 2.1.1 Mean Stress Modifications | 6 |
| 2.1.2 Eurocode 3: Design of steel structures - Part 1-9: Fatigue | 7 |
| 2.2 Fatigue Crack Propagation | 7 |
| 2.2.1 Stress Intensity Factor | 8 |
| 2.2.2 Fatigue Crack Growth | 9 |
| 2.2.3 Plastic Zone Size..... | 10 |
| 2.3 Mixed-Mode Fatigue..... | 11 |
| 2.3.1 Plastic Zone Shape | 12 |
| 2.3.2 Evaluation of Crack Growth Angle | 13 |
| 2.4 Standardized Procedures for Measurement of Fatigue Crack Growth Rates | 13 |
| 2.5 Specimen Configurations used for Mixed-mode Fatigue Crack Growth Studies | 15 |
| 2.6 Compact Tension Shear (CTS) Specimen | 16 |
| 2.7 Crack Length Measurements Techniques | 18 |
| 3 Feasibility Study..... | 19 |
| 3.1 Design Discussion..... | 19 |
| 3.1.1 Specimen Choice | 19 |
| 3.1.2 Design of Loading Device | 20 |
| 3.1.3 Production Method | 21 |
| 3.2 Method for Monitoring of Crack Propagation..... | 22 |
| 3.3 Experience from Earlier Tests | 23 |
| 4 CTS Specimen Calculation | 24 |
| 4.1 Maximum Allowable Load for CTS Specimens | 25 |
| 4.1.1 Loads on CTS Specimen Holes | 25 |
| 4.2 Crack Propagation Life | 26 |
| 4.3 Plastic Zone Size and Shape..... | 27 |
| 4.4 Crack Propagation Angle | 28 |
| 5 Design and Analysis of the Loading Device | 30 |
| 5.1 Finite Element Analysis of the Loading Device..... | 30 |

| | | |
|------------|--|-----------|
| 5.1.1 | Connections | 31 |
| 5.1.2 | Meshing | 31 |
| 5.1.3 | Constraints..... | 33 |
| 5.1.4 | Forces | 33 |
| 5.2 | Results of Simulation | 34 |
| 5.3 | Bolt Calculation..... | 37 |
| 5.4 | Material Choice of Loading Device | 38 |
| 5.5 | Fabrication of Loading Device | 41 |
| 6 | Fatigue Crack Propagation Testing | 43 |
| 7 | Results..... | 46 |
| 7.1 | Fatigue Crack Propagation Testing of CTS Specimens | 46 |
| 8 | Discussion..... | 53 |
| 8.1 | Functionality of Loading Device..... | 53 |
| 8.1.1 | Possible Reasons for Deviations in Results..... | 54 |
| 8.1.2 | Solutions to Improve the Loading Device | 55 |
| 8.2 | Crack Monitoring Using a Camera | 57 |
| 9 | Conclusion | 58 |
| 9.1 | Future use of the Loading Device | 58 |
| 10 | References | 59 |

Appendixes

Appendix-A Procedure for performing mixed mode I and II fatigue crack propagation tests

Appendix-B Machine drawings of fabricated parts

Appendix-C Revised machine drawings for improvement

Appendix-D Material certification AL 5754-H22

List of Abbreviations

| Word | Description |
|-------------|--|
| LEFM | Linear Elastic Fracture Mechanics |
| CTS | Compact Tension Shear |
| CT | Compact Tension |
| MT | Middle Tension |
| CCT | Center Cracked Tension |
| BSI | British Standard Institution |
| ISO | International Organization for Standardization |
| ASTM | American Society for Testing and Materials |
| EDM | Electrical Discharge Machining |
| FEA | Finite Element Analysis |
| CAD | Computer Aided Design |

List of Symbols

| Variable | Description |
|----------------------|--|
| $\Delta\sigma$ | Stress range |
| σ_{\max} | Maximum stress |
| σ_{\min} | Minimum stress |
| σ_a | Stress amplitude |
| σ_m | Mean stress |
| R | Stress range |
| $\sigma_a \sigma_m$ | Stress amplitude for fully-reversed loading |
| σ_{TS} | Tensile strength |
| σ_{YS} | Yield strength |
| K | Stress intensity factor |
| Y | Stress intensity modification factor |
| a | Crack length of specimen |
| da/dN | Crack growth rate |
| C | Crack propagation constant in Paris Law |
| m | Crack propagation exponent in Paris Law |
| ΔK | Stress intensity factor range |
| K_{\max} | Maximum stress intensity factor |
| K_{\min} | Minimum stress intensity factor |
| N | Number of cycles |
| r_y | Length of plastic zone for linear-elastic material behavior |
| r_p | Length of plastic zone for elastic-plastic material behavior |
| K_v | Comparative stress intensity factor |
| ΔK_v | Comparative stress intensity factor range |
| θ | Crack propagation angle |
| K_I | Stress intensity factor Mode I loading |
| K_{II} | Stress intensity factor Mode II loading |
| W | Width of CTS specimen |
| B | Thickness of CTS specimen |
| α | Angle of loading direction |
| F | Applied load |
| τ_{bolt} | Bolt shear stress |
| d | Bolt diameter |
| F_m | Mean load |
| F_a | Amplitude load |

Acknowledgements

This thesis concludes a two-year master's degree in Mechanical and Structural Engineering and Materials Science, specialization in Mechanical Systems, at the University of Stavanger. I chose this thesis due to the desire to learn more about fatigue strength of materials, combined with my interest in fatigue behavior of materials. Writing this thesis has been a great experience, and I have several persons to thank.

Firstly, I would like to thank my supervisors; Kristen Rege and Professor Dimitrios G. Pavlou for giving me the opportunity to work on this project. I would also give a huge thank for the possibility to participate in fatigue testing of pipe specimens during this work. This gave me good insight regarding the experimental process of fatigue testing and a much better understanding of fatigue behavior. I would also like to give an additional thank to Kristen Rege for very good feedback and help during the thesis.

I would also thank Martin Bae for guidance with regards to choosing the best-suited fabrication method for the loading devices, as well as Johan Andreas Thorikaas for the valuable help and guidance with the laboratory work.

I would also like to express my gratitude to Smed. T Kristiansen for good help and for producing all the parts needed for free.

Stavanger, Thursday 14th June 2018

Jonas Olsvik Rydland

1 Introduction

1.1 Background

Components and structures are often subjected to cyclic loadings caused by different loading conditions, such as environmental impact or operating conditions, and exist virtually everywhere. Offshore structures, such as oil rigs and windmills, are subjected to a combination of wave loads, currents and wind loads. Structural members in bridges are repeatedly subjected to loads from passing traffic and wind loads while piping and other pressurized systems, which is commonly used in the Norwegian oil industry, can be subjected to pressure fluctuations or repeated temperature changes. Further, vehicles and other machinery with rotating axles and gears are constantly subjected to fluctuating loads [1]. Damage to structures and components are often caused by small cracks present due to material defects or as a result of service condition. Thus, most fatigue cracks initiate and grow from structural defects [2], [3]. When such structures or components are subjected to continual loading and unloading over a sufficient amount of time, cracks will nucleate in the material. Over time, these cracks will grow larger until it finally leads to a fracture [2]. In order to evaluate the safety of structures or components, knowledge about fatigue behavior is therefore of great importance in various fields of engineering [3].

Many experimental investigations of fatigue behavior of cracks exposed to mode I loadings have been conducted over the years. However, many of the realistic loading conditions in engineering components and structures are due to mixed-mode loading. Such loading situations in practical cases may occur as a result of complex state of stress in a structure component, sharply bent or ramified cracks, multiple cracks, inclining or curved cracks, cracks initiation from notches, cracks at welded and bonded joints or cracks in composite materials as a result of dynamic or thermal stresses or of superimposed load, thermal and internal stresses [4]. Any change in the loading condition of a component can result in a change of crack path [5].

Since very few experimental testing results are obtained for mixed-mode loading, it is of great interest to obtain more experimental data also for mixed-mode fatigue crack propagation. Two of the main issues with regards to mixed-mode fatigue crack propagation is to establish the crack growth rate and predict the direction of crack growth. There are several theories that have been proposed to predict this path [6], but very few experimental testing results. Different specimen configurations have been used for investigations of mixed-mode loading [7], however, a common problem with many of these are the limited or absent opportunity for a transition from mode I to mode II loading. Thus, initiation of fatigue pre-cracking under mode I loading is very problematic [3]. For this reason, it is desirable to make a device which simplifies the transition from pure traction stress (Mode I) to pure shear stress (Mode II) of

the specimen [8], see Figure 1-1. Introducing such a loading device makes testing of Mode I, Mixed-Mode I and II and Mode II loadings easier and a universal fatigue testing machine can be used.

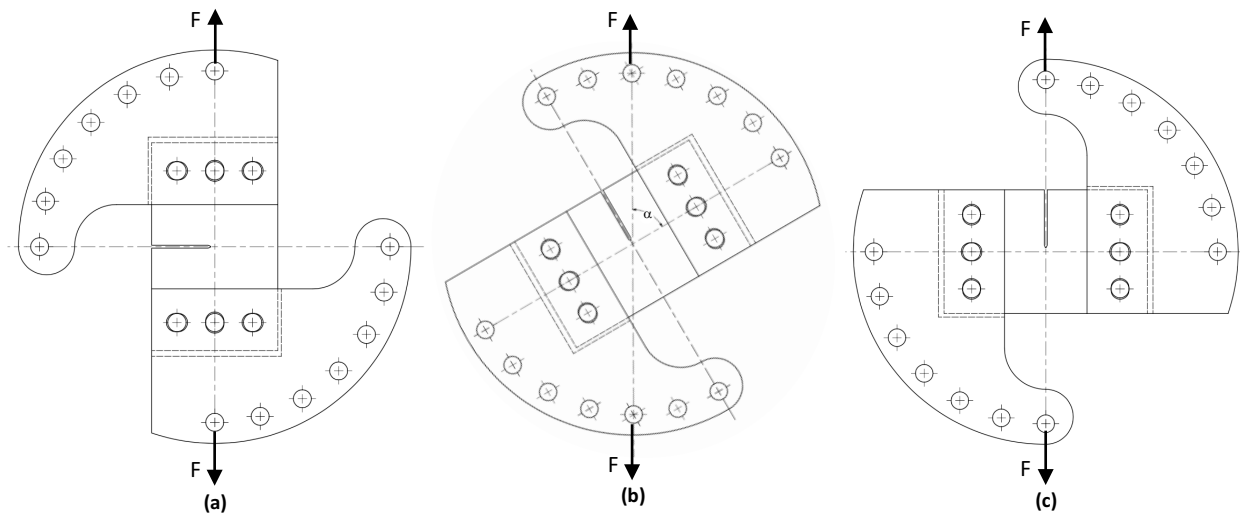


Figure 1-1 Position of loading device for (a) mode I loading ($\alpha = 0^\circ$), (b) mixed-mode loading ($0^\circ < \alpha < 90^\circ$) and (c) mode II loading ($\alpha = 90^\circ$) [8].

1.2 Scope

In this thesis, a loading device suitable for mixed mode I and II loading is designed and used to test three compact tension shear (CTS) specimens, see Figure 1-2. It is desirable to use the loading device to test a selection of the most commonly used materials in the Norwegian offshore industry. Four materials are chosen: EN S355, AISI 316L, API 5L X52 and the 5754 aluminum alloy. The loading device is designed for fatigue testing within the assumptions of linear elastic fracture mechanics (LEFM). In order to follow LEFM, the maximum loading applied to the CTS specimen is limited according to requirements given by the American Society for Testing and Materials (ASTM). The finite element analysis software, ANSYS Workbench 17, is used to determine the von Mises stress and displacement the loading devices are exposed to during fatigue testing. Based on these results, a suitable material for fabrication of the loading device is chosen.



Figure 1-2 Test setup for fatigue test of CTS specimen using designed loading device.

In addition, an appropriate method for crack growth monitoring is introduced. Commonly used methods for monitoring of crack growth under mode I loading are mainly adapted for monitoring of crack growth in the direction of the starter notch. This offers challenges for monitoring of an inclined crack. Thus, different monitoring methods are discussed, and necessary equipment preparations are performed in order to achieve a suitable monitoring technique for mixed mode I and II loading.

Further, experimental investigation of three CTS specimens of the 5754-H22 aluminum alloy is conducted in order to verify the function of the designed loading device. The fatigue crack propagation testing is performed using an MTS fatigue testing machine located in the workshop of the University of Stavanger. Tests are performed for both mode I loading and mixed-mode I and II loading. Fatigue crack growth rates and crack propagation angles are measured, and the experimental results are compared against the restrictions provided by ASTM in order to determine the validity of the results.

Finally, in order to give guidance for later use of the designed loading device, a procedure for performing mixed mode I and II fatigue crack propagation tests are prepared.

2 Theory

This chapter covers much of the theory which is used in the performed project. In addition, a brief literature study of earlier specimen configurations used for mixed-mode fatigue tests and available crack measurement methods are given.

2.1 Fatigue Strength

In order to determine the strength of materials subjected to fatigue loading, load is applied to specimens with either repeated or varying forces while the cycles are counted to destruction [9]. Applied stresses for fatigue testing is described by three parameters. The stress range, $\Delta\sigma$, which is the difference between the maximum and minimum stresses in one cycle, the mean stress, σ_m , which is the average of the maximum and minimum stresses in one cycle and the stress amplitude, σ_a , which is half the value of the stress range. When performing a fatigue test, it is common to apply constant amplitude loading, and the applied stress conditions are then usually written $\sigma_m \pm \sigma_a$ [2].

$$\Delta\sigma = \sigma_{max} - \sigma_{min} \quad (2.1.1)$$

$$\sigma_a = \frac{\Delta\sigma}{2} = \frac{\sigma_{max} - \sigma_{min}}{2} \quad (2.1.2)$$

$$\sigma_m = \frac{\sigma_{max} + \sigma_{min}}{2} \quad (2.1.3)$$

In addition to equations above, the mean stress is also characterized in terms of the stress ratio R. The R ratio has a significant influence on the crack growth rate and is frequently used concerning fatigue loading [10].

$$R = \frac{\sigma_{min}}{\sigma_{max}} \quad (2.1.4)$$

If the R ratio is equal to -1, the stresses are fully reversed, as Figure 2-1(a) illustrates. If the stress is cycled between a maximum stress and no load, the stress ratio R becomes zero. If the stress is cycled between two tensile stresses, the stress ratio R becomes a positive number less than 1 [2], illustrated in Figure 2-1 (b).

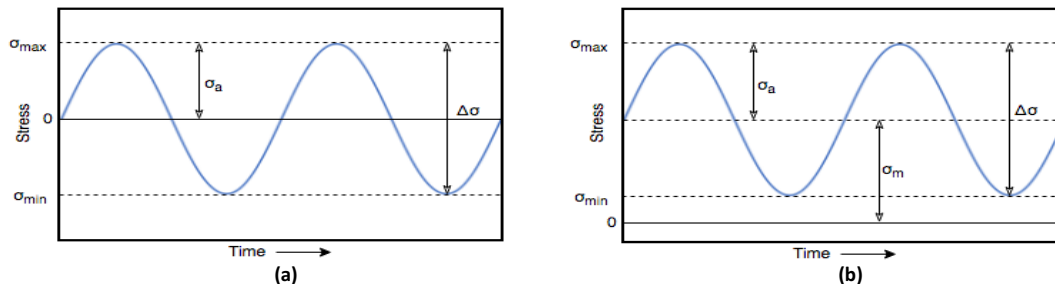


Figure 2-1 Constant amplitude loading and the associated nomenclature. (a) Stresses are fully reversed, ($R = -1$ and $\sigma_m = 0$) (b) Fluctuating stress with nonzero mean stress, ($R > 0$).

Due to the statistical nature of fatigue, several tests are necessary in order to establish the fatigue strength of a material. The first test is made using a stress that is slightly below the tensile strength of the material, continuing to slightly reduce the applied stress for each test. This process is continued for quite a number of test, and the results are plotted as stress amplitude, maximum stress or stress range to number of cycles, N , to failure. The stress can be plotted either using a linear or logarithmic scale, while number of cycles is plotted using a logarithmic scale. The resulting plot of the data is called an S-N curve [9][2].

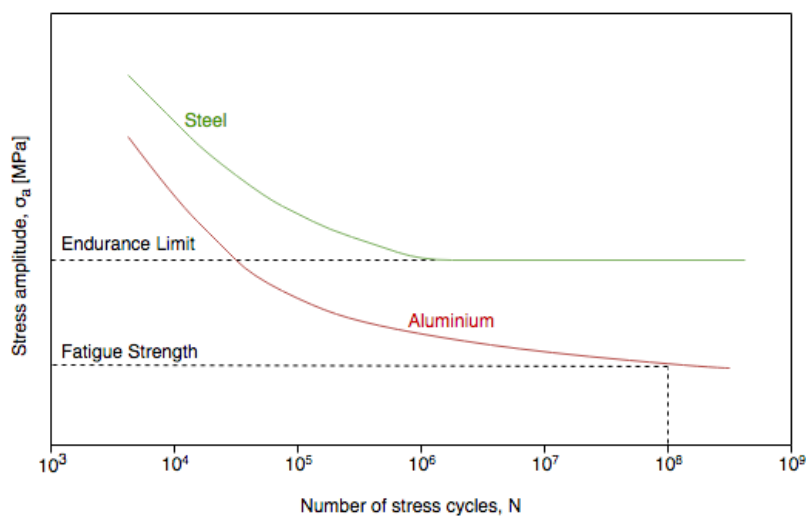


Figure 2-2 Typical S-N Curves.

From this curve the stress a material can endure for a specific number of cycles before failure can be found, called the fatigue strength. As Figure 2-2 illustrates, the fatigue strength decreases with increasing number of cycles. It is also shown that for materials such as steel, the S-N curve becomes horizontal at a given stress value. Below this stress value, the material can withstand an infinite number of cycles without failure and is called the endurance limit or the fatigue limit. For most nonferrous metals an alloys, such as aluminum, the curve does not become horizontal, and therefore they do not have an endurance limit. Instead, the S-N curves continue to slowly drop even at high numbers of cycles. For such metals, it is normal to report the fatigue strength rather than fatigue limit, which is the stress the metal can be subjected to for a specific number of cycles [2].

2.1.1 Mean Stress Modifications

It is known that mean stress play an important role in influencing the fatigue life of materials. In order to take the influence of different mean stresses on the fatigue life into account, mean stress effects in fatigue can be represented using a constant-life diagram, as illustrated in Figure 2-3. Different combinations of stress amplitude and mean stress which provides a constant fatigue life are plotted. The three most know models are those due to Gerber, Godman and Soderberg [11]. The life plot represented in Figure 2-3, the *Modified Godman relation*, is described by the expression given below

$$\sigma_a = \sigma_{a|\sigma_m=0} \left\{ 1 - \frac{\sigma_m}{\sigma_{TS}} \right\} \quad (2.1.5)$$

Where σ_a is the stress amplitude giving the fatigue strength for a nonzero mean stress, $\sigma_{a|\sigma_m=0}$ is the stress amplitude for fully-reversed loading ($\sigma_m = 0$ and $R = -1$), and σ_{TS} is the tensile strength of the material. It can also be useful to plot the yield line in the diagram, as a reminder that first-cycle yielding might be the reason of failure rather than fatigue [9].

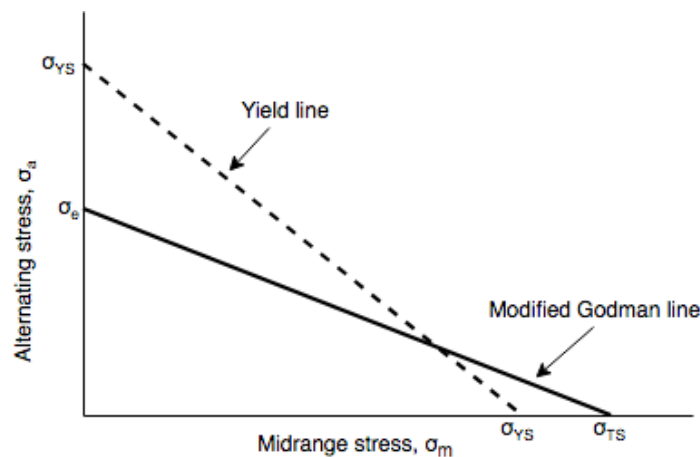


Figure 2-3 Constant-life curve for fatigue loading with a nonzero mean stress [9].

The following observations for the different models are important to take into account. The model given by Gerber provides a conservative estimate of fatigue life for most engineering alloys, while Godman's model matches experimental observations quite well for brittle metals, however, for ductile alloys it is conservative. The model given by Soderberg is generally good for ductile alloys for tensile mean stresses but does not separate between the difference in fatigue life due to compressive and tensile mean stresses [11].

2.1.2 Eurocode 3: Design of steel structures - Part 1-9: Fatigue

In order to establish the fatigue strength of the loading device, information from the NS-EN 1993-1-9 standard is used [12]. This standard includes different methods for estimation of fatigue resistance of members, connections, and joints subjected to fatigue loading. These methods are derived from fatigue tests of large-scale specimens, including effects of geometry and structural imperfections. The method that is described most comprehensive is the fatigue strength based on S-N curves. Separate S-N curves are given for a range of different detail categories, found in table 8.1 to 8.10 in NS-EN 1993-1-9. The tables cover, among other things, plain materials and bolted connections.

Effect of varied stress range is also considered in this standard. A transition line is introduced to the S-N curves for damage summation, which is expressed in the Palmgren-Miner rule, stated below.

$$D = \sum \frac{n_i}{N_i} = \left(\frac{n_1}{N_1} + \frac{n_2}{N_2} + \frac{n_3}{N_3} + \dots \right) \quad (2.1.6)$$

Where n_i is the number of cycles with stress range of $\Delta\sigma_i$ and N_i is the design value of the fatigue endurance for that stress. For a satisfactory assessment, D is less than or equal to 1.

The assessment methods provided in this standard can be used for all grades of structural steel, stainless steel, and unprotected weathered steels. For some of the details, there may be exceptions, which then is noted in the category tables. The fatigue strengths given in EN 1993-1-9 applies only to structures under normal atmospheric conditions and structures with sufficient corrosion protection.

2.2 Fatigue Crack Propagation

For large structural bodies, the presence of a crack does not necessarily mean that failure of the part will occur. The objective of fatigue crack propagation testing is to determine the crack growth rates of preexisting cracks under cyclic loadings before they reach a critical size for fracture [2]. In order to predict the crack growth of structures subjected to fatigue loadings, linear fracture mechanics (LEFM) is used. The growth of a fatigue crack exposed to cyclic loading is mainly controlled by the stress ratio and maximum load. Fatigue crack propagation testing generally involves constant amplitude loading of notched specimens that have been introduced to fatigue pre-cracking [2]. The crack length is then measured as a function of number of cycles. Further, the crack growth rate, da/dN , is then established using the data found subjected to numerical analysis. This fatigue crack growth data are typically presented in a logarithmic plot of crack growth rate, da/dN , versus the stress-intensity factor range ΔK [2].

2.2.1 Stress Intensity Factor

In order to calculate crack growth rates when following LEFM, it is important to determine the stress intensity factor. The stress intensity factor, K , is a measure of the severity of stress concentrations around the crack tip and is necessary in order to find the fatigue crack propagation rate. K is a function of the size of the crack, cracked specimen geometry and the type of loading and shape [9], [13]. When defining K , it is important that the material is assumed to behave in a linear-elastic manner, according to Hook's law. For this reason, the approach being used is linear-elastic fracture mechanics [14]. For different load and geometric configurations, the stress intensity factor for mode I loading can be expressed as

$$K = Y\sigma\sqrt{\pi a} \quad (2.2.1)$$

Where Y is the *stress intensity modification factor*, which depends on the geometry and mode of loading, σ is the nominal stress and a is the length of the crack.

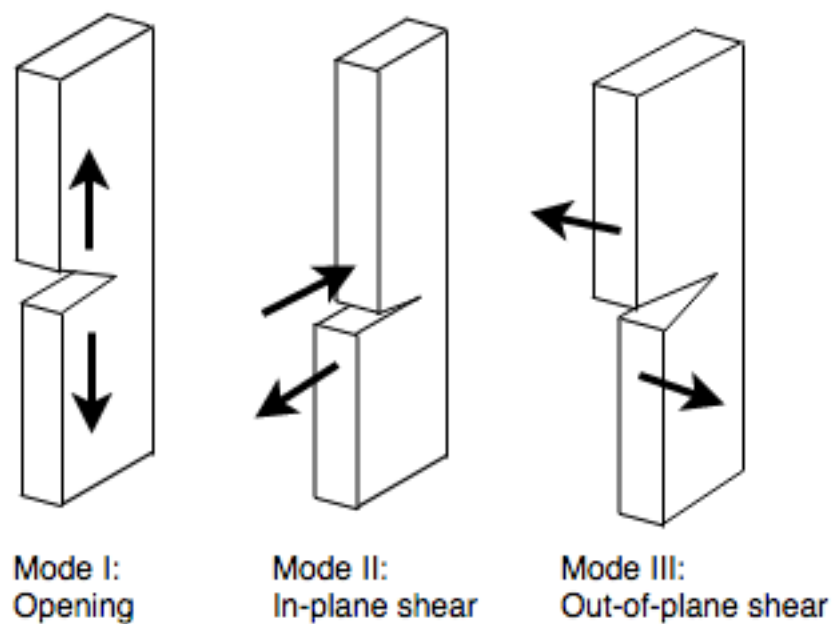


Figure 2-4 Crack propagation modes.

A crack can experience three types of loading, as Figure 2-4 illustrates. Mode I loading is called the *opening mode* and tends to open the crack. Here the load is applied normal to the crack plane. Mode II is called the *sliding mode* and tends to slide on the crack face with respect to the other due to in-plane shear loading. Mode III involves sliding of the crack faces due to out-of-plane shear. This mode is called the *tearing mode* and the crack faces are sliding parallel to the leading edge. A cracked structure can be loaded in each of these modes, or a combination of two or three modes [15][16]. The stress intensity factor is specific for each of the three modes mentioned above and is usually defined as K_I , K_{II} and K_{III} . This thesis will consider only mode I and II loading.

2.2.2 Fatigue Crack Growth

In the 1960's, Paris et al. [16] demonstrated that application of fracture mechanics to fatigue was useful for characterizing crack growth. He suggested that the crack growth rate could be presented by the power-law relationship, also known as the Paris Law.

$$\frac{da}{dN} = C(\Delta K)^m \quad (2.2.2)$$

Where da/dN is the growth rate of the crack, C and m are material constants that are determined experimentally and ΔK is the stress intensity factor range, given by

$$\Delta K = K_{max} - K_{min} = (1 - R)K_{max} \text{ for } R \geq 0$$

Crack initiation and crack propagation are caused by the tensile component of the loading. If R is below zero the applied loading will vary between tension and compression, meaning that the estimation of crack growth rate will be wrong since the crack will not grow under compressive loading. In order to achieve comparative data for fatigue crack growth rates, a stress ratio equal to 0.1 is frequently used in fatigue testing [2].

Fatigue crack growth data are typically presented in a logarithmic plot of crack growth rate, da/dN , versus the stress-intensity factor range ΔK , as Figure 2-5 illustrates. Most structural alloys are anticipated to have a plot of similar shape, however, the values of da/dN and ΔK varies with the material. The curve in Figure 2-5 illustrates typical fatigue crack growth behavior for metals [16]. Based on results of fatigue crack growth rate tests for a wide range of different metallic structural metals, it is found that the curve in Figure 2-5 has three distinct regions [2].

Region I illustrate the threshold value ΔK_{th} , which is the stress intensity factor range were da/dN approaches zero. Below this stress intensity factor range, no crack growth will occur. In region II the crack growth rate increases steadily at intermediate stress intensity factor range, ΔK , values [16]. The data in this region is usually described by a straight line on a log-log plot of ΔK versus da/dN , which is characterized by the Paris Law given in equation 2.2.2. In region III, the crack growth rate is rapidly increased to the point where K_{max} reaches the fracture toughness of the material, K_c , and failure occurs [2]. Due to the simplicity of the Paris law, it is only valid for determination of crack growth rates of region II behavior under constant cyclic loading [1].

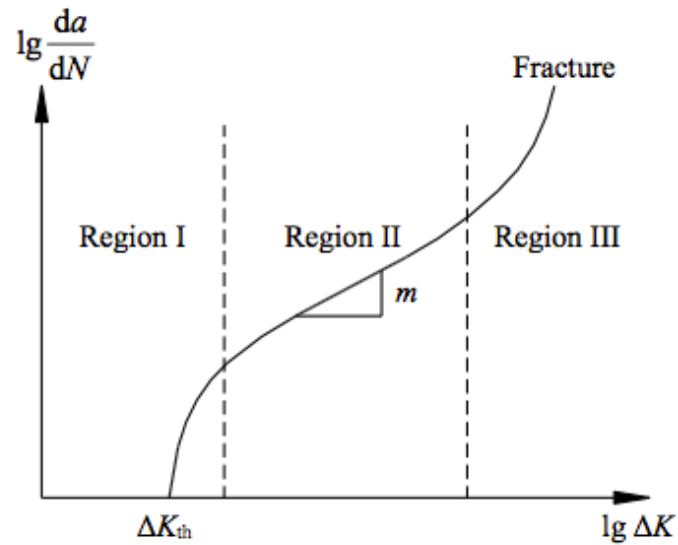


Figure 2-5 Typical fatigue crack growth behavior for metals [1].

In order to develop a mathematical model for prediction of fatigue life, N , for a given stress range at a constant load amplitude, the Paris law can be integrated. The number of cycles required for a crack to grow from initial length a_0 to final length a_f can then be found.

$$N_f = \int_{a_0}^{a_f} \frac{da}{C(\Delta K)^m} \quad (2.2.3)$$

2.2.3 Plastic Zone Size

In order to follow LEFM and for K to characterize the crack-tip conditions, the plastic zone size around the crack-tip must be small compared to any remaining distance between the crack-tip and boundaries of the specimen. If the plastic zone is sufficiently small, there will be an area outside it where the elastic stress field equation still applies, and K uniquely defines the crack tip conditions [14]. In other words, the elastic stress analysis becomes more inaccurate as the inelastic region at the crack tip grows. An equation for the size of the yielding zone of the crack tip can be estimated for plane stress situations from the elastic stress field equation. By substituting yield strength into the elastic stress field equation and solving for r gives [16].

$$r_y = \frac{1}{2\pi} \left(\frac{K}{\sigma_{YS}} \right)^2 \quad (2.2.4)$$

Which is the distance ahead of the crack tip where the elastic stress distribution exceeds the yield criterion for plane stress [14]. Note that for this expression, linear-elastic behavior is assumed, thus, this expression is not strictly correct. For elastic-plastic material behavior the

stresses cannot exceed the yield strength of the material, thus, forces above the yield strength present in an elastic material cannot be carried in the elastic-plastic material. In order to accommodate for these forces, yielding will extend even farther, which leads to a final estimate for plastic zone size for plane stress [16]

$$r_p = \frac{1}{\pi} \left(\frac{K}{\sigma_{YS}} \right)^2 \quad (2.2.5)$$

This expression shows as might be expected that the plastic zone will increase with increasing stress.

2.3 Mixed-Mode Fatigue

If the applied force is not normal to the crack, or if there is a complex state of stress, there may exist a combination of fracture modes I, II and III [14]. When a structure is subject to mixed-mode I and II loading, the stresses that arise at the crack tip are characterized by the stress intensity factors K_I and K_{II} [4]. In order to evaluate the characteristics of mixed mode fatigue crack propagation, a comparative stress intensity factor K_v is necessary to introduce, which consider K_I and K_{II} simultaneously [1]. Several comparable stress intensity factors have been proposed over the years, among them are those of Tanaka and Richard & Henn [17],[7]. The Richard/Henn-criterion, which has been found to yield good agreement with results [18], is given by

$$K_v = \frac{K_I}{2} + \frac{1}{2} \sqrt{K_I^2 + 6K_{II}^2} \quad (2.3.1)$$

Additionally, when conducting mixed mode fatigue calculations, a defined comparative stress intensity factor range, ΔK_v , may be used in the Paris Law.

$$\Delta K_v = \frac{\Delta K_I}{2} + \frac{1}{2} \sqrt{\Delta K_I^2 + 6\Delta K_{II}^2} \quad (2.3.2)$$

Where ΔK_I and ΔK_{II} are the stress intensity factor range for mode I and mode II respectively.

2.3.1 Plastic Zone Shape

Golos and Wasiluk (2000) [19] proposed an expression for the plastic zone boundary based on the elastic stress field around a mixed-mode I and II crack derived using the von Mises yield criterion under plane stress conditions. The expression defines the approximate boundary between elastic and plastic behavior and is estimated based on linear-elastic material behavior.

$$r_p = \frac{1}{2\pi\sigma_{YS}^2} \left[K_I^2 \cos^2 \frac{\theta}{2} \left(1 + 3 \sin^2 \frac{\theta}{2} \right) + K_I K_{II} \sin \theta (3 \cos \theta - 1) + K_{II}^2 \left\{ 3 + \sin^2 \frac{\theta}{2} \left(1 - 9 \cos^2 \frac{\theta}{2} \right) \right\} \right] \quad (2.3.3)$$

Where $\theta = 0$ along the parallel extension of the crack tip. Substituting values for K_I and K_{II} for different loading angles, θ , gives the plastic zone boundaries, as illustrated in Figure 2-6.

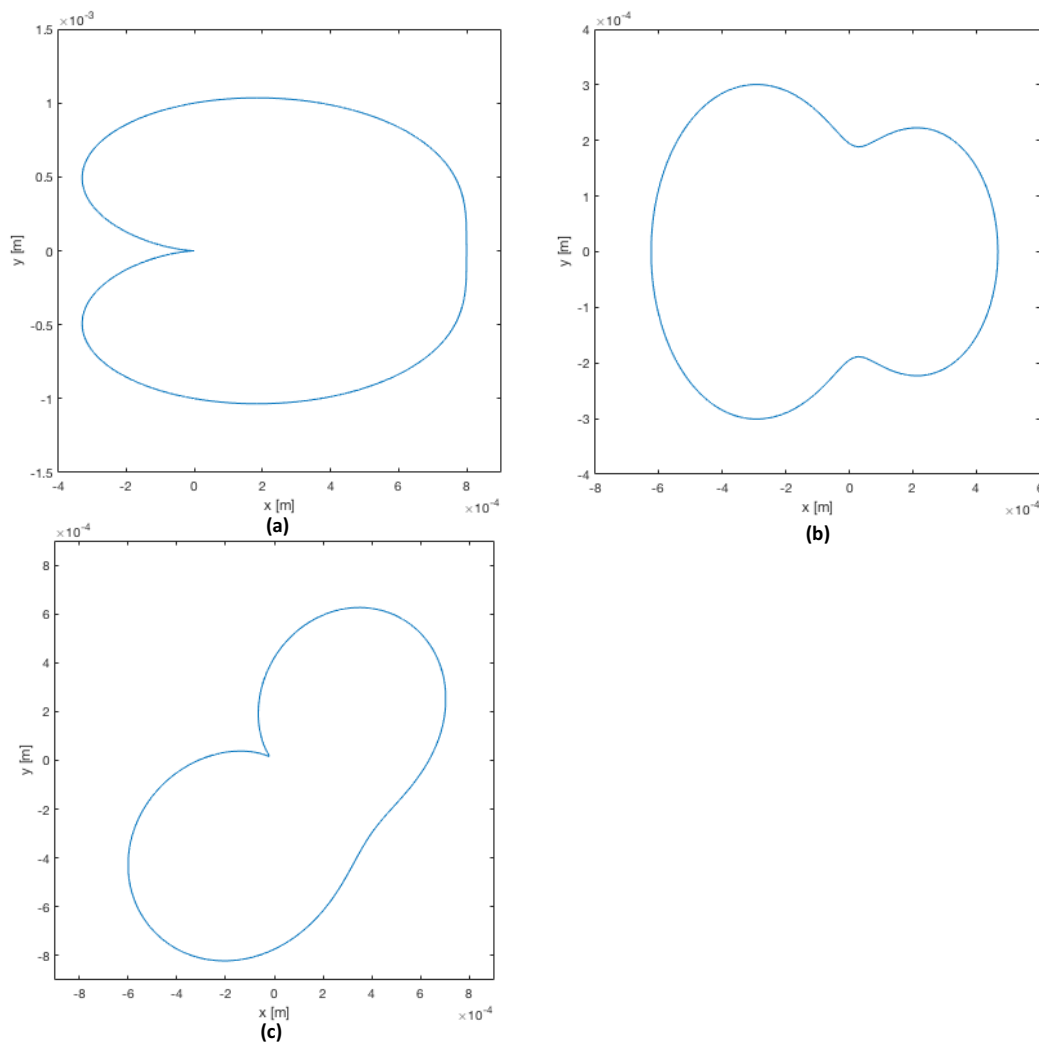


Figure 2-6 Crack-tip plastic zone boundaries for (a) Mode I (b) Mode II and (c) Mixed-mode I+II loadings.

2.3.2 Evaluation of Crack Growth Angle

When a crack is subjected to mixed-mode loading, the crack usually follows the path which offers the least resistance to propagate. In order to avoid rubbing their faces, fatigue cracks will attempt to propagate in mode I or try to minimize the amount of mode II loading, curving their paths if necessary [6]. To choose the propagating path of the crack, several theories have been proposed. The three most used are the criteria of maximum tangential stress, minimum strain energy density and maximum energy release rate [1]. Bittencourt [20] have shown that for brittle materials the three criteria mentioned basically predicts the same crack growth path. However, no general agreement on which of the theories that should be used exists [1], [21].

Concerning the criterion of maximum tangential stress, the crack extension should occur in a direction corresponding to the maximum tangential stress. This criterion has been found to yield good agreement with experimental observations [5], and due to its simplicity, this criterion has been widely used. In order to determine the angle of crack growth under mixed-mode fatigue loadings, Erdogan and Sih proposed the following expression [6]

$$\theta = 2 \arctan \left(\frac{1}{4} \frac{K_I}{K_{II}} \pm \sqrt{\left(\frac{K_I}{K_{II}}\right)^2 + 8} \right) \quad (2.3.4)$$

Where the sign of θ is the opposite of the K_{II} sign, and K_I and K_{II} are the stress intensity factors for mode I and mode II loadings.

2.4 Standardized Procedures for Measurement of Fatigue Crack

Growth Rates

There exist several standardized procedures for measurement of fatigue crack growth rates, including the British Standards Institution (BSI), the International Institute of Standards (ISO), and the American Society for Testing and Materials (ASTM). Since the ASTM standards are the most widely used throughout the world with regards to fatigue testing of materials [16], it was decided to follow the ASTM E 647 [22] standard in this thesis.

ASTM E 647 covers the determination of fatigue crack growth rates from near-threshold to K_{max} for compact tension C(T) and middle tension M(T) specimens. However, the general procedures regarding pre-crack length, crack size measurement and K_{max} limitations is also used for the compact tension shear (CTS) specimen used in this thesis.

The ASTM standard for fatigue crack growth measurement requires that data must be examined within the linear elastic fracture mechanics. The following expression gives the K_{max} limitation in order for LEFM to be valid.

$$(W - a) \geq \frac{4}{\pi} \left(\frac{K_{max}}{\sigma_{YS}} \right)^2 \quad (2.4.1)$$

Where $(W - a)$ is the uncracked length of the specimen.

The ASTM E 647 standard does not contain any specific requirements on specimen thickness, however, the fatigue properties can depend on thickness, so the thickness of the test specimen should match the structure of interest [16].

Following the ASTM standard, all specimens must be fatigue pre-cracked before the actual test. The length of the pre-crack should according to ASTM E 647 not be less than 0.1B, h or 1mm, whichever is greater. There are several procedures for notch preparation, depending on the material. The notch for a standard specimen may be made by electrical-discharge machining (EDM), milling, broaching, or saw cutting. The latter is only recommended for aluminum alloys. The purpose of pre-cracking is to obtain a sharpened fatigue crack of sufficient size and straightness. It is important that the final K_{max} during pre-cracking does not exceed the initial K_{max} in the fatigue test.

During the test, the length of the crack must be measured periodically. Measurements should be at intervals such that da/dN data are nearly evenly distributed with respect to ΔK . ASTM also recommends a minimum Δa of 0.25mm. The suggested intervals for the C(T) specimen is given by

$$\Delta a \leq 0.04 W \text{ for } 0.25 \leq \frac{a}{W} \leq 0.40 \quad (2.4.2)$$

$$\Delta a \leq 0.02 W \text{ for } 0.40 \leq \frac{a}{W} \leq 0.60 \quad (2.4.3)$$

$$\Delta a \leq 0.01 W \text{ for } \frac{a}{W} \geq 0.60 \quad (2.4.4)$$

If crack size is measured visually, an average value of crack lengths of the front and back side of the specimen should be used.

According to ASTM, the data are invalid if the crack deviates more than $\pm 20^\circ$ from the orientation of the initial notch over a distance equal of greater then 0.1W. The data are also

invalid if the crack size measured on the front and back side of specimen differ by more than 0.25 times the thickness of the specimen.

The ASTM standard E 647 suggest two numerical methods for plotting of da/dN versus ΔK , which is *the secant method* or *the incremental polynomial method*.

2.5 Specimen Configurations used for Mixed-mode Fatigue Crack

Growth Studies

A wide range of different specimen geometries has been used to simulate different combinations of mixed-mode loadings. Since there does not exist any standardized specimen geometries for mixed-mode loading, it is difficult to compare experimental results from different specimen geometries with regards to mixed-mode crack growth [7]. Nine different specimens have been presented by Richard [3], shown in Table 2-1, which have been used in mixed mode fracture and fatigue studies [7].

Table 2-1 List of different specimen geometries used for mixed-mode loading.

| | |
|--------------------------|--|
| <i>Richard [3]</i> | (S1) Plate specimen with inclined central crack under tension. |
| | (S2) Plate specimen with inclined edge crack under tension. |
| | (S3) Disc specimen with inclined inside crack. |
| | (S4) Cruciform specimen with inclined central crack. |
| | (S5) Shear specimen with inclined central crack. |
| | (S6) Pipe specimen with inclined through crack. |
| | (S7) Pipe specimen exposed to superimposed tensile and torsional stress. |
| | (S8) Three-point bend specimen with offset crack. |
| | (S9) Compact tension and shear specimen (CTS). |
| <i>Lal</i> | (S10) Double oblique edge crack specimen. |
| <i>Mahanty and Maiti</i> | (S11) CT specimen with inclined loads. |
| <i>Chamers et al.</i> | (S12) Double CT specimen with inclined loads. |
| <i>Otsuka and Tohgo</i> | (S13) CCT specimen loaded in tension and shear. |

Richard [3] also listed some criteria in order to obtain an optimal mixed-mode specimen, designed for fracture and fatigue tests. Following these was found useful in order to be able to evaluate specimens under mixed-mode loading systematically. The most critical once are; the possibility to apply full range of mixed mode I and mode II combinations, compactness of specimen, ease of manufacture, the ability to form fatigue pre-cracks under mode I loading and ease clamping and loading conditions. In addition, Richard analyzed the different specimen configurations (S1 to S9) based on the criteria's mentioned above. He found that

there was not possible for a transition from pure mode I to pure mode II for specimens S1, S2 and S6, thereby problematic to introduce pre-cracking. Also, there is neither possible to vary the K_{II}/K_I ratio for S1 and S1. Further, the presence of two crack tips was also listed unfavorable, due to the possibility for that the crack propagation does not start simultaneously at both crack tips. Richard then concluded that the CTS specimen (S9) was best suited for fatigue tests under mixed-mode loadings.

Several other specimen geometries have also been used for mixed mode I and II crack growth studies [7]. Among them are a double oblique edge crack specimen (S10), used for mixed-mode fatigue studies for different steels. For this specimen, force can be applied in both horizontal and vertical direction. However, due to the angled cracks, there is no possibility for fatigue pre-cracking under mode I loading. Further, a compact tension (CT) specimen (S11) with inclined load was used for studying stable crack growth under mixed-mode I and II loadings. Not either this specimen does allow for initiation of fatigue pre-cracking in the direction of the starter notch. Neither is there any possibility for the K_{II}/K_I ratio to be varied. In addition, a double CT specimen (S12) with inclined loads were also used in order to produce mixed-mode I and II loadings. This specimen configuration gives the possibility for initiating fatigue pre-cracking under mode I loading, and the opportunity to vary the K_{II}/K_I ratio. However, a fatigue testing machine with biaxial loading is required, which is not possible to perform on the MTS fatigue machine used in this thesis. The same problem also applies to the center cracked (CCT) specimen (S13) loaded in tension and shear for studying of the fatigue crack growth under static mode I and cyclic mode II loadings.

2.6 Compact Tension Shear (CTS) Specimen

In order to determine the forces the loading device is exposed to, it is necessary to calculate the loads that will be applied for testing of the CTS Specimen. Richard [4] obtained expressions for determination of the stress intensity factors K_I and K_{II} for the CTS geometry with an edge crack, plane and normal to lateral faces. To stay within the limits of LEFM, the maximum force can then be found by inserting maximum stress intensity factor, K_{max} , found from equation 2.4.1.

$$K_I = \frac{F\sqrt{\pi a}}{WB} \frac{\cos \alpha}{1 - \frac{a}{W}} \sqrt{\frac{0.26 + 2.65 \left(\frac{a}{W-a}\right)}{1 + 0.55 \left(\frac{a}{W-a}\right) - 0.08 \left(\frac{a}{W-a}\right)^2}} \quad (2.6.1)$$

$$K_{II} = \frac{F\sqrt{\pi a}}{WB} \frac{\sin \alpha}{1 - \frac{a}{W}} \sqrt{\frac{-0.23 + 1.40 \left(\frac{a}{W-a}\right)}{1 - 0.67 \left(\frac{a}{W-a}\right) + 2.08 \left(\frac{a}{W-a}\right)^2}} \quad (2.6.2)$$

Where W is the specimen width, B is the thickness of the specimen, a is the crack length, α is the angle of loading direction with respect to the crack plane and F is the applied force, as illustrated in Figure 2-7 (a). The given expressions are only valid in the range from $0.5 \leq a/W \leq 0.7$ [4].

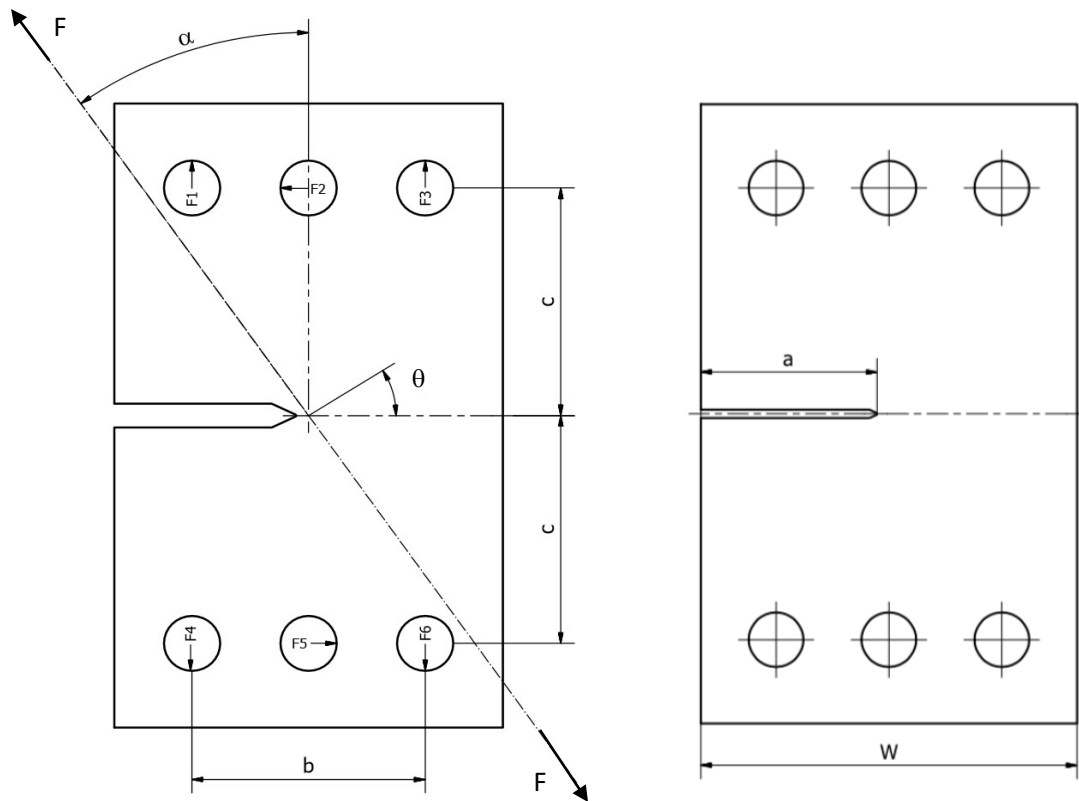


Figure 2-7 Dimension, forces and angle of loading direction on CTS specimen [17].

Richard also found the relation between the uniaxial load F related to punctual loads in the holes according to expressions [23]

$$F_1 = F_6 = F \left(\frac{1}{2} \cos \alpha + \frac{c}{b} \sin \alpha \right) \quad (2.6.3)$$

$$F_2 = F_5 = F \sin \alpha \quad (2.6.4)$$

$$F_3 = F_4 = F \left(\frac{1}{2} \cos \alpha - \frac{c}{b} \sin \alpha \right) \quad (2.6.5)$$

Where $\alpha = 0^\circ$ for Mode I loading, $\alpha = 90^\circ$ for Mode II loading and $0^\circ < \alpha < 90^\circ$ for Mixed Mode loading. These forces will be necessary when analyzing the loading device later on in this thesis.

2.7 Crack Length Measurements Techniques

Several different methods can be used to monitor the crack growth during fatigue testing. Among them are optical, including both visual and photographic monitoring, electrical, compliance, ultrasonic and acoustic emission monitoring techniques [2].

Visual observation can be done in several ways, including observing the crack at the specimen surface using a traveling microscope at a magnification of 20 to 50 times [2], [22], or by using a photo camera documenting the propagating crack length. In the latter case, the photos can be analyzed afterward, finding the crack propagation rate. For visual monitoring, measurements of crack length are made at intervals according to ASTM standard E 647. If the specimen surface is carefully polished and oxidation doesn't occur during testing, the visual monitoring technique gives accurate results [2]. In order to achieve a better optical measurement, surface crack detection coating can be used. Research and testing done by Three Bond Co. LTD [24], has shown that such a coating makes it easier to detect cracks on the surface. When a crack propagates, capsules in the coating will break, releasing pigments which will color the surface for easier detection of cracks. Other coloring technics can also be used in order to achieve color contrast between the surface and crack, thus, with the possibility for reduced quality.

Another monitoring technique is the compliance method of crack extension measurement. Here the crack opening displacement and applied tensile load are measured in order to determine the crack length, a , from the load line to the crack tip. As the crack length increases, the opening displacement will also increase. Both specimen load and crack opening displacement are measured simultaneously, using a displacement gauge and electronic loading cell, directing the outputs to the same data-acquisition system [2].

3 Feasibility Study

3.1 Design Discussion

In this chapter, there will be given an insight into the different choices in terms of which specimen type that were used, decisions that are done with regards to the design of the loading device and the chosen fabrication method.

3.1.1 Specimen Choice

Based on the knowledge gained from the research work, it was decided to use the CTS specimen (S9) with a specially designed loading device introduced by Richard for mixed mode I and II crack propagation testing. This specimen type was chosen considering the available clamping for the fatigue testing machine in the workshop at the University of Stavanger, combined with the opportunity to follow the most critical criteria for mixed mode fatigue testing proposed by Richard. Using this specimen combined with the specially designed loading device gives the possibility to introduce pre-cracking under mode I loading, the ability to apply a full range of mixed-mode loading combinations and easy clamping and loading using the fatigue testing machines CT grip.

Another suitable specimen type is the pipe specimen (S7), which gives the possibility for mixed-mode loading under combined tensile and torsional stresses. Based on already ongoing work at the University of Stavanger using this specimen type, it was found to be some disadvantages with the pipe specimen compared to CTS specimen. Concerning monitoring of crack growth, due to the centered crack of the pipe specimen, cracks will arise from both crack tips. Combined with the curved surface of the specimen, it was found difficult to get photos with good visibility of the crack on both sides at the same time. This problem increased with increasing crack length, meaning that manually photos had to be taken. Also by using a microscope, the crack monitoring will be much more time consuming for the pipe specimen compared to the CTS specimen, due to crack growth in both directions. As mentioned in Ch.2.5, there may also occur problems with two crack tips due to the possibility for uneven crack propagation. Another disadvantage with the pipe specimen is concerning the specimen fabrication. In order for the pipe specimen to be suited for testing, specially designed end pieces have to be welded on at both sides. Fabrication of a pipe specimen is therefore much more time consuming and costly than for a CTS specimen. Based on these experiences, it was desirable to try the CTS specimen for testing of mixed mode fatigue crack propagation.

3.1.2 Design of Loading Device

In order to use the selected CTS specimen for mixed mode I and II fatigue crack propagation testing, a special loading device has to be designed. The loading device designed in this thesis was based on similar loading devices that already have been introduced and used for experimental investigations of fatigue behavior under mixed-mode loading [8], [17], [18], [23].

Due to the size of the CT grip available for the fatigue testing machine, the loading device was restricted to have a maximum thickness of 12.7 mm. On the other hand, a thicker section could be used in the area which is not affected by the CT grip, as done by Huang *et. al* [25]. However, due to the fabrication method used for the loading device, this design would have increased the production costs a lot. In order to use this design, a machining process would have been required after water jet cutting. In addition, a thicker plate would have been necessary for the two side plates, resulting in higher material costs. Based on the increased cost for a device with varying thickness, combined with results obtained from the finite element analysis performed, the best solution was found to be using a constant thickness of the entire loading device.

Due to the pin size of the CT grip, the holes for attaching the loading device to the fatigue testing machine were set to have a diameter of 12.7 mm. Seven holes were made, making it possible for testing of pure Mode I, Mixed-Mode I and II and pure Mode II loading. The holes were made such that the angle of loading direction increases with 15 degrees for each hole, see Figure 3-1.

Three holes were made for connecting the loading device and the CTS specimen using bolts. In order to ensure a statically applied load transfer, the loading device is provided with elongated holes, while the CTS specimen is provided with circular holes. The external holes are elongated parallel to the direction of the notch, while the center hole is elongated perpendicularly to the notch [3], [18]. It was decided to use M12 bolts for connecting the loading device and specimen, thus, based on the standard for clearance holes for bolts, screws and studs [26], a radius of 6.5 mm was used. Drawings of the loading device can be found in Appendix-B.

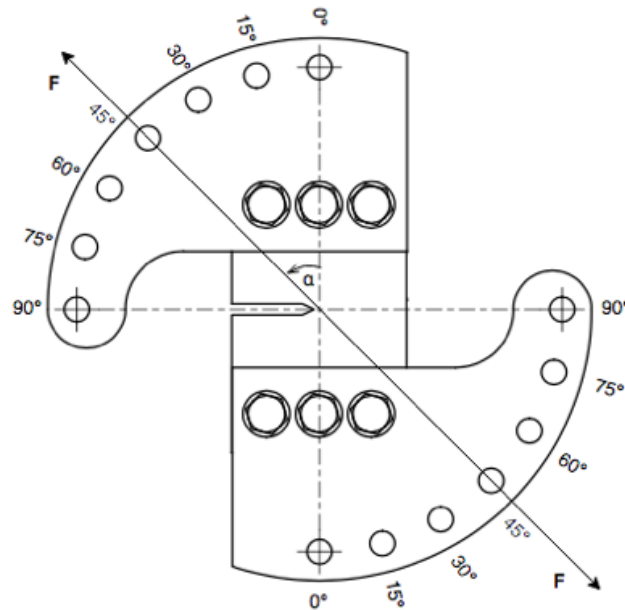


Figure 3-1 Loading device for testing of mixed-mode fatigue crack propagation [4].

3.1.3 Production Method

Through close collaboration with Martin Bae, workshop engineer at the University of Stavanger, it was decided to fabricate the loading device using three plates prepared by water jet cutting and then spot welded together. For simplicity, plates with a thickness of 4 mm were used, giving a total thickness of 12 mm. The loading device will then consist of two similar side plates and one middle plate, giving a 4 mm gap for insertion of the CTS specimen, see Appendix-B. This method was found to be the most cost-efficient way to manufacture the loading device, but still giving a satisfactory result.

Another production method that was considered was milling the loading device using a CNC-machine. However, due to the geometry of the loading device, it was found hard to get the workpiece properly fastened in the machine. In addition, machining the device would be a much costlier production method than water jet cutting. Some of the advantages of using a CNC-machine instead of water jet cutting are; increased accuracy of machined surfaces and edges, and avoiding weaknesses and inaccuracy with regard to welding.

Results found from the finite element analysis showed that the influence of the middle plate was almost absent. Based on this result, combined with recommendation received from Martin Bae, it was decided that water jet cutting followed by spot welding was a satisfactory fabrication method to use in this thesis. In addition, if the accuracy after water jet cutting and welding is too bad, it was still possible to mill the loading device afterward in order to achieve a better accuracy using a CNC-machine available at the workshop of the University of Stavanger.

3.2 Method for Monitoring of Crack Propagation

For monitoring of the crack growth, it was decided to use a photo camera attached to an adjustable tripod, as illustrated in Figure 3-2. The camera was connected to a computer for the possibility of shooting at preset intervals. The desired advantage with the use of a photo camera was the possibility to reduce the work amount with regard to monitoring of the crack growth compared to using a traveling microscope. Using a camera with the ability for automatic shooting do not require the same presence during testing. When using a traveling microscope, the operator physically has to move the microscope between each measurement of the crack growth. Another disadvantage with the use of a traveling microscope is the eventual equipment preparations needed for monitoring of mixed-mode fatigue testing. Microscopes for monitoring of fatigue crack propagation is usually delivered with a sliding rig for horizontal movement only. Thus, for monitoring of an inclined crack, an additional sliding rig for vertical movement has to be designed. For the work in this thesis, there was no time for such additional work. In addition, the equipment cost for a traveling microscope is much higher than for a photo camera.

One disadvantage of using a camera is the challenge of getting good visibility of the crack growth in the photos. However, based on knowledge gained from the research work done, there are several coating techniques available for enhanced visibility of cracks on the specimen surface. Therefore, based on the assumptions and research done for the two different crack measurement methods, it was decided to try using a photo camera in this work.



Figure 3-2 Monitoring of crack growth with the use of a photo camera.

3.3 Experience from Earlier Tests

During this Master thesis, the author has participated in fatigue crack propagation testing of pipe specimens. For this specimen type, mixed-mode loading was possible to obtain using a combination of axial and torsional loading. A total of three specimens were tested, all under pure mode I loading. Since the fatigue testing machine was new to the University of Stavanger, the first three tests were time consuming and used to gain experience with the machine. For this reason, there was no time for mixed mode I and II loading of the pipe specimen. During this work, good experience operating the fatigue testing machine was obtained.

A photo camera was used for monitoring of the crack propagation, which gave the author good experience regarding crack monitoring with the use of a camera. Based on this testing, it was found difficult to see the crack on the photos. Several technics were tried in order to make the crack more visual, namely a green coating, a red and a yellow marker pen. It was found that the yellow marker pen gave the best result, making it easier to detect the surface crack on the photos. The red marker pen made the surface in some cases too dark for the camera to handle, giving a photo with reduced quality. The green painting did not stick perfectly to the surface around the crack, causing the crack to partly grow under the painting, making it difficult to tell the exact crack length. However, using a similar coating technique as given by Three Bond Co., LTD [24], would possibly have given a better result.

4 CTS Specimen Calculation

In order to determine the forces the loading device would be exposed to, it was necessary to calculate the loads that would be applied for testing of the CTS Specimen. It was desirable to design the loading device in such a way that it was possible to test specimens of different materials. For this reason, calculations were done for four commonly used materials within the Norwegian offshore industry, namely EN S355, EN 316L, API 5L X52 and the 5754 aluminum alloy. The loading device was designed for fatigue testing within the assumption of LEFM. To stay within the limits of LEFM, the maximum applied loading to the CTS specimens follows requirements given by the ASTM E 647 standard. It was also desirable to determine how many cycles that was necessary for completing a crack propagation fatigue test of a specimen. These results were used later on to choose a suitable material for the loading device.

Mixed-mode fatigue crack propagation tests were performed using CTS specimens with width, $W = 90\text{mm}$, initial notch length, $a = 42.5\text{ mm}$ and a thickness $B = 4\text{ mm}$, see Figure 4-1. The selected dimensions for the CTS specimen was based on earlier work done by Richard [4], [8]. Using stress-analytical investigations carried out with the photo-elastic method and the finite-element method, he found the optimal dimensions for a CTS specimen.

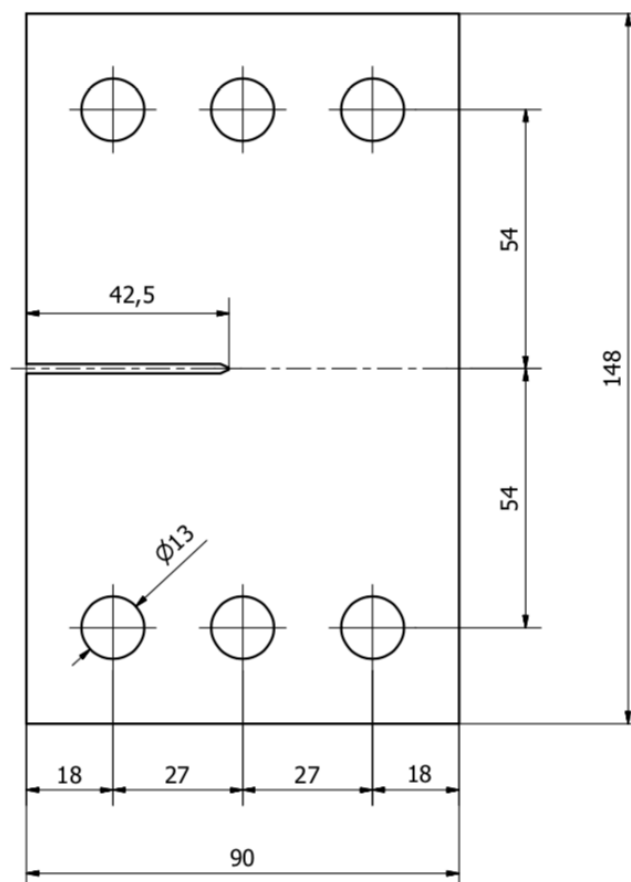


Figure 4-1 Dimensions of tested CTS specimen. Thickness: 4 mm.

4.1 Maximum Allowable Load for CTS Specimens

For simplicity, the following calculations were based on mode I loading only. In order to determine the maximum loadings used for fatigue testing of the CTS specimens, the maximum stress intensity factor, K_{max} , had to be found. It was desired to stay within the limits of LEFM, thus, the maximum allowable stress intensity factor was found using the expression given in ASTM E 647, Eq.(2.6.1). Stresses occurring at the crack tip increases with increasing crack length, thus, the maximum stress intensity factor will occur at the final crack length. In order to use the expression given by Richard, Eq.(2.5.1), the final crack length of the CTS specimens was limited to 63 mm. As can be seen from expression below, K_{max} varies for different yield strengths, hence for different materials. Calculations for all the selected materials was therefore performed.

$$K_{max} \leq \sigma_{YS} \sqrt{\frac{\pi}{4} (0.09 - 0.063)}$$

By inserting the calculated K_{max} values into the stress intensity factor expression for Mode I loading given by Richard (Equation 2.5.1), the maximum applied force, F_{max} was found. Table 4-1 shows the maximum allowable stress intensity factors for the selected materials, along with the maximum applied forces in order to follow LEFM.

Table 4-1 Maximum allowable stress intensity factors and maximum applied loading for the different materials.

| Material | Yield Strength [MPa] | K_{max} [MPa \sqrt{m}] | F [N] |
|-------------|----------------------|-----------------------------|-------|
| EN S355 | 355 | 51.7 | 6720 |
| 316L | 170 | 24.8 | 3224 |
| API 5L X52 | 300 | 43.7 | 5680 |
| Al 5754 H22 | 130 | 18.9 | 2460 |

4.1.1 Loads on CTS Specimen Holes

In order to determine the forces that would act on the loading device during fatigue testing, the punctual forces acting on each hole of the CTS specimen was desired to be found, illustrated in Figure 2-7. Similar forces will also act in the elongated holes of the loading device, just of opposite direction. Using expressions given by Richard, Eq.(2.6.3 – 2.6.5), the punctual forces for all the different loading angles were calculated for fatigue testing of steel grade EN S355, shown in Table 4-2. The calculations were done for this material since it has the highest yield strength of the selected materials, hence the highest applied load.

Table 4-2 Punctual loads acting on each hole of the CTS Specimen of steel grade EN S355.

| Loading Angle | $F_1 = F_6 [N]$ | $F_2 = F_5 [N]$ | $F_3 = F_4 [N]$ |
|---------------|-----------------|-----------------|-----------------|
| 0° | 3360 | 0 | 3360 |
| 15° | 4985 | 1739 | 1506 |
| 30° | 6270 | 3360 | -450 |
| 45° | 7483 | 5718 | -3953 |
| 60° | 7500 | 5820 | -4140 |
| 75° | 7361 | 6491 | -5621 |
| 90° | 6720 | 6720 | -6720 |

4.2 Crack Propagation Life

In order to know how many cycles that are necessary for fatigue crack propagation testing of the CTS specimen, it was desirable to find the crack propagation life. The calculations were based on region II behavior; hence the use of the Paris law expression. Carrying out the Paris law integration and inserting the stress intensity factor range for mode I loading, ΔK_I , the number of cycles to reach the final crack length of 63 mm were found. The stress ratio, R, were set to 0.1 in order to reduce the influence of crack closer during the test. The Paris Law constants, C and m, were found from earlier experiments and literature. Calculations and associated plots were computed using MATLAB.

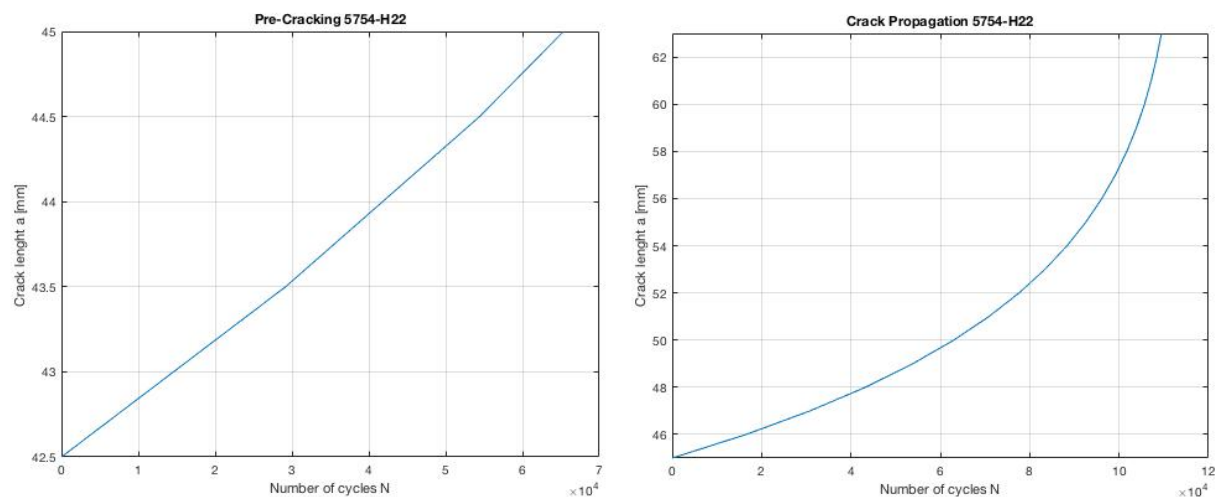


Figure 4-2 Numbers of cycles for fatigue pre-cracking and fatigue crack propagation testing of the 5754-H22 aluminum alloy.

Figure 4-2 shows the crack length versus the number of cycles for a CTS specimen of the 5754 – H22 aluminum alloy for both pre-cracking and crack propagation. The total number of cycles, including pre-cracking, for fatigue testing of all four materials, and the associated Paris Law constants, C and m, are listed in Table 4-3. It must be mentioned that there is a great

uncertainty regarding the Paris law constants. These constants have to be determined experimentally, thus a correct value for each of the materials was hard to find. The constants, C and m , were found from different works of literature and experimental work. However, for some of the metals constants from materials with similar properties were used.

Table 4-3 Paris Law constants and estimated number of cycles for different materials (ΔK in $\text{MPa}\sqrt{\text{m}}$, and da/dN in m/cycle).

| Material | C | m | Number of cycles Pre-cracking | Number of cycles Crack propagation |
|------------------|-------------------------|-------|----------------------------------|---------------------------------------|
| EN S355 [27] | 3.47×10^{-12} | 3.31 | 65 000 | 111 000 |
| AISI 316L [28] | 5.61×10^{-12} | 3.25 | 600 000 | 900 000 |
| API 5L X52 [29] | 1.427×10^{-12} | 3.523 | 145 000 | 275 000 |
| AL 5754-H22 [30] | 1.759×10^{-10} | 3.040 | 65 000 | 110 000 |

4.3 Plastic Zone Size and Shape

To control that the size of the plastic zone is sufficiently small during the crack propagation fatigue test, such that LEFM applies, r_y were calculated according to Eq.(2.2.4). As stated earlier in Ch. 2.2.3, this is an estimate of the extent of the plastic zone ahead of the crack tip based on linear-elastic material behavior. A plot of plastic zone size divided by crack length were created using MATLAB, showing the percentage of the plastic zone size relative to the crack length. Figure 4-3 shows that the plastic zone size reaches a maximum of 5.5 % of the crack length for fatigue testing of the 5754 – H22 aluminum alloy, which was found sufficient in order to reduce plasticity effects.

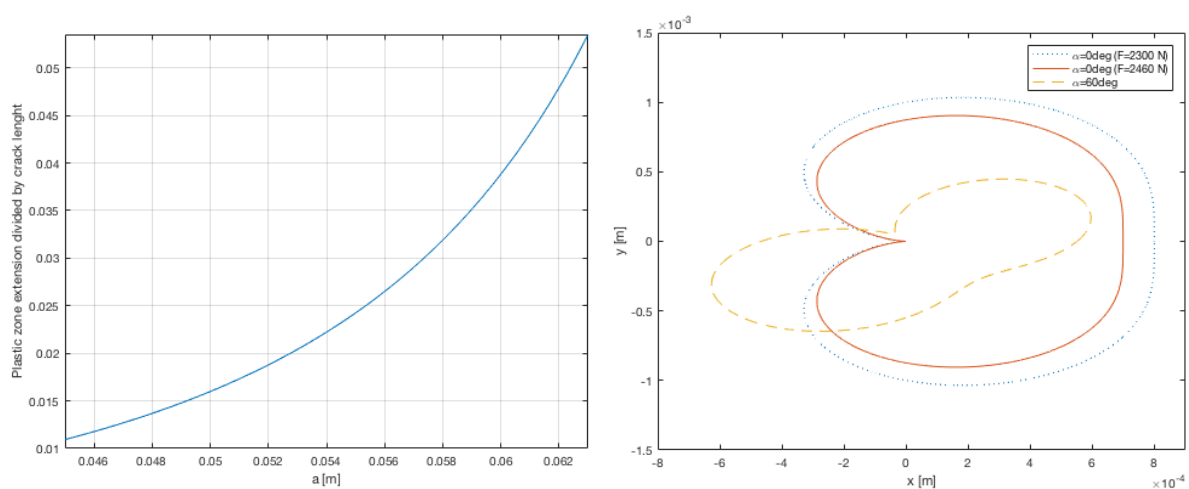


Figure 4-3 Percentage of plastic zone size relative to the crack length and plastic zone shape for mode I and mixed mode I+II.

In addition, it was desirable to investigate if the plastic zone shape obtained during pre-cracking would influence the result of the mixed-mode fatigue crack propagation testing. As stated earlier in Ch.2.3.1, the plastic zone boundaries are different for different angles of loading. A plot of plastic zone shape for pre-cracking under mode I loading and mixed-mode loading for a loading angle of $\alpha = 60^\circ$ was created, as illustrated in Figure 4-3. Plastic zone boundaries obtained during pre-cracking were plotted for two different loadings. As shown, reducing the applied load during pre-cracking decreases the plastic zone size, hence, affects the result of mixed-mode fatigue testing less. Since the size of the plastic zone is so small, it was decided to introduce pre-cracking under a loading of 2300 N.

4.4 Crack Propagation Angle

Using the criteria of maximum tangential stress, Eq.(2.3.4), the predicted crack propagation angles were calculated for every possible loading angles, as shown in Table 4-4. This result was used later on comparing against the actual angle obtained during mixed-mode fatigue crack propagation testing.

Table 4-4 Theoretically calculated crack propagation angle.

| <i>Loading Angle, α [$^\circ$]</i> | <i>Predicted Crack Propagation Angle, θ [$^\circ$]</i> |
|---|---|
| 15 | 13.1 |
| 30 | 25.7 |
| 45 | 37.5 |
| 60 | 48.6 |
| 75 | 59.5 |
| 90 | 70.5 |

In addition, predicted crack growth paths were plotted for every possible loading angles, see Figure 4-4. Based on the criteria of maximum tangential stress, the crack-tip angle will slightly decrease with increasing crack length. However, for simplicity, the different paths were plotted as straight lines along the predicted initiation angle.

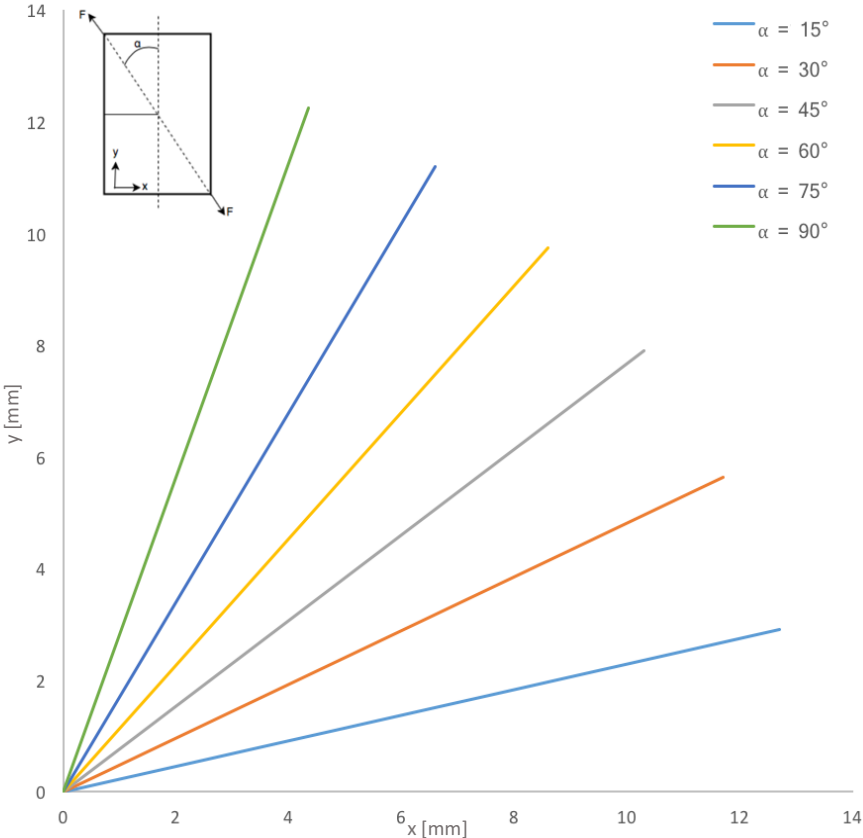


Figure 4-4 Predicted crack growth paths for mixed-mode loading under different loading angles.

5 Design and Analysis of the Loading Device

5.1 Finite Element Analysis of the Loading Device

Two computer software's were used to design and perform analysis of the loading device in this thesis. The finite element analysis program ANSYS Workbench 17 was used for analyzing the loading device. ANSYS Workbench also allows creating 3D models of the geometry using the built-in *Design Modeler*. However, due to previous experience with the CAD software Autodesk Inventor, this was used instead for modeling of the loading device geometry. There exists an import function between Inventor and ANSYS making it possible to export the 3D assembly from Inventor to an ANSYS model.

A project in ANSYS workbench consists of seven steps, which all have to be defined in order to execute an analysis.

1. Analysis system
2. Engineering data
3. Geometry
4. Model
5. Setup
6. Solution
7. Results

Before starting the simulation setup in ANSYS Workbench, a suitable analysis system has to be chosen. There are many different environments to choose from, depending on what type of analysis to perform. For this thesis, it was desirable to find the maximum stress and displacement occurring in the loading device, thus the *Static Structural* analysis system was used.

Further, the material properties of the desired material have to be defined in the *Engineering Data*, such as tensile strength, yield strength, poisson's ratio, etc. To get an accurate result of the analysis, material properties as identically as possible to the real material should be used.

Autodesk Inventor was used instead of the built-in *Design Modeler* available in ANSYS to create a 3D model of the loading device geometry. Two plate geometries were made, a side plate and a middle plate, see Appendix-B. Then the assemble function in Inventor was used in order to make the loading device, consisting of the middle plate in between the two side plates. Further, the assembly was saved as a STEP file before imported to ANSYS using the *Design Modeler*.

The remaining four steps take place in the Workbench *Mechanical* module. Here a suitable mesh was generated before forces and constraints were applied. Before running the simulation, desired result parameters also had to be determined. For this analysis, maximum von Mises stress and total deformation were used.

Since the values and directions of the forces acting in the elongated holes related to the total applied force are already known, it gives a more accurate result applying forces instead of constraints in the elongated holes. In order to simulate the correct load acting on the loading device, it was therefore chosen to apply forces in the elongated holes and a constraint in the upper circular hole.

5.1.1 Connections

Since the loading device will consist of three separate plates spot welded together, a suitable connection between the plates had to be chosen. The *mechanical* software in ANSYS *Workbench* automatically defines a fixed connection between the three plates. Since there does not exist an easy approach for simulating the case of spot welded connections, both fixed and frictionless connection between the plates were tested. The results for both cases gave a similar result, which means that the center plate isn't bearing any considerable load. This result shows that the connection method isn't critical for the resulting analysis and that any of the two methods mentioned can be used.

Based on this result, another possible solution is to perform the simulation based on a geometry consisting only of the two side plates, neglecting the effect of the middle plate. This would have reduced the number of meshed parts and the opportunity for a finer overall meshing. However, since the majority of the meshing is located around the elongated holes, it turned out to not have any significant influence. Thus, it was decided to perform the analysis using the actual geometry with a fixed connection between the three plates.

5.1.2 Meshing

The loading device was meshed using the automatic meshing method with 10-node tetrahedral elements in ANSYS Workbench [31], applied utilizing element sizing control. Quadrilateral dominant elements were not available for this analysis, thus tetrahedral elements were found to be the best-suited method. To localize the critical areas regarding stress concentrations in the loading device, a simulation was first executed using a mesh with element sizing control set to 5 mm. The given result showed that maximum stress occurred in and around the elongated holes of the loading device. However, for the 45 degree loading case, high stresses also occurred in the circular hole. Thus, a different mesh was used for analyzing the case of loading for 45 degrees.

For the 45 degree loading case, mesh refinement was used both around the elongated holes and the circular hole. For the other loading cases, mesh refinement was only used for the local mesh around the elongated holes. Mesh refinement around the circular hole for these loading angles was also tested, but it proved to not result in any changes. Since the ANSYS Workbench software license at the University of Stavanger has limitations on the allowable number of elements, a finer general mesh size was prioritized for these cases. Figure 5-1 shows the final meshing used for the simulation.

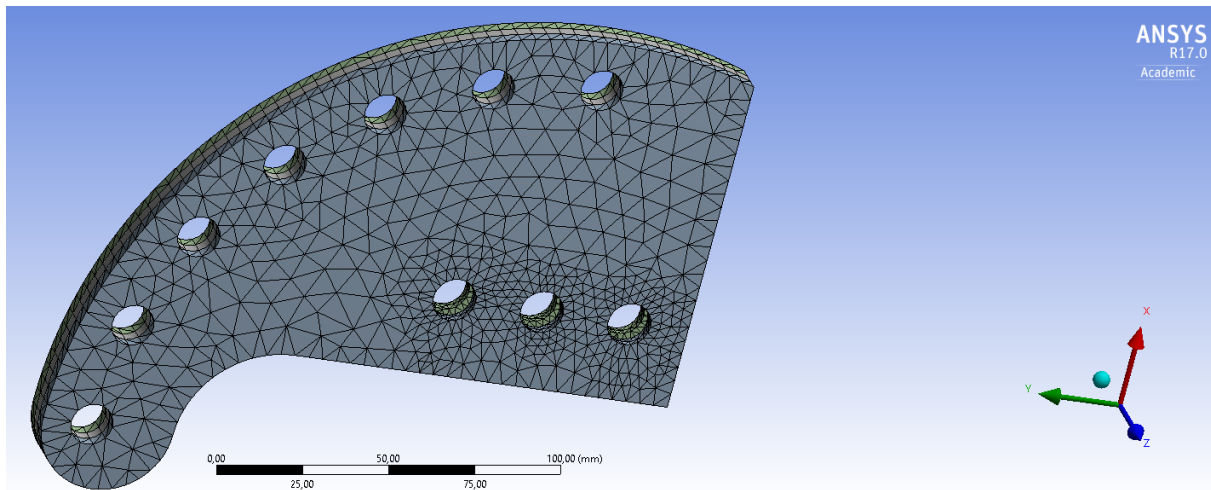


Figure 5-1 General meshing used for analysis in ANSYS Workbench. Source: ANSYS® Workbench, R17.0, Academic.

5.1.2.1 Mesh Convergence Test

In order to ensure a satisfactory meshing accuracy, a mesh convergence test using a decreasing range of mesh sizes was performed. The maximum von Mises stress based on nodal average stress were plotted for an increasing number of elements. If the corresponding plot is converging, the given mesh is satisfactory. Since the geometry is relatively simple, a satisfactory meshing was obtained even though there is some limitation to the ANSYS software regarding the allowable number of elements.

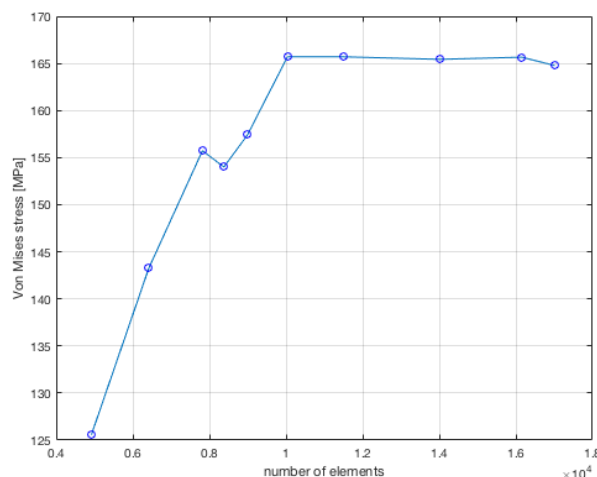


Figure 5-2 Mesh convergence test.

5.1.3 Constraints

The loading device was constrained in the circular hole where the device will be connected to the fatigue testing machine's CT grip. Different holes are constrained, depending on which loading angle that is to be analyzed. *ANSYS Workbench 17* has a built-in constraint function called *cylindrical support* for simulation of bolted or pinned connections. This function can control displacement in three directions, radial, axial and tangential direction. Since the loading device will be locked, hence no movement in any direction, all three directions were set to fixed.

In addition, fixed displacement in z-direction was applied in the open space between the two side plates where the CTS specimen would be installed during testing. Figure 5-3 shows applied constraints for the case of a loading direction of $\alpha = 90^\circ$.

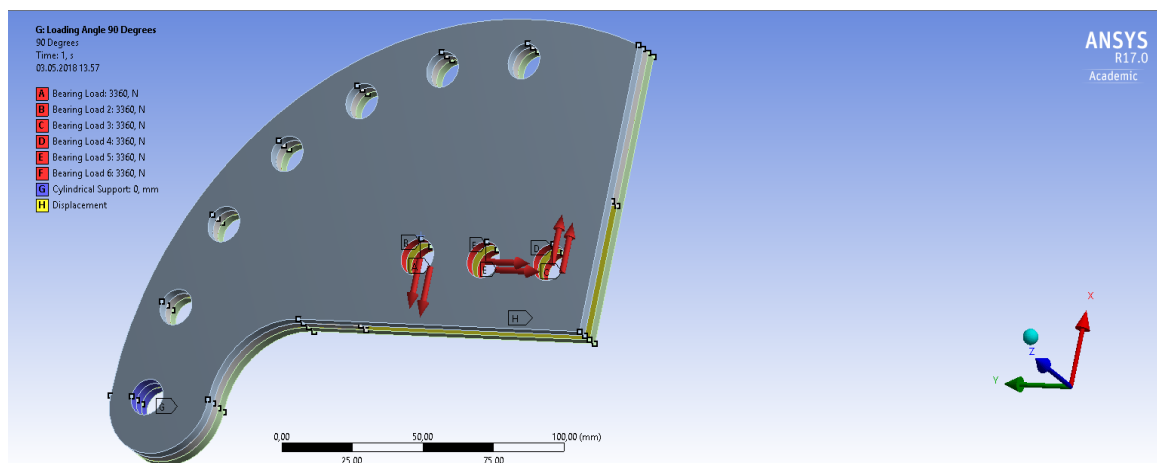


Figure 5-3 Applied constraints and forces for ANSYS Workbench analysis. Source: ANSYS® Workbench, R17.0, Academic.

5.1.4 Forces

The forces acting on the loading device were applied in the elongated holes, which is the bolted connection with the CTS specimen. The calculated values shown in Table 4-2 were used, only that they are acting in the opposite direction. For simplicity, circular holes were used instead of elongated holes for the FEA analysis. A simple study of the two different approaches was performed, showing that both circular holes and elongated holes gave a similar result. When running the analysis using elongated holes, a surface simulating the connection area between the bolts and the elongated holes had to be created. Then point loads were applied to the created bolt surface. Figure 5-4 shows the simulation results for both cases for a loading direction of $\alpha = 90^\circ$.

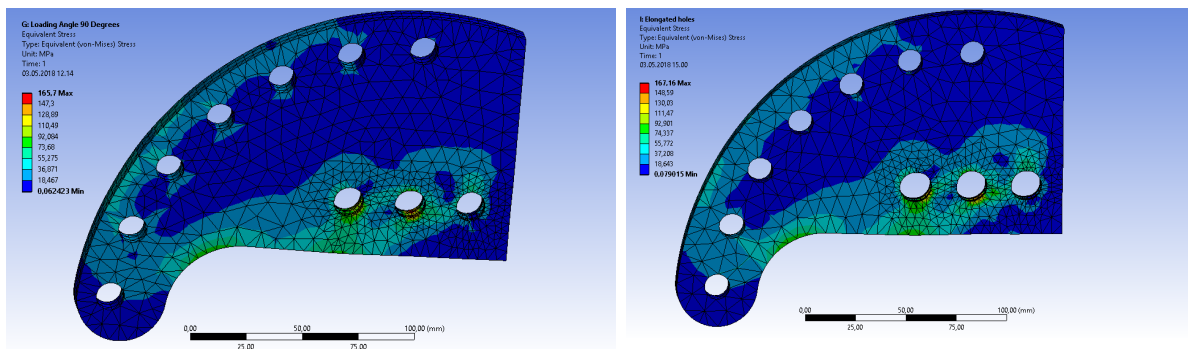


Figure 5-4 Comparison between using elongated holes and circular holes. Source: ANSYS® Workbench, R17.0, Academic.

Using circular holes made it possible to use the *bearing load* function for simulation of the bolted connection. A bearing load represents a typical load that will occur from a bolt in a cylindrical contact area. Using this function instead of modeling a virtual part for the connection is much less time-consuming, due to the reduction of meshed parts. In addition, a very fine mesh is required for a correct simulation of the contact area between the holes and the bolt. Since the used ANSYS license had a restriction on the allowable number of elements, using an extra part would have reduced the overall mesh sizing, leading to a more inaccurate result. Forces given in Table 4-2 were applied for the different angles of loading direction. Figure 5-3 shows the forces applied using the *bearing load* function for a loading direction of $\alpha = 90^\circ$.

5.2 Results of Simulation

The finite element analysis using ANSYS showed that the loading device is exposed to a maximum von Mises stress of 166 MPa, which occurs for a loading direction of $\alpha = 90^\circ$. Following are the results for total displacement and von Mises stress occurring in the loading device for every possible loading direction. These results are based on fatigue testing of a CTS specimen of steel grade EN S355, hence an applied total force of 6720 N. However, as long as all stresses remain below the yield strength of the material, the problem is linear, and the stress components can be multiplied in order to find stresses for different loadings. Table 5-1 shows the maximum von Mises stress occurring in the loading device during fatigue testing of all the four materials that are taken into account in this thesis.

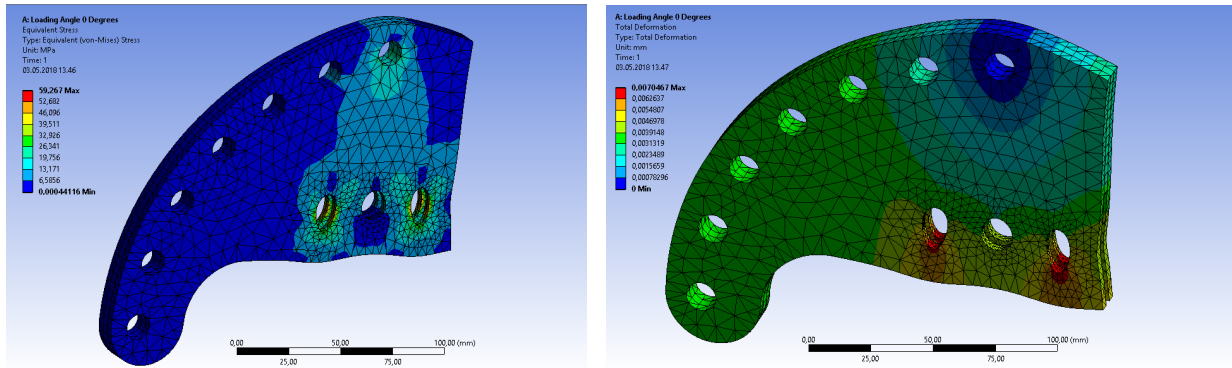


Figure 5-5 von Mises stress and total displacement for a loading direction of $\alpha = 0^\circ$. Source: ANSYS® Workbench, R17.0, Academic.

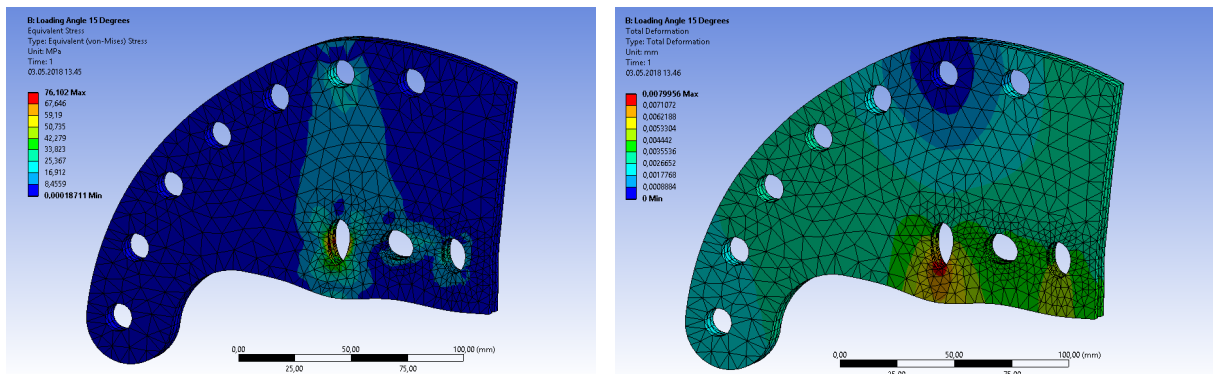


Figure 5-6 von Mises stress and total displacement for a loading direction of $\alpha = 15^\circ$. Source: ANSYS® Workbench, R17.0, Academic.

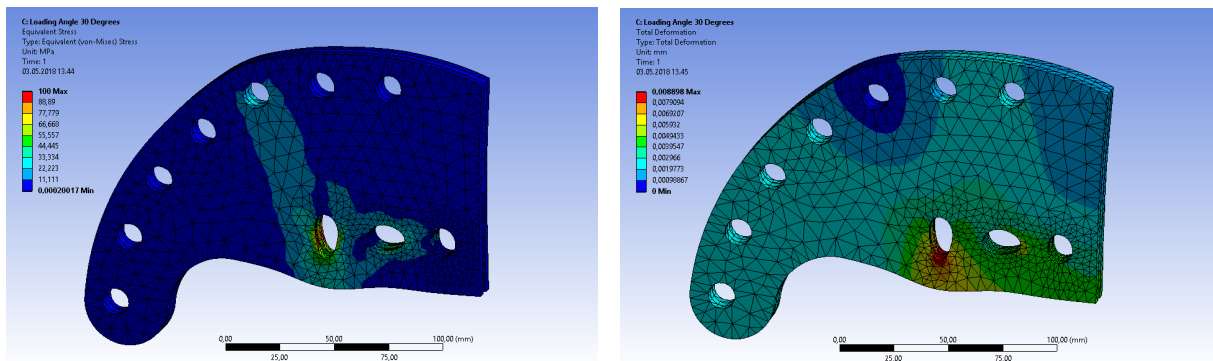


Figure 5-7 von Mises stress and total displacement for a loading direction of $\alpha = 30^\circ$. Source: ANSYS® Workbench, R17.0, Academic.

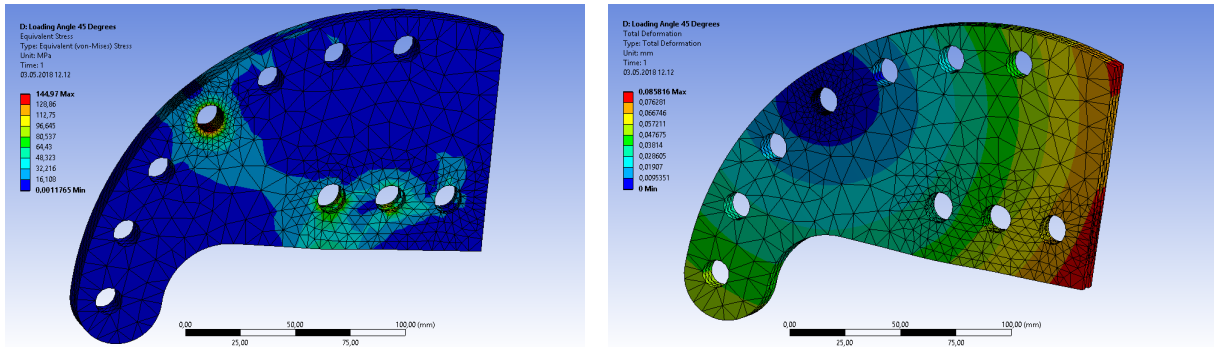


Figure 5-8 von Mises stress and total displacement for a loading direction of $\alpha = 45^\circ$. Source: ANSYS® Workbench, R17.0, Academic.

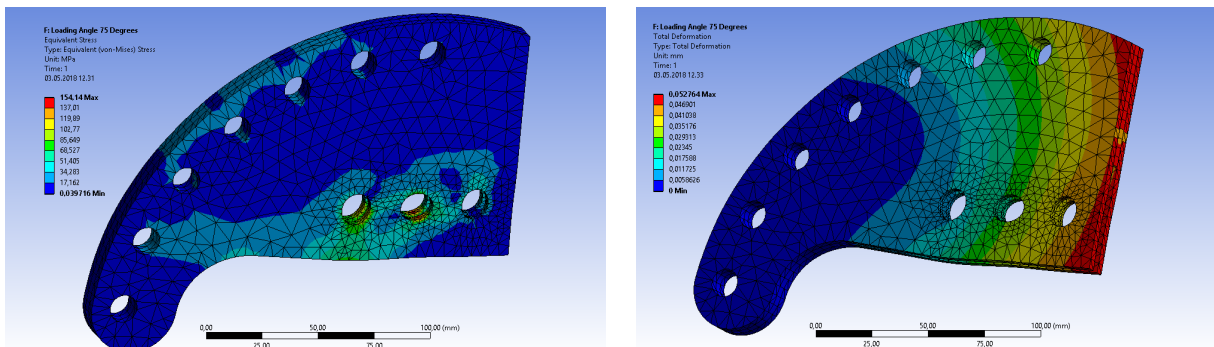


Figure 5-9 von Mises stress and total displacement for a loading direction of $\alpha = 60^\circ$. Source: ANSYS® Workbench, R17.0, Academic.

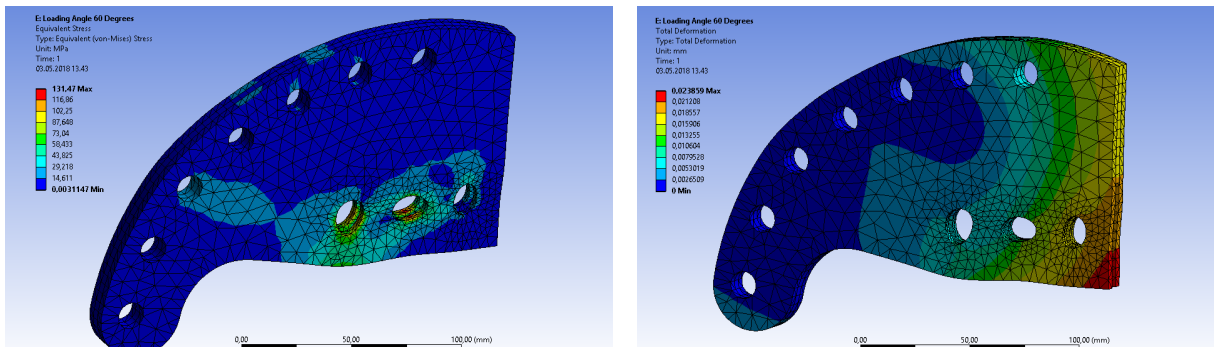


Figure 5-10 von Mises stress and total displacement for a loading direction of $\alpha = 75^\circ$. Source: ANSYS® Workbench, R17.0, Academic.

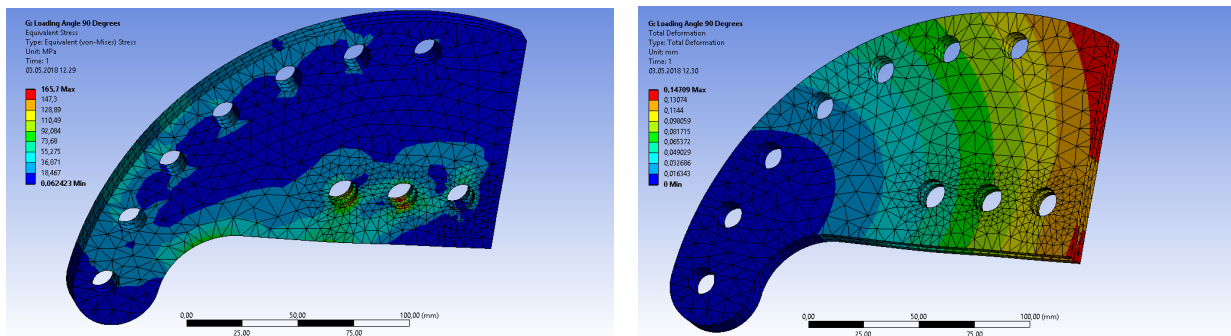


Figure 5-11 von Mises stress and total displacement for a loading direction of $\alpha = 90^\circ$. Source: ANSYS® Workbench, R17.0, Academic.

Table 5-1 Maximum von Mises stress occurring in the loading device for fatigue testing of different materials and for different angles of loading direction.

| Loading Angle, α [$^\circ$] | Maximum von Mises stress [MPa] | | | |
|--------------------------------------|--------------------------------|-----------|------------|---------------|
| | EN S355 | AISI 316L | API 5L X52 | AL 5754 – H22 |
| 0 | 59 | 28 | 50 | 22 |
| 15 | 76 | 37 | 64 | 28 |
| 30 | 100 | 48 | 85 | 37 |
| 45 | 145 | 70 | 123 | 53 |
| 60 | 132 | 63 | 112 | 48 |
| 75 | 154 | 74 | 130 | 56 |
| 90 | 166 | 80 | 140 | 61 |

5.3 Bolt Calculation

It was desirable to find the shear forces acting on each individual bolt. Partial thread M12 bolts of grade 8.8 with a length such that the thread is not in the shear plane were used. The maximum shear forces acting on each of the three bolts connecting the CTS specimen to the loading devices was calculated for an applied load of 6720 N, which is the maximum load used for consideration. Due to a missing pin for the CT grip, M12 bolts were used here as well. Thus, the shear stress in the bolt connecting the loading device with the CT grip in the fatigue testing machine was also calculated. All of the bolts will be loose, and due to the design of the joint, the bolts will be exposed to double shear. The expression for shear stress in a bolt under double shear is

$$\tau_{bolt} = \frac{2F}{\pi d^2} = \frac{2 \times 6720 \text{ N}}{\pi (12 \text{ mm})^2} = 29.7 \text{ MPa} \quad (5.3.1)$$

Where F is the applied force and d is the bolt diameter. According to Eurocode 3, detail category 100, a bolt in double shear of grade 8.8 will have a cut-off limit of approximately 67 MPa, which is well above the calculated shear stress of 29.7 MPa. This means that every bolt will have an infinite life.

5.4 Material Choice of Loading Device

Based on the results obtained from the ANSYS Workbench analysis, a suitable material for the loading device had to be chosen. Since the loading device is exposed to a maximum von Mises stress of around 166 MPa, a material with an endurance limit above this was desirable. In addition, it should also be possible to apply double overload to the CTS specimens, making a material with yield strength higher than 332 MPa necessary. Due to the chosen fabrication method, the material also needed to have good weldability. Another factor to account for was the material and production cost. If a durable material with infinite life would be much more expensive than a common material, there could be more cost efficient to make several loading devices of a cheaper material with a given fatigue life.

Several different materials were investigated. Based on material properties and information gained from different S-N curves, a high strength low carbon martensitic/austenitic stainless steel, S165 [32], was found to have all the desired material properties. From the S-N curve shown in Figure 5-12 [33], a mean value for the fatigue limit is approximately 535 MPa for testing with $R = -1$, and 457 MPa for testing performed with a stress ratio equal zero. Using the modified Goodman relation, it was found that the material has a fatigue limit of approximately 400 MPa for a stress ratio of $R = 0.1$. It is important to mention that only one S-N curve was found for this material, which leads to a high uncertainty. In addition, the source of the data is not the best.

However, even if the material properties are well suited, there were some disadvantages to the use of this steel alloy. The material cost for the steel alloy S165 and similar high strength steels is much higher than for common structural steels. Hence, using a cheaper steel grade with lower strength could be more economic. Even though the loading device would not have the same durability, it could be possible to produce multiple devices at a lower price. Another problem regarding steel alloys of this strength was that they are only delivered in round bar, making the production cost increase due to extra work. If using round bar, the material first has to be cut into suitable slices and then machined in order to achieve an approved surface finish. Several companies providing a wide range of materials was contacted in order to find steel alloys of this strength in plates with a thickness of 4 mm, without any success.

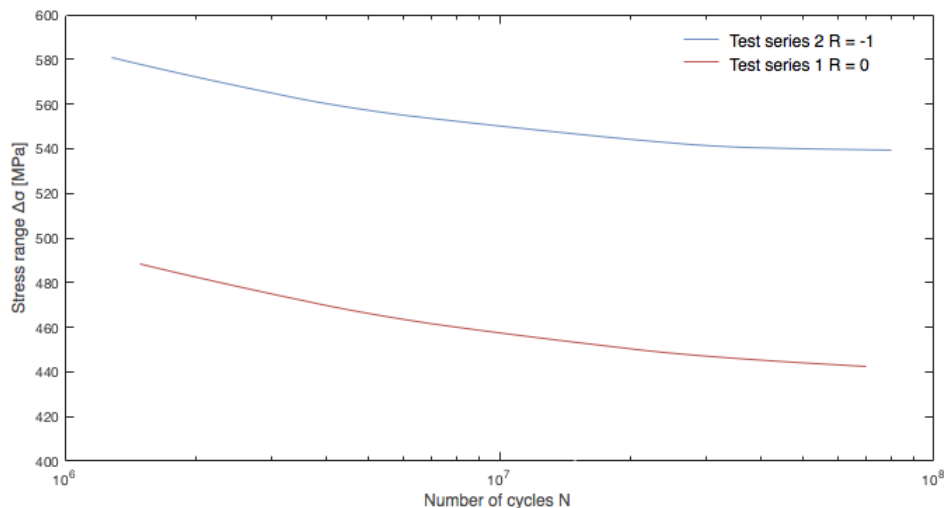


Figure 5-12 S-N curves for S165 based on experimental results obtained by [33].

In addition, the company that provided water jet cutting of the loading device parts, Smed T. Kristiansen AS, offered to produce the loading device for free if a common steel alloy was used, namely EN S355. Based on information gained from different S-N curves and the Eurocode 3 standard, combined with the fact that production and material costs were free, it was decided to fabricate the loading devices using this steel alloy.

Based on notch detail 160, derived from Eurocode 3, the loading device will have an infinite life for stress ranges below 119 MPa. Meaning, that for mixed-mode fatigue crack propagation testing of a CTS specimen made of AISI 316L and AL 5475 – H22 aluminum alloy, testing using a stress ratio of $R = 0.1$, the loading device will theoretically have an infinite life. The same also applies for testing of API 5L X52, except for a loading direction of $\alpha = 90^\circ$, and for EN S355 for loading directions of $\alpha = 0^\circ, 15^\circ, 30^\circ$ and 60° .

Based on this information, the loading device will have a given fatigue life for the case of testing of API 5L X52 for a loading direction of $\alpha = 90^\circ$, and for testing of EN S355 for both a loading direction of $\alpha = 75^\circ$ and 90° . Thus, it was desirable to estimate the minimum number of cycles the loading device would endure. According to Eurocode 3, the loading device will have a fatigue life of approximately 2 million cycles for testing of the steel grade EN S355 under a loading angle of $\alpha = 90^\circ$. In addition, when variable amplitude loading is applied, the cut-off limit is reduced. The endurance limit is therefore reduced after tests were the stresses exceed the fatigue limit. According to Eurocode 3, using the extended fatigue strength curve, this leads to a reduction of the cut-off limit to approximately 65 MPa.

In addition to the S-N curve provided by Eurocode 3, two other S-N curves were found. Based on experimental testing with regard to the steel grade EN S355 by Ungermann *et. al* [34], the corresponding S-N curve gave a mean fatigue limit of approximately 157 MPa, see Figure 5-13. The tests were performed using a constant stress range under sinusoidal cycle with a stress

range of $R = 0.05$. Using the modified Godman relation, the fatigue limit for a stress range of $R = 0.1$ was found to be a stress range of 155 MPa.

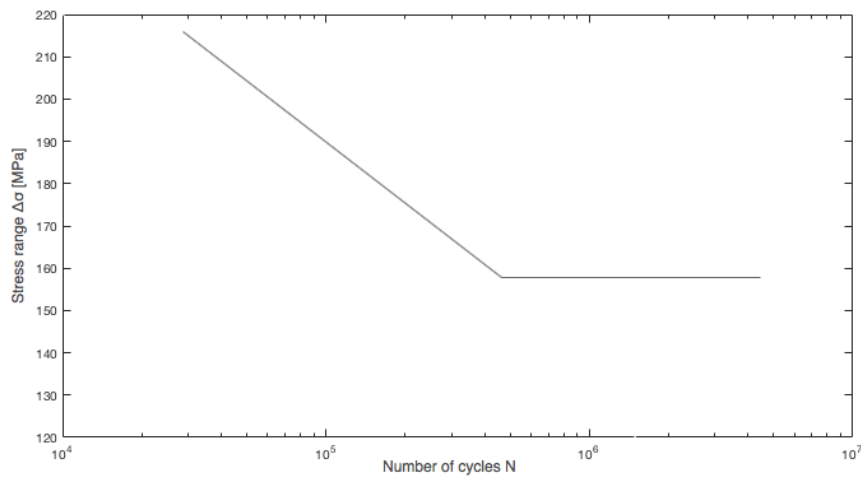


Figure 5-13 S-N curve for steel alloy EN S355 based on experimental results by Ungermann et. al. [34].

Results from the second studied S-N curve for S355J2 steel, based on experimental results by Ulewicz et al. [35], showed a fatigue limit of 290 MPa, as illustrated in Figure 5-14. Here 12 specimens were tested using a stress ratio of $R = -1$. For this S-N curve, the stresses are reported as stress amplitude instead of stress range. Using the modified Godman relation, the fatigue limit for a stress ratio of $R = 0.1$ was found to be 234 MPa, which is well above the maximum amplitude stress occurring in the loading device. Based on this result the loading device will have an infinite life. However, since the results deviate so much compared to the S-N curve found by Ungermann et al. and those results gained from the Eurocode 3 standard, a great uncertainty must be assumed. In addition, the source of the last discussed S-N curve is highly unsure.

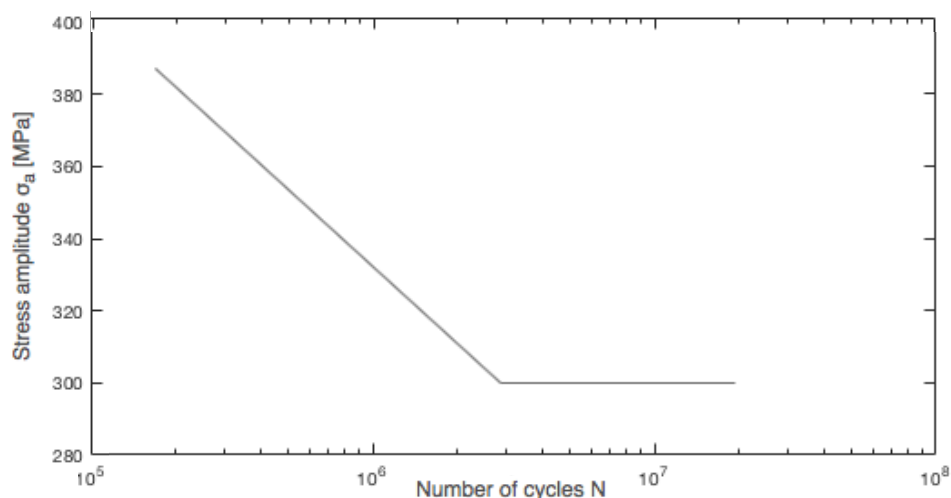


Figure 5-14 S-N curve for steel alloy EN S355 based on experimental results by Ulewicz et al. [35].

Based on the knowledge gained from studied standard and S-N curves, the use of steel grade EN S355 was found sufficient. Combined with the fact that material and production cost when using this steel grade was free, it was found to be the best solution for this thesis. Based on results from Eurocode 3 combined with results from the two other studied S-N curves, it is safe to say that the loading device will endure testing of many specimens before failure. However, due to the fact that the loading device will not have an infinite life for all testing cases considered, it was decided to produce two sets of the loading device.

5.5 Fabrication of Loading Device

As mentioned earlier, it was decided that the loading device would consist of three plates. Each of the plates was prepared by water jet cutting, and then spot welded together. It was also considered to rout the holes on the loading device after welding to obtain a better accuracy and surface finish of the holes. Since the loading device was found to not last forever, it was decided together with Martin Bae that the precision and surface finish obtained by water jet cutting would be sufficient. However, if a material giving infinite life would have been used, such as the high strength steel alloy S165, extra work with regard to achieving a finer finish and accuracy would have been preferred.

The geometry of the loading device drawn in Inventor was imported into AUTOCAD, where dxf files of the side plate and a middle plate was generated. These were then sent over to Smed T. Kristiansen AS for water jet cutting. A total of 8 side plates and 4 middle plates were produced in order to have two sets of the loading device. After water jet cutting, a thin layer of rust had settled on the surfaces and edges of the plates. Prior to welding, the plates were sandblasted in order to remove the rust, see Figure 5-15. This was done in the workshop at the University of Stavanger.



Figure 5-15 Sandblasting of plates before welding.

Prior to welding, the three plates were clamped tight together using a vise and two screw clamps. The lower flat side of the plates was placed in the vise in order to align the plates correctly in relation to each other, see Figure 5-16. In addition, it was checked that all the holes were perfectly aligned before the two screw clamps were attached. The clamps were used to make sure that there was no movement between the plates during welding. The welding was performed in the workshop at the University of Stavanger by Johan Andreas Thorakaas.

TIG – welding was used, which is well suited for thin materials and small specimens. Since the three plates were laying on top of each other, no filler wire was used, meaning that the three plates were just melted together. Before welding of the loading device, two test plates were welded together in order to make sure that a sufficient result was obtained. Seven spot welds were evenly distributed around the loading device. In order to make sure that the material strength around the holes would not be influenced by the welds, the spot welds were placed as far away as possible from the holes.



Figure 5-16 Clamping of loading device prior to welding.

To prevent new rust from forming, a lanoline-based lubricant from Fluid Film [36] was applied to the loading devices after welding. It was then left overnight in order for the lubricant to penetrate to the base of the metal, then was the excess fluid removed with a paper towel. Since the loading device is exposed to repeated cyclic loadings, this was found to be a more durable protection than paint coatings.

6 Fatigue Crack Propagation Testing

The fatigue crack propagation testing was conducted using the 5754 aluminum alloy furnished in the H22 temper. In order to achieve this temper, the aluminum is work hardened by rolling and then annealed to quarter hard. The mechanical properties and chemical composition of the aluminum alloy are shown in Table 6-1 and Table 6-2. The certification of the material is found in Appendix-D.

Both Mode I and Mixed-Mode I+II fatigue crack growth tests were conducted on CTS specimens with a thickness of 4 mm. All dimensions of the CTS specimen are shown in Figure 4-1. Three CTS specimens were made using water jet cutting by Smed T. Kristiansen AS. The initial notch length, a , after water cutting was 41 mm. Then a jeweler saw was used in order to get a total initial notch length of 42.5 mm. The saw used in this project was obtained from a jeweler and had a saw blade thickness of 0.48 mm. However, a suitable saw can be purchased online from K.A. Rasumssen Norway.

Table 6-1 Chemical composition of 5754-H22 aluminum alloy [% weight].

| <i>Si</i> | <i>Fe</i> | <i>Cu</i> | <i>Mn</i> | <i>Mg</i> | <i>Cr</i> | <i>Zn</i> | <i>Ti</i> | <i>Al</i> |
|-----------|-----------|-----------|-----------|-----------|-----------|-----------|-----------|-----------|
| 0.4 | 0.4 | 0.1 | 0.5 | 2.6-3.6 | 0.3 | 0.2 | 0.15 | Rem. |

Table 6-2 Mechanical Properties of 5754 – H22 aluminum alloy.

| | |
|-------------------------|-----------|
| Tensile Strength, [MPa] | 220 - 270 |
| Yield Strength, [MPa] | 130 Min |

The tests were conducted using the loading device created in this thesis, see Figure 6-1. This device allows applying mixed-mode loading to the CTS specimen as well as pure Mode I and pure Mode II loading by changing the loading angle, α .

The crack propagation tests were performed using a fatigue testing machine from MTS installed in the workshop at the University of Stavanger. The fatigue testing machine was connected to a computer for machine control. Every test was performed in air at room temperature. The loads were applied with a sinusoidal waveform at a frequency of 8 Hz. A loading ratio of 0.1 was kept constant for all the fatigue tests. Applied mean and amplitude loadings used for the pre-cracking and crack propagation testing are shown in Table 6-3. The procedure for the crack propagation testing is shown in Appendix-A.

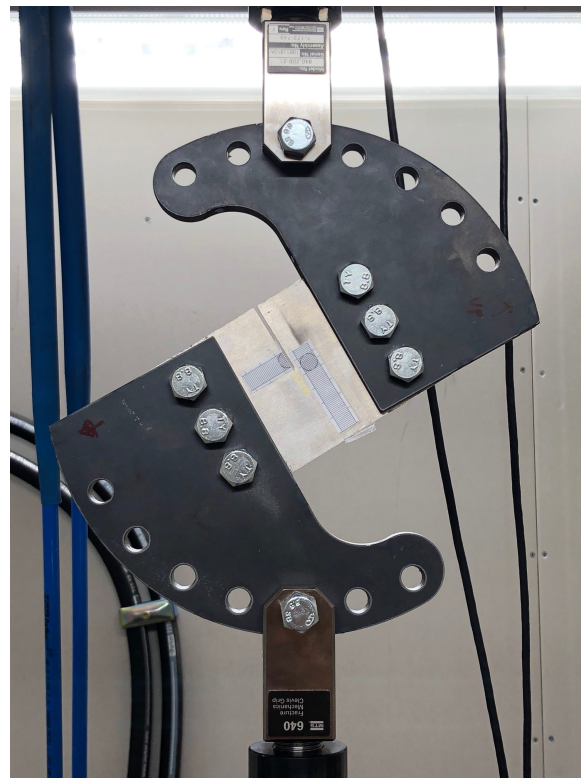


Figure 6-1 Setup for mixed-mode loading ($\alpha = 60^\circ$).

For mode I loading, it was found that the fatigue testing machine did not manage to deliver the targeted loads for such low loadings. Thus, the actually applied load and stress ratio was slightly higher than those inserted in the machine control. However, for mixed-mode testing under a loading angle of 60 degrees, the actual values delivered by the machine were almost identical to the input values. One possible reason for this is that the assembly of the loading device and specimen is stiffer when rotated. For mode I loading a slight vibration of the specimen was observed, which may be caused due to the low thickness of the specimen. This vibration was not present during mixed-mode loading.

Table 6-3 Values for calculated and actual obtained loadings.

| | Loading Mode | R | F_m [N] | F_a [N] |
|----------------------|-------------------|------|-----------|-----------|
| Input values | Pre-cracking | 0.1 | 1265 | 1035 |
| | Crack Propagation | 0.1 | 1353 | 1107 |
| Actual values | Pre-cracking | 0.15 | 1460 | 1080 |
| | Crack Propagation | 0.14 | 1560 | 1170 |

Fatigue pre-cracking was performed under mode I loading ($\alpha = 0$) to a total crack length of 45 mm was achieved. This crack length gives an a/W ratio of 0.5, which is within the region where the stress intensity factor expressions given in Eq.(2.6.1 – 2.6.2) are valid. For mixed-mode testing, the loading device was adjusted after pre-cracking such that a loading direction of $\alpha=60^\circ$ was obtained.

The crack growth was measured using a Canon photo camera connected to a computer allowing to take photos at preset intervals. A tripod with an adjustable height was used to install the camera in front of the specimen. Based on experience from participation in fatigue testing of pipe specimens, it was found that the best camera position relative to the test specimen vary from test to test. Therefore, the best-suited camera angle has to be found for each test after pre-cracking. In order to make it easier to measure the crack length in the photos, length scales were attached to the specimen.

Knowledge gained during participation in fatigue testing of pipe specimens showed that using a yellow marker pen was the best available method to achieve enhanced visibility of the crack in the photos. No place that sold the coating introduced by *ThreeBond Co.* were found. It was therefore not possible to acquire such a coating for use in this project. As mentioned in Ch.3.3, a green paint was tried during participation in fatigue testing in order to achieve a similar effect. However, this coating turned out to give a poor result. Figure 6-2 shows photos of the cracked surface without any coating, with a red marker pen and with a yellow marker pen. The pictures were taken at almost the same time, clearly showing that using a marker pen increases the visibility of the crack in the photos. In this example, both the red and the yellow marker pen gave a good result, however, the red marker pen was found to be more sensitive to the light condition in the room.

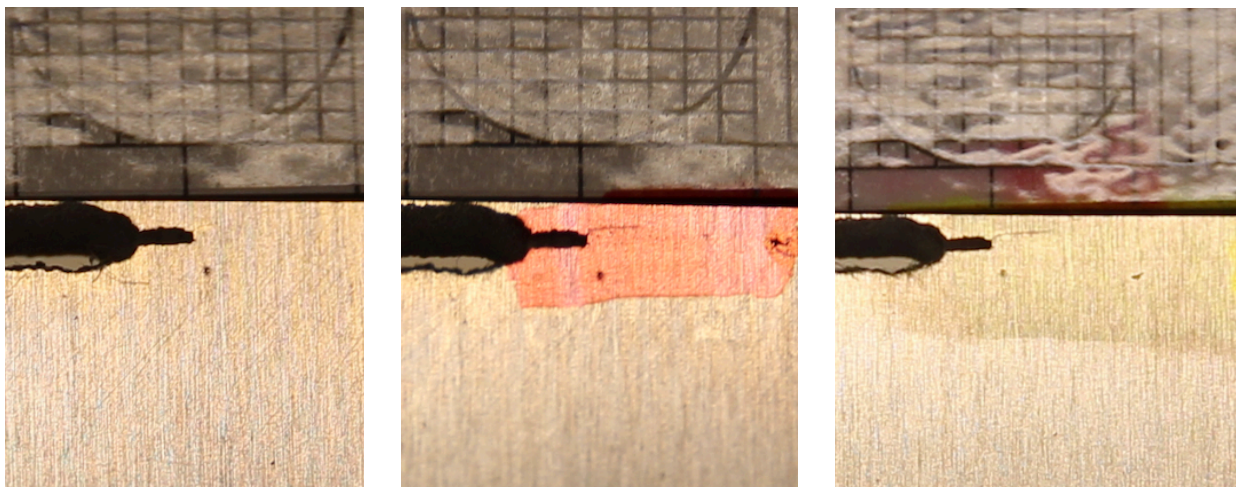


Figure 6-2 Crack visibility using two different marker pens compared to a clean surface.

Two specimens were tested under mode I loading in order to test the loading device and to determine suitable Paris law constants for the 5754 aluminum alloy. The last specimen was tested for mixed-mode loading for a loading direction of $\alpha = 60^\circ$. The influence of the different loadings was then investigated in the Paris regime and the crack growth rates were determined using the incremental polynomial method.

7 Results

Three CTS specimen were tested during this master thesis, two specimens under mode I loading and one specimen for mixed-mode loading for a loading direction of $\alpha = 60^\circ$. The first specimen was tested to failure in order to verify that the loading device was functional and that found Paris law constants was somewhat correct. The obtained results showed a big deviation between the calculated number of cycles and the actually used number of cycles. Thus, new Paris law constants that fitted better with the achieved results were derived.

7.1 Fatigue Crack Propagation Testing of CTS Specimens

The result from the test of the second specimen showed a deviation in crack length of the front and the back side after pre-cracking of approximately 2 mm, which is a bigger deviation than allowable according to ASTM. This difference of the crack length continued for the crack propagation testing, meaning that obtained results are not valid according to restrictions given by ASTM. It was also observed that the crack on the back side stopped growing when a crack length of 15 mm was obtained, while the crack on the front side continued to grow. In addition, a slight deviation in the direction of the crack was observed for both sides of the specimen. Over a distance of 9 mm, this angle was calculated to be 6.7° for the front side and 6° for the back side. Meaning that deviation with regard to crack direction was well within the limits according to ASTM.

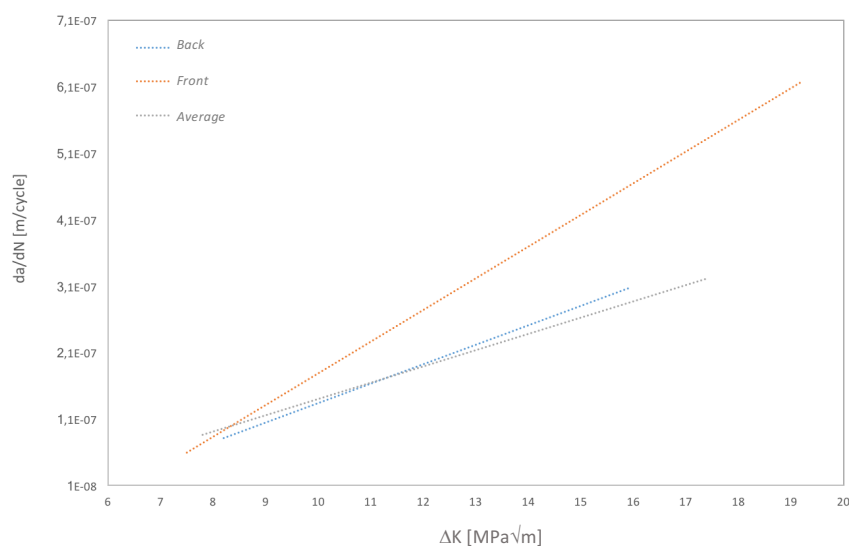


Figure 7-1 Crack growth rate versus stress intensity factor range, ΔK , based on average crack growth, crack growth of front side and crack growth of back side of CTS specimen.

The photos taken from both the back and front side of the second specimen were investigated and crack length at various number of cycles was noted. This was then used to determine the crack growth rate, da/dN . Further, the incremental polynomial method was used to determine the crack growth behavior, as illustrated in Figure 7-2. MATLAB was used in to calculate the

stress intensity factor range and a plot of crack growth rate versus the stress intensity factor range were made. The obtained Paris law constants, C and m , for mode I loading were obtained by fitting the results using a power law function. Due to the big deviation in crack length of the front and the back side of the specimen, the crack growth rate versus stress intensity factor range was plotted for both the front and the back. In addition, an average crack growth length of the front and the back were calculated and used to plot the crack growth behavior, see Figure 7-1. Table 7-1 shows the obtained Paris law constants for the front, the back and an average value. Possible reasons for deviation of crack lengths for the front and the back side will be discussed later on.

Table 7-1 Obtained Paris law parameters and R^2 correlation coefficients (ΔK in $\text{MPa}\sqrt{\text{m}}$ and da/dN in m/cycle).

| | C | m | R² |
|----------------|-------------------------|----------|----------------------|
| Front | 1.0994×10^{-9} | 2.1705 | 0.9169 |
| Back | 3.7075×10^{-9} | 1.5411 | 0.3819 |
| Average | $3,3392 \times 10^{-9}$ | 1.6071 | 0.8489 |

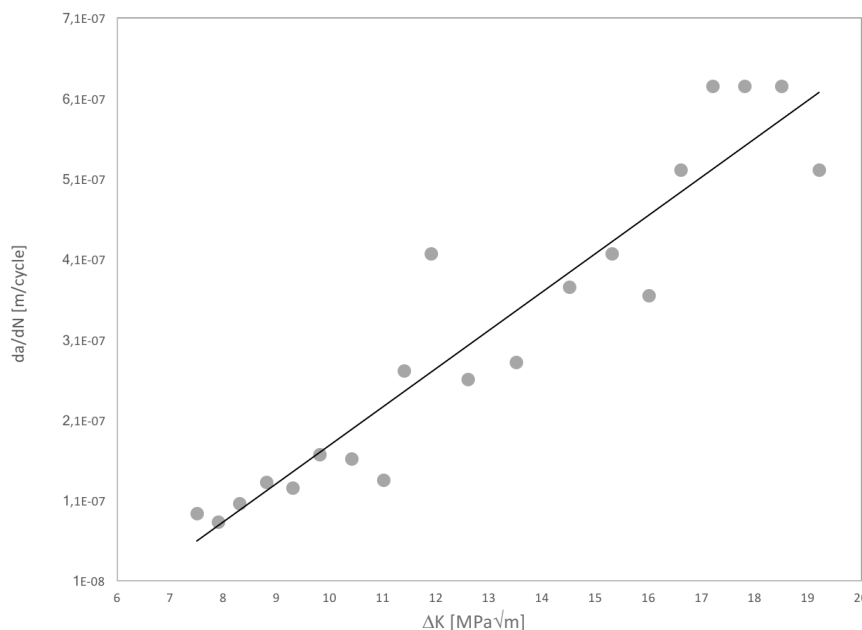


Figure 7-2 Crack growth rate versus stress intensity factor range, ΔK , based on crack growth of the front side of the CTS specimen.

For the third specimen pre-cracking were introduced under mode I loading with loads as given in Table 6-3. It was observed that the crack in the front grew straight, while the crack on the back side grew downwards at an angle of approximately 14.5 degrees. When the first planned pre-crack length of 45 mm was obtained, there was a length difference of 2.6 mm, combined with the difference of the crack direction, as shown in Figure 7-3. Due to the big difference in crack length and crack direction of the front and back side during pre-cracking, it was decided to extend the length of the pre-crack to a total of 50 mm in order to see if the crack would

stabilize. Further, it was observed that the crack on the back side started to grow upwards again, as can be seen from Figure 7-3. When a final pre-crack length of 50 mm was obtained, the differences between the front and back side had improved, but there was still a difference in length of 1.7 mm.



Figure 7-3 Difference in crack growth of the front and the back side during pre-cracking of the third specimen.

After pre-cracking, the loading direction was changed to an angle of 60 degrees, but due to the clearance between the bolts and elongated holes, the actual loading angle was slightly lower than this, see Figure 7-4. A loading similar to the one used during pre-cracking were applied for the crack propagation testing. After approximately 30 000 cycles, no crack growth had been observed, thus, the loading was increased to the same value as used for the second specimen. When the applied load was increased, the crack almost immediately started to grow on the front side. However, as can be seen from Figure 7-5, the crack on the back side of the specimen started to grow later than for the front side. In fact, the crack on the front had grown approximately 4 mm before the crack on the back side started to grow. A possible reason being the difference in crack length that occurred during pre-cracking. When the crack started to grow, it was observed that the fatigue crack growth direction changed immediately from the fatigue pre-crack orientation.

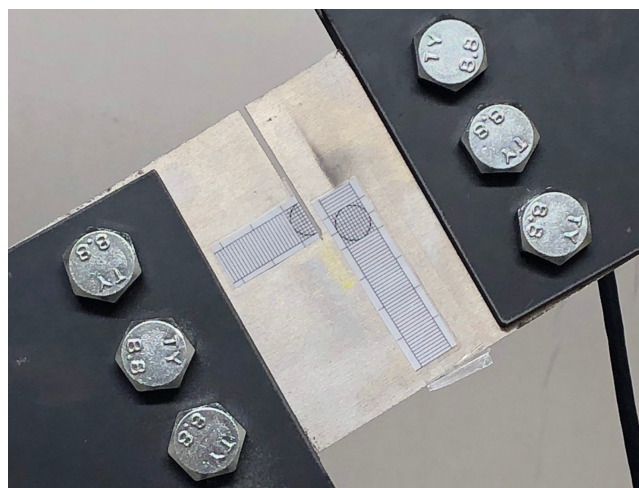


Figure 7-4 Offset of CTS specimen for mixed-mode loading due to bolt hole clearance.

Due to the time limitations of the project, there was no time for calculation of the comparative stress intensity factor range for the third specimen, meaning that a plot of crack growth rate versus the comparative stress intensity factor range was not obtained for the mixed-mode fatigue test. However, for testing of mixed-mode loading, the crack growth path was plotted as shown in Figure 7-5. Here a_x is the horizontal crack length and a_y the vertical crack length. Both values for the front and the back side are shown, and the corresponding number of cycles are noted. In addition, a straight line along the predicted crack growth angle of 48.6° is plotted for comparison.

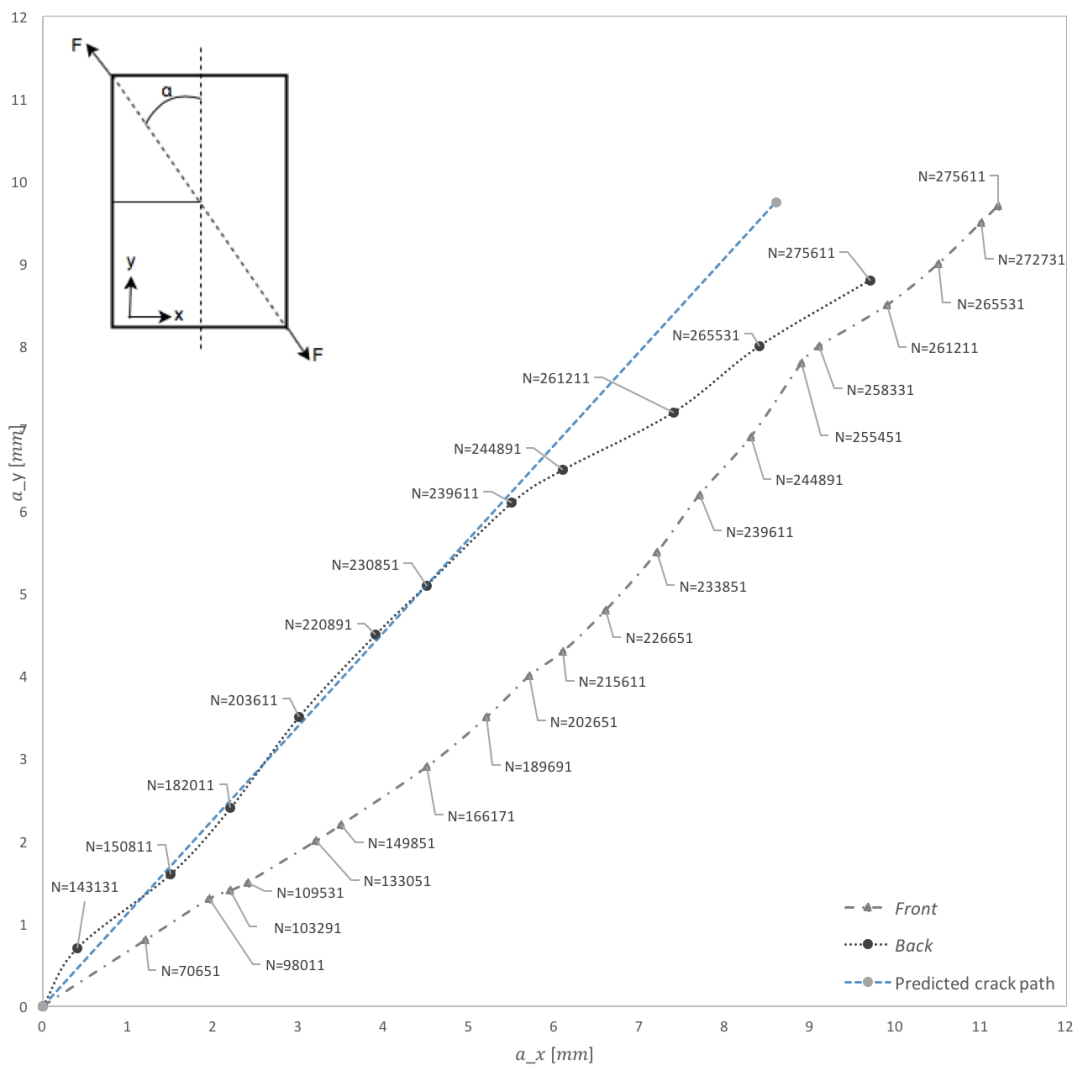


Figure 7-5 Crack growth paths for the front and the back side of the third specimen.

The measured values of the crack length were then used to calculate the crack propagation angle. The initial slope at the crack tip for a loading angle of 60 degrees was found for both the front and the back side of the specimen. In addition, an average value was calculated due to the big difference between the two sides of the specimen, as shown in Table 7-2.

Table 7-2 Comparison of calculated and experimentally obtained crack angle.

| Front | Back | Average | Theoretically calculated |
|-------|-------|---------|--------------------------|
| 33.7° | 46.6° | 37.5° | 48.6° |

Figure 7-6 shows crack length versus the number of cycles recorded for both mode I and mixed-mode I and II loading for $\alpha = 60^\circ$. As can be seen from this figure, for the mixed-mode test the crack did not start to grow before approximately 30,000 cycles. One possible reason for this is that a lower loading than for the mode I test was used. As soon as the loading was increased, the crack started to grow. The mode I fatigue crack propagation test needed 102,848 to reach a total crack length of 63 mm, while the mixed-mode fatigue test needed 261,211 cycles in order to reach the same length. Since the specimen for mixed-mode testing were pre-cracked to a total crack length of 50 mm, the length of crack growth during fatigue testing was shorter for the third specimen. Further, pictures of the final cracked specimens are shown in Figure 7-7 to 7-9.

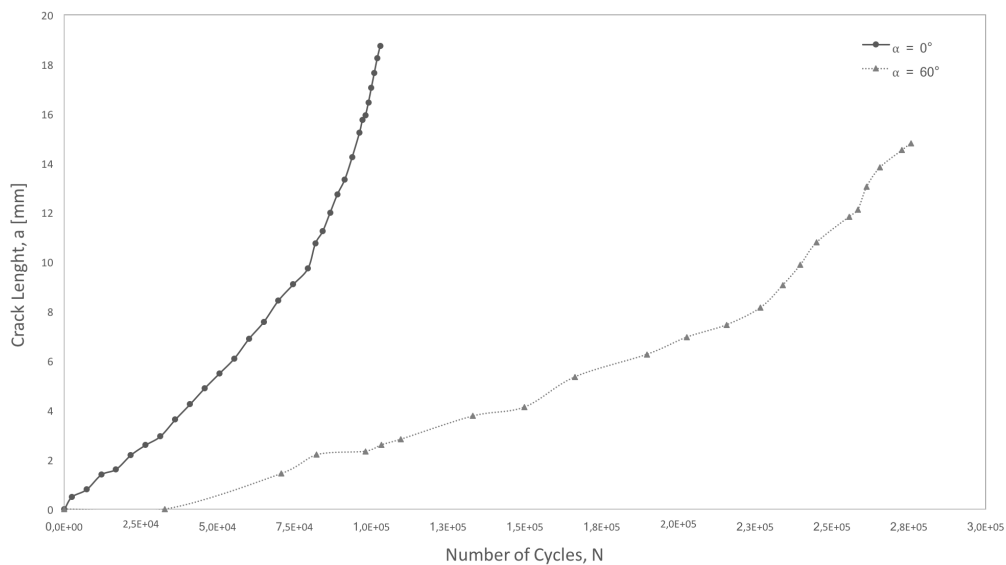


Figure 7-6 Crack length versus number of cycles for mode I and mixed-mode I+II loading.

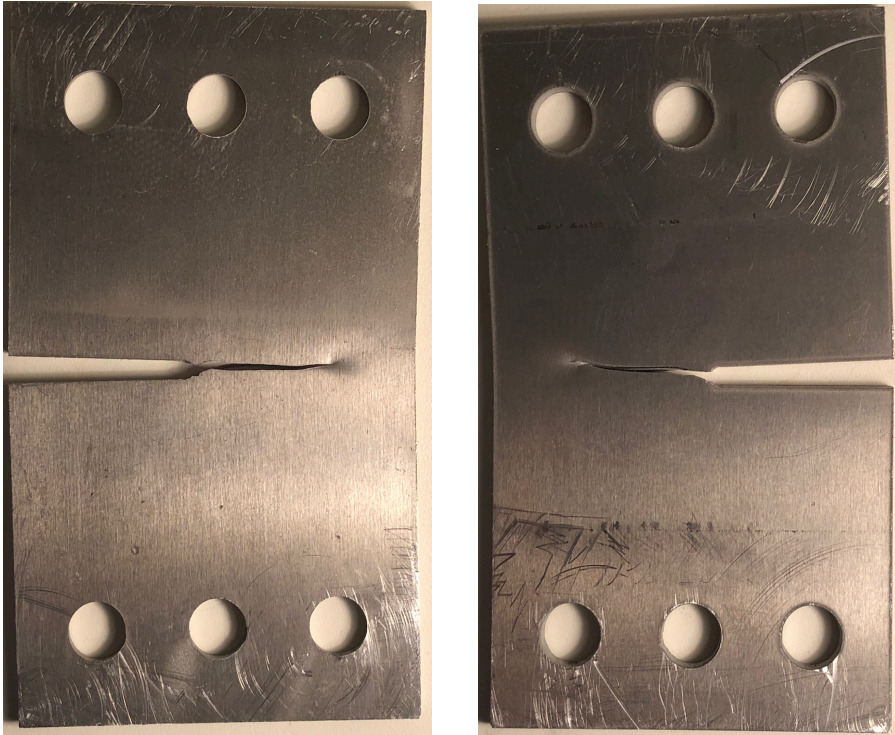


Figure 7-7 Pictures of specimen number 1 after testing. The front side of the specimen is shown to the left.

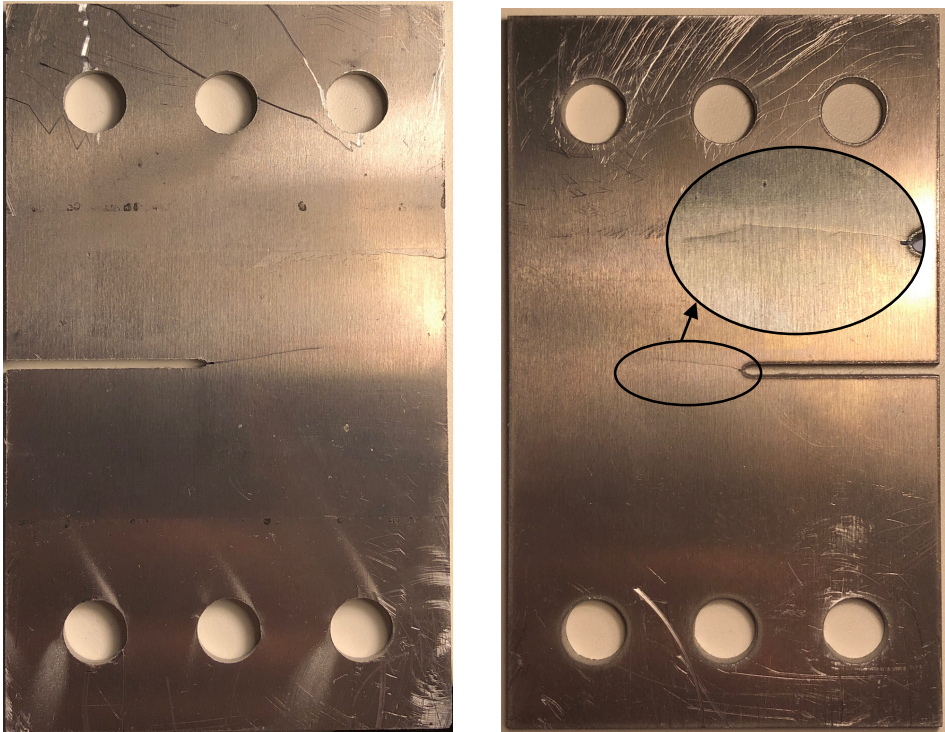


Figure 7-8 Pictures of specimen number 2 after testing. The front side of the specimen is shown to the left.

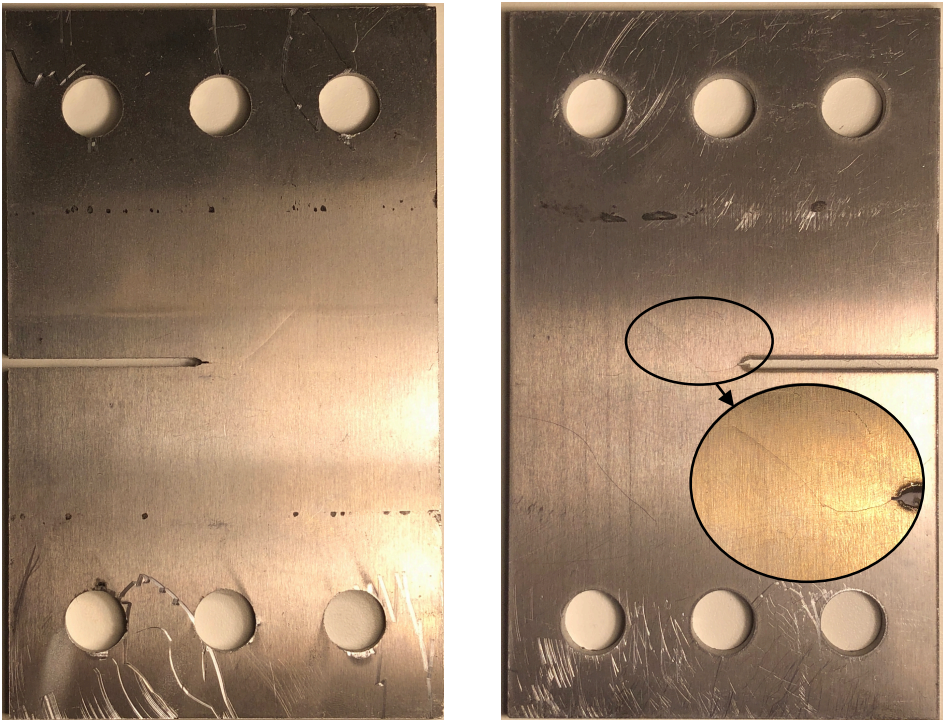


Figure 7-9 Pictures of specimen number 3 after testing. The front side of the specimen is shown to the left.

8 Discussion

The objective of this thesis was to make preparations for mixed-mode fatigue crack propagation testing. Hence, a suitable loading device for testing of CTS specimens was constructed and used for testing of three specimens. Both fatigue tests for mode I and mixed-mode loading was performed. In addition, a suitable method for crack growth measurements was prepared. Functionalities and possible improvements with regards to both the loading device and the prepared measurement method is discussed in the following subsections.

8.1 Functionality of Loading Device

Despite the fact that obtained results for the fatigue tests gave invalid results according to restrictions given by ASTM, some of the results from fatigue testing were found to yield agreement with other experimental results [18], [30]. In Figure 4-2, estimated crack length at various number of cycles is plotted for the 5754-H22 aluminum alloy. The figure has been generated in MATLAB by integrating the Paris law expression Eq.(2.2.3) and then crack length versus the number of cycles is plotted. Used values for the Paris law constants, $C = 1.759 \times 10^{-10}$ and $m = 3.040$, was found from an experiment by Meilinger et al. [30]. Comparing this result to the actual number of cycles used for fatigue testing in this thesis, Figure 7-6, shows relatively good agreement. This estimate shows only a difference of approximately 8.000 cycles between estimated and experimentally achieved results. With regard to the mixed-mode fatigue crack propagation test, some typically crack growth behaviors were found to be corresponding to other observations [18]. When the loading direction was changed after pre-cracking, the crack growth direction immediately changed from the orientation of the initial notch. Another observation that matched with previous results was that the crack tip angle decreased with increasing crack length, see Figure 7-5. This also agrees with the crack path prediction given by the criteria of maximum tangential stress stated in Eq.(2.3.4). However, a direct comparison of the actually obtained crack path direction against those calculated was difficult due to the high deviation of the result. From Figure 7-5, it can be seen that the crack path of the back side of the specimen fits well with the predicted path given by the criteria of maximum tangential stress, whereas the crack path on the front side deviates considerably.

Further, several desired features with the use of this loading device were found to be fulfilled. Firstly, the loading device was found well suited to use in a standard uniaxial MTS fatigue testing machine. Easy off and on clamping of both the CTS specimen and installation of the loading device in the fatigue testing machine was achieved. However, it should be mentioned that some vibrations were detected for testing using high frequency's. In order to reduce this vibration, a frequency of 8 Hz was used. One possible reason for vibrations at high frequency's is the low thickness of the CTS specimen. In addition, it was experienced that for loadings as low as used in this thesis, the machine did not manage to deliver the desired values. Actual

values applied during testing were therefore slightly higher than desired. However, for higher loads, this problem was not present. Further, from the performed fatigue tests it was found successful to introduce fatigue pre-cracking under mode I loading. Due to the importance of fatigue pre-cracking in order to obtain good results for fatigue testing, this was one of the most important criteria to fulfill. It was also experienced that a transition from pure mode I loading to mixed-mode loading was uncomplicated due to the design of the loading device and the easy off and on clamping. Thus, the loading device can be used for testing of a variety of K_{II}/K_I ratios.

Since only three CTS specimens of the 5754-H22 aluminum alloy were tested during this thesis, there was not possible to verify if the actual strength and endurance of the loading device were as estimated. However, after the conducted tests no wear and tear or defects could be observed in the holes of the loading device.

Based on the observations discussed above, the loading device was found well suited for mixed-mode fatigue crack propagation testing. It fulfills the desired criteria's and provides a simple test procedure. From tests performed in this thesis, both the design and material quality used for the loading device was found successful. However, in order to reduce deviation in the results, some adjustments and modifications has to be done to the loading device.

8.1.1 Possible Reasons for Deviations in Results

Based on the gained results from conducted fatigue tests, deviations in crack growth length of the back and the front side of the specimens were observed. According to restrictions given by ASTM, these deviations were too high for the results to be valid. In addition, both for pre-cracking and for mode I loading of the CTS specimen, it was observed that the crack propagated with a small angle. Even if the obtained angle was within the claim of ASTM, this could influence the direction of the crack path under mixed-mode loading. There may be several possible reasons for the deviations experienced.

The first factor is the accuracy of the water jet cutting. A slight inclination of the surfaces inside the holes could be spotted, meaning that the load distribution of the CTS specimen could be unevenly partitioned. Thus, a difference in the crack path and crack length of the front and the back side could arise. In addition, a deviation in the distance from the external elongated holes to the lower edge of the loading device was measured to have a slight deviation. Thus, the CTS specimen will be loaded under a small angle, which can explain the angled direction of crack growth during mode I loading. In addition, the welding gave a slight offset between the three plates, reinforcing the already existing inclination and inaccuracy of the holes.

Another factor that can affect the results of the fatigue testing is the big bolt hole clearance of the elongated holes. They were designed using recommended values for a tight fit with regards to bolted structures, meaning, that a clearance between the holes and the bolts were approximately 1 mm. Based on the experience gained through the performed fatigue tests, this clearance is desirable to be as small as possible. For mode I loading using a stress ratio of $R = 0.1$, this will not necessarily have a great significance, since a load always will be applied, and thus no movement of the bolts. However, for mixed-mode testing, this clearance will cause the obtained loading angle to be slightly different than estimated, as can be seen from Figure 7-4. For testing using a stress ratio equal to 0.1, no movement of the bolts inside the elongated holes was observed. However, if testing is to be performed using a stress ratio equal to or lower than zero, this clearance will most likely have an influence on the result.

Natural defects in the tested aluminum alloy may also cause some deviation in the results. As mentioned in Ch.2.3.2, a growing crack tends to seek the path of least resistance. Since the crack growth during pre-cracking for the first two specimens were straight, local defects in the microstructure may therefore be a possible reason for the unexpected crack growth during pre-cracking of the third specimen. Local defects in the microstructure can also be the reason that caused the crack growth on the back side of the second specimen to stop, followed by a sudden change of crack growth path, see Figure 7-8.

8.1.2 Solutions to Improve the Loading Device

In order to obtain better results for both crack growth rates and crack propagation direction, some modifications of the loading device were necessary. Possible solutions for fixing the loading device and necessary changes for future production of the loading device is given in this subchapter. The following suggestions are based on assumptions and observations made in the previous chapters.

To improve the already produced loading devices, both the elongated holes and the circular holes are recommended to be machined in order to achieve a better accuracy and finish. The elongated holes are recommended to be machined to a radius of 7.05 mm. M14 bolts can then be used instead of M12 bolts. In addition, the circular holes were found to have a diameter smaller than supposed. They were measured to have a diameter of 12.5 mm. It is therefore recommended to machine these to the supposed diameter of 12.7 mm. These modifications will both reduce the bolt hole clearance of the elongated holes and improve the accuracy and finish of all the holes in the loading device, correcting the inclination inside the holes. A new analysis was performed in order to check that increasing the size of the elongated holes would not influence the strength and durability of the loading device. The results are given in Figure 8-1, showing that increasing the radius of the elongated holes does not significantly weaken the loading device.

No CNC-operator was available at the workshop of the University of Stavanger during this thesis, thus, the modifications mentioned above were not completed. It is therefore recommended before further use of the produced loading device that the holes are CNC-milled according to suggested values, see Appendix-C.

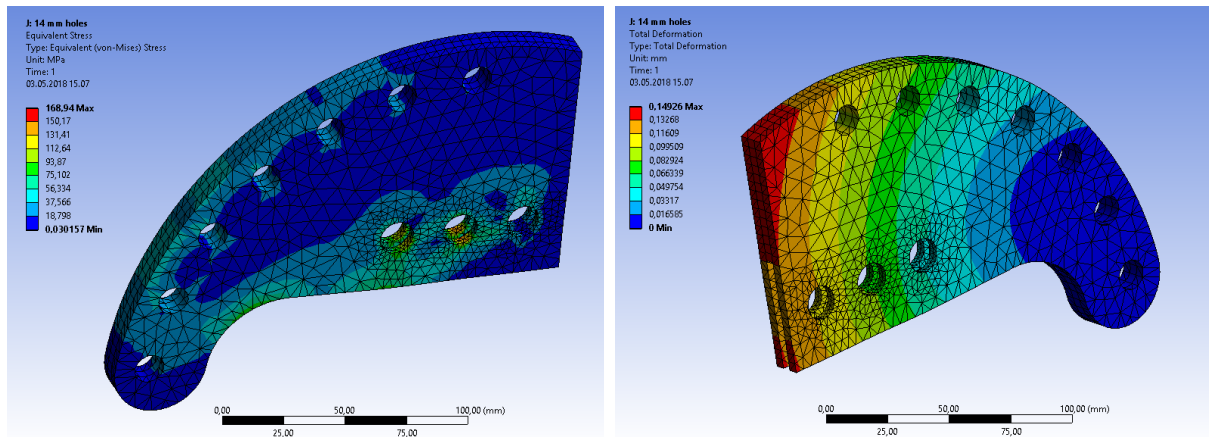


Figure 8-1 The von Mises stress and total deformation from ANSYS analysis for elongated holes with radius of 7.05 mm. Source: ANSYS® Workbench, R17.0, Academic.

Since the used manufacturing method of the loading device did not give the wanted accuracy, the achieved result was not satisfactory. It is therefore recommended for future production to machine the holes to desired dimensions after welding the plates together. This will improve the accuracy and finish of the edges of the holes. A second revision was made of the drawings, where the circular holes of the side and middle plates were reduced to 12 mm prior to water jet cutting. The loading device can then after water jet cutting and welding be machined to the desired dimensions of 12.7 mm for the circular holes and a radius of 7.05 mm for the elongated holes. Since the new design proposition requires to use M14 bolts, the holes in the CTS specimen was changed to a diameter of 14.1 mm. The modified drawings are found in Appendix-C.

For further use of this loading device, fabrication of the loading device using a CNC-machine can also be considered. If materials with higher yield strength than what was accounted for in this thesis is to be tested, the loading device is recommended to be fabricated using a material with higher strength than the steel alloy EN S355. As mentioned earlier, high strength materials such as the steel alloy S165 were only delivered in round bars. Thus, the use of a CNC-machine for manufacturing may be a good solution. Due to the extra work with regard to material preparation prior to water jet cutting for the round bars, the cost savings of water jet cutting compared to machining decreases.

8.2 Crack Monitoring Using a Camera

For monitoring of crack growth under mode I loading, the camera worked well, considering the visibility of the crack if a colored surface were used. In addition, it allowed for automatic shooting, meaning that presence during the test was not necessary. However, the work analyzing the photos afterward was very time consuming. The hoped advantage with regard to saving time compared to the use of a traveling microscope therefore disappeared.

When it came to monitoring of crack growth during mixed-mode fatigue testing, a good quality photo was about impossible to obtain when the camera was attached to the tripod. However, if the camera were handheld, photos of the same quality as for mode I loading were possible to obtain. In order to get this quality, the camera had to be tilted in the same direction as the angled crack. Different attempts showed that in order to achieve a good photo of the crack, the camera had to be located below the crack shooting upwards, making the light reflect in such a way that the crack became visible. One possible solution to this problem is to design a wall mounted stand for the camera, with the possibility of rotating and tilting the camera in different directions. Using a tripod gave a very reduced opportunity for camera positioning.

Based on testing done in this thesis, the use of a photo camera for crack monitoring was found to be a sufficient method. However, this method was both more time consuming and challenging than first assumed. One possible solution that simplifies this method is to use a better coating technique for increased crack visibility, as the one introduced by *Three Bond Co.* This will most likely improve the accuracy of the measured crack lengths and simplify the work analyzing the photos. In addition, an improved coating will possibly give better results when the camera is attached to the tripod. Unfortunately, such a coating technique was not available for use in this thesis.

It is also possible to use a traveling microscope for monitoring of crack growth, which was done by Peixoto and de Castro [17]. Since the microscope only measured the crack length precisely in the horizontal direction, they used a microscope equipped with two digital micrometers to draw the crack profile. However, this is a much more expensive and complicated method than using a camera. Due to the extensive preparations needed in order to use this method, it was not possible to use in this thesis.

9 Conclusion

The goal of this project was to design a loading device for mixed-mode fatigue crack propagation testing. Based on results gained from fatigue tests conducted in this thesis combined with knowledge gained from research of previous work done using a similar loading device, it was found well suited for mixed-mode fatigue crack propagation testing. However, it was also found that in order to achieve better results, a high accuracy regarding fabrication of the loading device is necessary. To improve the produced loading device, several suggestions have been proposed, mainly reduction of bolt hole clearance and measures to improve the accuracy with regard to manufacturing of the loading device.

Based on knowledge gained through this thesis, the use of a photo camera for monitoring of crack growth was found to give sufficient results. However, the desired benefit in terms of saving time making the crack monitoring more automatic was not achieved. For monitoring of mixed mode fatigue crack propagation testing, the camera had to be handheld in order to achieve usable photos.

9.1 Future use of the Loading Device

For further use of this loading device, suggested changes would be recommended. In addition, if mainly materials with high yield strength are to be tested, the use of a material with higher strength than used in this thesis would be recommended for fabrication of the loading device, such as the S165 steel alloy discussed.

With regard to crack monitoring, designing a new mounting device or trying better surface coatings would be recommended for further use of a photo camera. Another possibility is to use a traveling microscope in combination with a specially designed device for monitoring of crack length in both vertical and horizontal direction.

10 References

- [1] K. Rege and H. G. Lemu, "A review of fatigue crack propagation modelling techniques using FEM and XFEM," *IOP Conf. Ser. Mater. Sci. Eng.*, vol. 276, no.1, pp. 12–27, 2017.
- [2] H. E. Boyer, *Atlas of Fatigue Curves*. Materials Park, Ohio: ASM International, 1986.
- [3] H. A. Richard, "Specimens for Investigating Biaxial fracture and fatigue processes," *Biaxial Multiaxial Fatigue*, ed. M. W. Brown K. J. Miller. Mech. Eng. Publ. London, 1989, pp. 217–229.
- [4] H. A. Richard, "Some theoretical and experimental aspects of mixed mode fracture," in *6th International Conference on Fracture*, 1984, vol. 5, pp. 3337–3344.
- [5] H. A. Richard, M. Fulland, and M. Sander, "Theoretical crack path prediction," *Fatigue Fract. Eng. Mater. Struct.*, vol. 28, no. 1–2, pp. 3–12, 2005.
- [6] A. C. O. Miranda, M. A. Meggiolaro, J. T. P. Castro, L. F. Martha, and T. N. Bittencourt, "Fatigue life and crack path predictions in generic 2D structural components," *Eng. Fract. Mech.*, vol. 70, no. 10, pp. 1259–1279, 2003.
- [7] J. Qian and A. Fatemi, "Mixed mode fatigue crack growth: A literature survey," *Eng. Fract. Mech.*, vol. 55, no. 6, pp. 969–990, 1996.
- [8] H. A. Ricard and K. Benitz, "A loading device for the creation of mixed mode in fracture mechanics," *Int. J. Fatigue*, vol. 22, no. 2, pp. R55–R58, 1983.
- [9] R. G. Budynas and J. K. Nisbett, *Shigley's Mechanical Engineering Design*, 8th ed. New York: McGraw-Hill, 2005.
- [10] F. C. Campbell, *Elements of Metallurgy and Engineering Alloys*. Materials Park, Ohio: ASM International, 2008.
- [11] S. Suresh, *Fatigue of Materials*, 2nd ed. Cambridge: Cambridge University Press, 1998.
- [12] *Eurocode 3: Design of steel structures - Part 1-9: Fatigue, NS-EN 1993-1-9:2005+NA:2010*. 2010.
- [13] A. Ghahreman and J. A. Kakavand, "Evaluation of experimental test results of High Frequency Mechanical Impact improved welded details," M.S. thesis, Dept. of Civil and Environmental Eng., Chalmers Univ., Gothenburg, 2016.
- [14] N. E. Dowling, *Mechanical Behavior of Materials*, 4th ed. Boston: Pearson, 2012.
- [15] A. Seshadri, "Statical variation of weld profiles and their expected influence on fatigue strength," M.S. thesis, Dept. of Mech. Eng., Lappeenranta Univ., Lappeenranta, Finland, 2006.

- [16] T. L. Anderson, *Fracture Mechanics Fundamentals and Applications*, 3rd ed. Boca Raton: CRC Press/Taylor & Francis Group, 2005.
- [17] D. F. C. Peixoto and P. M. S. T. de Castro, "Fatigue crack growth of a railway wheel," *Eng. Fail. Anal.*, vol. 82, pp. 420–434, 2017.
- [18] L. P. Borrego, F. V. Antunes, J. M. Costa, and J. M. Ferreira, "Mixed-mode fatigue crack growth behaviour in aluminium alloy," *Int. J. Fatigue*, vol. 28, no. 5–6, pp. 618–626, 2006.
- [19] K. Golos and B. Wasiluk, "Role of plastic zone in crack growth direction criterion under mixed mode loading," *Int. J. Fract.*, vol. 102, pp. 341–353, 2000.
- [20] T. N. Bittencourt, P. A. Wawrzynek, A. R. Ingraffeat, and J. L. Sousa, "Quasi-automatic simulation of crack propagation for 2D LEFM problems," *Eng. Fract. Mech.*, vol. 55, no. 2, pp. 321–334, 1996.
- [21] D. G. Pavlou, G. N. Labeas, N. V Vlachakis, and F. G. Pavlou, "Fatigue crack propagation trajectories under mixed-mode cyclic loading," *Eng. Struct.*, vol. 25, no. 7, pp. 869–875, 2003.
- [22] *Standard Test Method for Measurement of Fatigue Crack Growth Rates, ASTM Standard E647-15e1*. 2015.
- [23] D. F. C. Peixoto and P. M. S. T. de Castro, "Mixed mode fatigue crack propagation in a railway wheel steel," *Procedia Struct. Integr.*, vol. 1, pp. 150–157, 2016.
- [24] Three Bond CO., "Surface Crack Detection Coating Argent," *ThreeBond Technical News*, no. 67, Tokyo, 2006.
- [25] Y. Huang, L. Huan, and L. Xiao, "Prediction of Low Cycle Fatigue Crack Growth under Mixed-mode Loading Conditions Using Cohesive Zone Models," *Procedia Eng.*, vol. 99, pp. 1317–1322, 2015.
- [26] *Clearance Holes for Bolts, Screws, and Studs, ASME Standard B18.2.8-1999 (R2017)*. 1999.
- [27] M. Stašević, "Fatigue Crack Growth Prediction from Low Cycle Fatigue Properties," *Strojarstvo*, vol. 53, pp. 171–178, 2011.
- [28] Ø. Å. Waløen, *Maskindeler. 1*. Trondheim: Tapir Forlag, 1989.
- [29] A. J. Slifka *et al.*, "Fatigue crack growth of two pipeline steels in a pressurized hydrogen environment," *Corros. Sci.*, vol. 78, pp. 313–321, 2014.

- [30] J. Lukács, Á. Meilinger, and D. Pósalaky, "High cycle fatigue and fatigue crack propagation design curves for 5754-H22 and 6082-T6 aluminium alloys and their friction stir welded joints," *Weld. World*, vol. 62, no. 4, pp. 737–749, 2018.
- [31] H.-H. Lee, *Finite Element Simulations with ANSYS Workbench 17*. Mission, Kansas: SDC Publications, 2017.
- [32] Sverdrup Steel., "ALLOY 1.4418 / S165M / 2387," 2018. [Online]. Available: <http://www.sverdrupsteel.com/products/alloy-1-4418-s165m>. [Accessed: 20-Feb-2018].
- [33] T. Lassen and Z. Mikulski, "Fatigue methodology for life predictions for the wheel-rail contact area in large offshore turret bearings," *Frat. ed Integria Strutt.*, vol. 10, no. 38, pp. 54–60, 2016.
- [34] D. Ungermann *et al.*, "Sustained Use of Hot-Dip Galvanizing in Steel and Composite Bridge Construction," presented at the 23rd Int. Galvanizing Conf. and Exhibition, Paris, 2012. [Online]. Available: https://www.researchgate.net/publication/283087542_Sustained_Use_of_Hot-Dip_Galvanizing_in_Steel_and_Composite_Bridge_Construction.
- [35] R. Ulewicz, P. Szataniak, and F. Novy, "Fatigue properties of wear resistant martensitic steel," presented at the 23rd Int. Conf. on Metallurgy and Materials, Brno, Czech Republic, May. 21-23, 2014. [Online]. Available: <http://konsyst.tanger.cz/files/proceedings/17/reports/2599.pdf>.
- [36] L. Stott Industrial Pty., "Fluid Film - Powerful protection to stop rust," 2018. [Online]. Available: <http://www.fluidfilm.com.au>. [Accessed: 28-Apr-2018].

Appendixes

Appendix-A Procedure for performing mixed mode I and II
fatigue crack propagation tests

Procedure for Performing Mixed-Mode I+II Fatigue Crack Propagation Tests

Using:

MTS 809 Axial/Torsional Test System

Model 319.25 Axial-Torsional Load Frame

Including:

Special Designed Loading Device for
Mixed-Mode I+II Fatigue Crack Propagation Tests of
CTS Specimens

Prepared by Jonas Olsvik Rydland

Rev. 01, 16.05.18

Department of Mechanical and Structural
Engineering and Materials Science
University of Stavanger

Necessary Manuals

The following is a list of necessary manuals for operating the fatigue machine provided by MTS. Any operator of the fatigue testing machine needs to read these three manuals before operating the machine.

Hardware

- Series 319 Axial-Torsional Load Frame Product Information
- Series 647 Hydraulic Wedge Grips Reference Manual (Only hard copy)

Control Software

- MTS Series 793 Control Software

In order to use this testing procedure for performing mixed-mode I+II crack propagation testing it is also necessary to have the *Guide for Operating the Fatigue Testing Machine* by Kristen Rege at hand.

1.Introduction

This procedure is written as a help for performing mixed-mode I+II fatigue crack propagation testing using a special loading device for testing of CTS specimens. This procedure includes description on how to install the loading device into the fatigue testing machine and monitoring of crack growth. This test does not describe how to operate the fatigue testing machine, therefore, this procedure must be used together with the *Guide for Operating the Fatigue Testing Machine* by Kristen Rege.

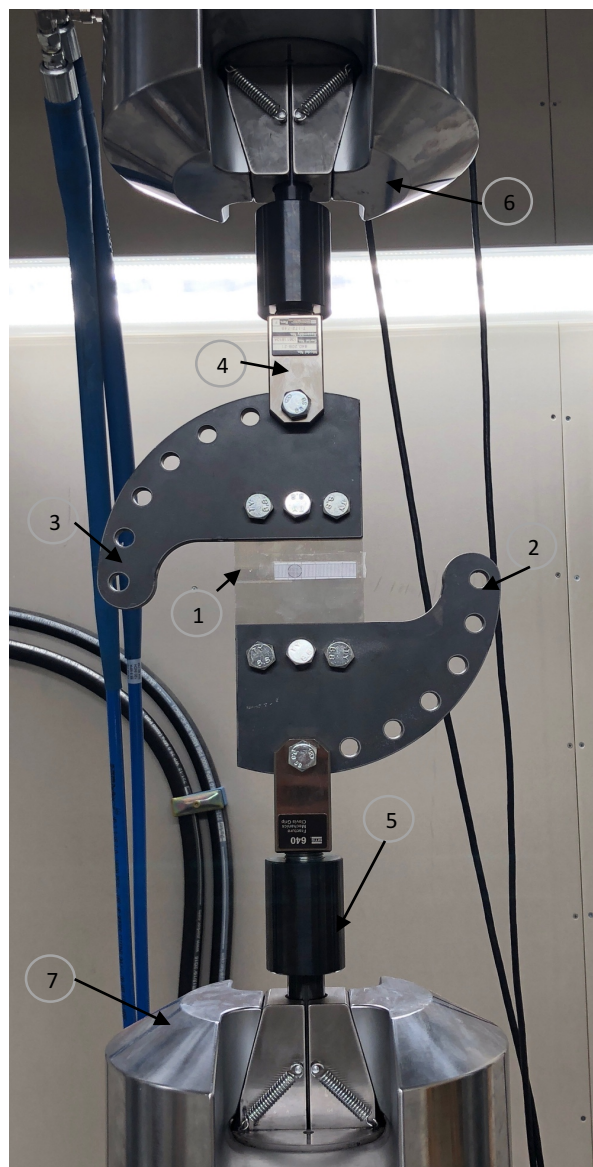


Figure 0-1 Installation of loading device and CTS specimen

2. Installation Setup

When performing this part of the procedure, chapter 3.4 in the *Guide for Operating the Fatigue Testing Machine* by Kristen Rege must be followed.

2.1 Specimen Installation

- 2.1.1 Ensure that the spacing for installation of CTS specimen in the loading device is clear of dirt.
- 2.1.2 Insert the CTS specimen (1) into the upper (3) and lower (2) part of the loading devices, insert the bolts and fasten the nuts, as illustrated in Figure 0-1. The bolts are of such a length that the nuts can be screwed in completely. If other bolts are used, make sure that no tightening torque are used.

2.2 Installation of Loading Device

- 2.2.1 Install the CT grip (4) in the upper grip of the machine (6).
- 2.2.2 Raise the crossbeam so that there is good space in between the fixtures to install the loading device.
- 2.2.3 Place the upper part of the loading device (3) in the upper CT grip, and fasten bolt or pin.
- 2.2.4 Attach the lower CT grip to the lower part of loading device (2).

Warning: When performing this operation your hands will be within the crush zone! Make sure to take necessary precautions!

- 2.2.5 Before extending the actuator upwards, make sure that the pin (5) attached to the CT grip is inside the lower grip (7) of the machine. If not, use the crossbeam to lower CT grip pin (5) into position.

Warning: Make sure that the lower grip pin does not hit the bottom inner edge of the lower grip wedges! This can cause damage to both the specimen and the machine!

- 2.2.6 Slowly extend the actuator upwards until the displacement is zero (Midstroke of the machine). If necessary, raise the crossbeam upwards to make more space for grip pin. It is recommended to be two persons for this operation.

- 2.2.7 When actuator is positioned at midstroke, if necessary, lower the crossbeam allowing a space of at least 3 mm but not greater than 6 mm between lower part of CT grip pin (5) and the inner lower edges of the wedges. Lock the lower grip.
- 2.2.8 Control that the specimen and loading device is positioned correctly, and that both the upper and lower CT grip is located parallel to each other. If not, open the lower grip (7) and adjust the placement of the lower CT grip.
- 2.2.9 Follow chapter 3.5 in the *Guide for Operating the Fatigue Testing Machine* by Kristen Rege before starting the test.

3. Monitoring of Crack Propagation

For this test procedure a photo camera (Canon EOS 1300D) is used for monitoring the crack propagation. A tripod with adjustable height is used in order to install the camera in front of the tested specimen.

3.1 Installation and Setup of Camera

- 3.1.1 Install the camera on the tripod and adjust the camera to desired position. Based on previous testing the best results were obtained when camera was placed below the crack and shooting upwards at an angle, as illustrated in Figure 0-2. However, the position giving the best results will vary from time to time, meaning, that the best suited placement of the camera must be found for every test.
- 3.1.2 Which camera setting to use can vary depending on surface of different materials and light conditions in the fatigue testing room. Thus, it is recommended to try different shooting modes, starting with the auto setting. If this doesn't give a satisfactory result, try using the program mode. This setting allows to predefine different parameters such as iso setting, white balance and whether to use blitz or not.
- 3.1.3 If the crack is hard to spot in the photos, try using a yellow marker pen on the crack surface and area around the crack.

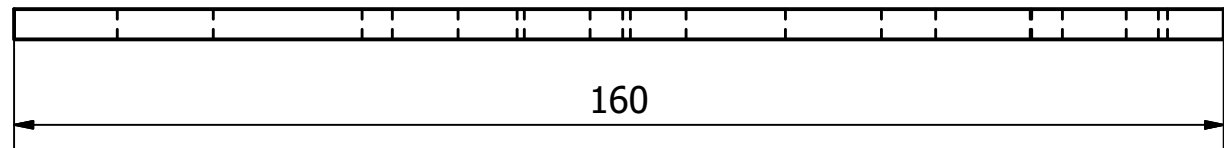
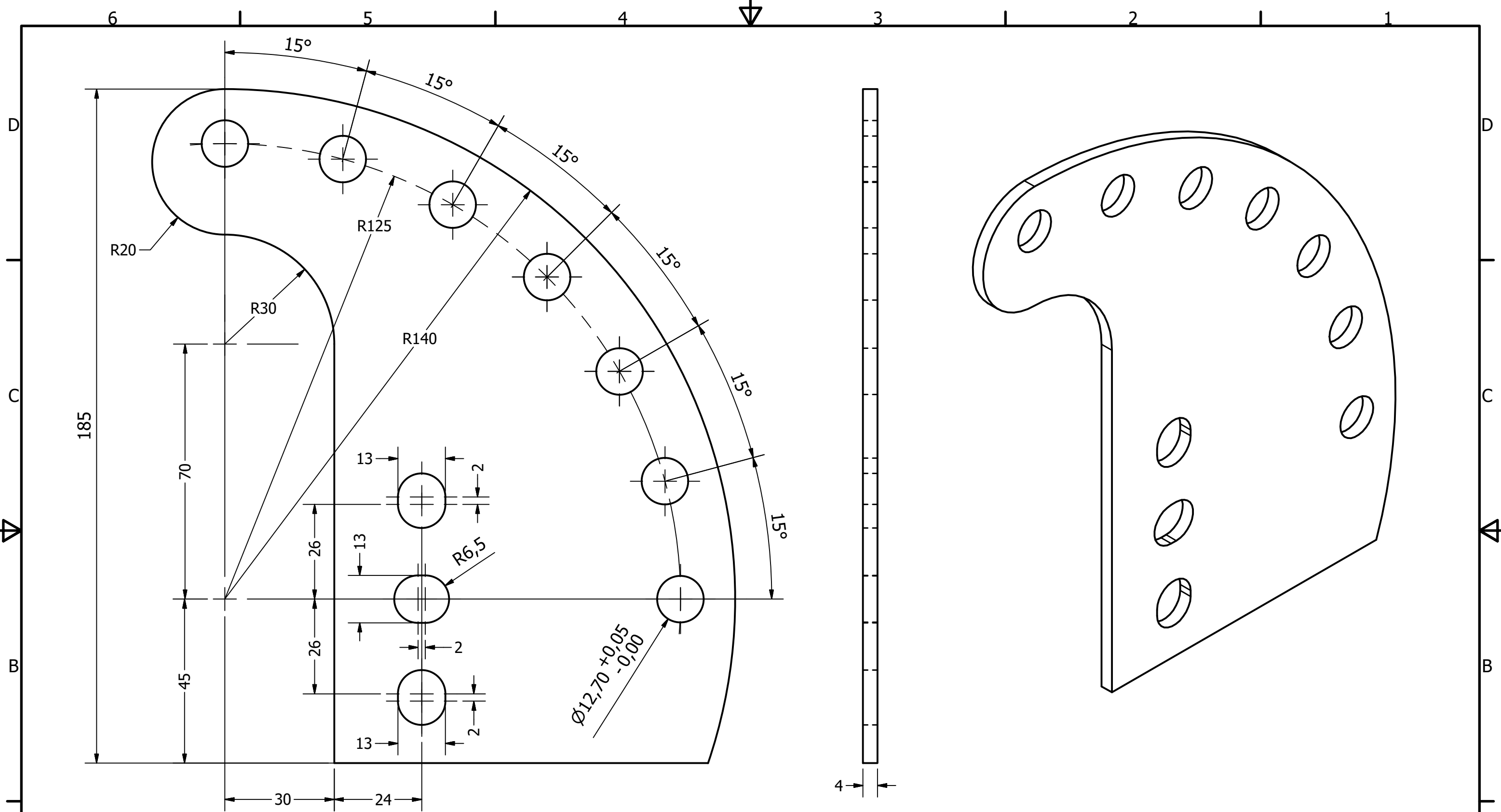
3.2 Monitoring

- 3.2.1 Use a camera software that allows for time interval shooting. The time intervals pictures should be set based on theoretically calculated crack growth and monitoring intervals acc to. ASTM E 657. If such a software is not present, shoot manually at the same time intervals. When testing a new material, it is recommended to be present during testing or check in at short time intervals.
- 3.2.2 Acc to. ASTM E647 pictures should also be taken from both the back and front side of the specimen. If there is a difference between crack length in the front and the back, manually shooting have to be done of the back side of the specimen.




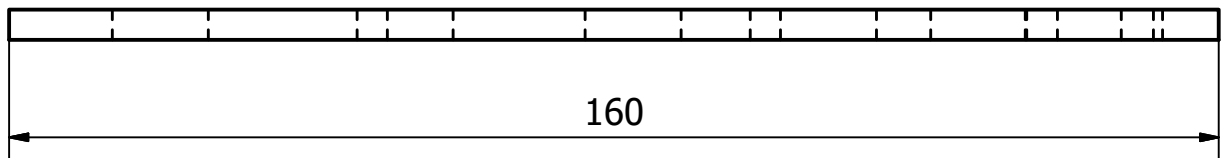
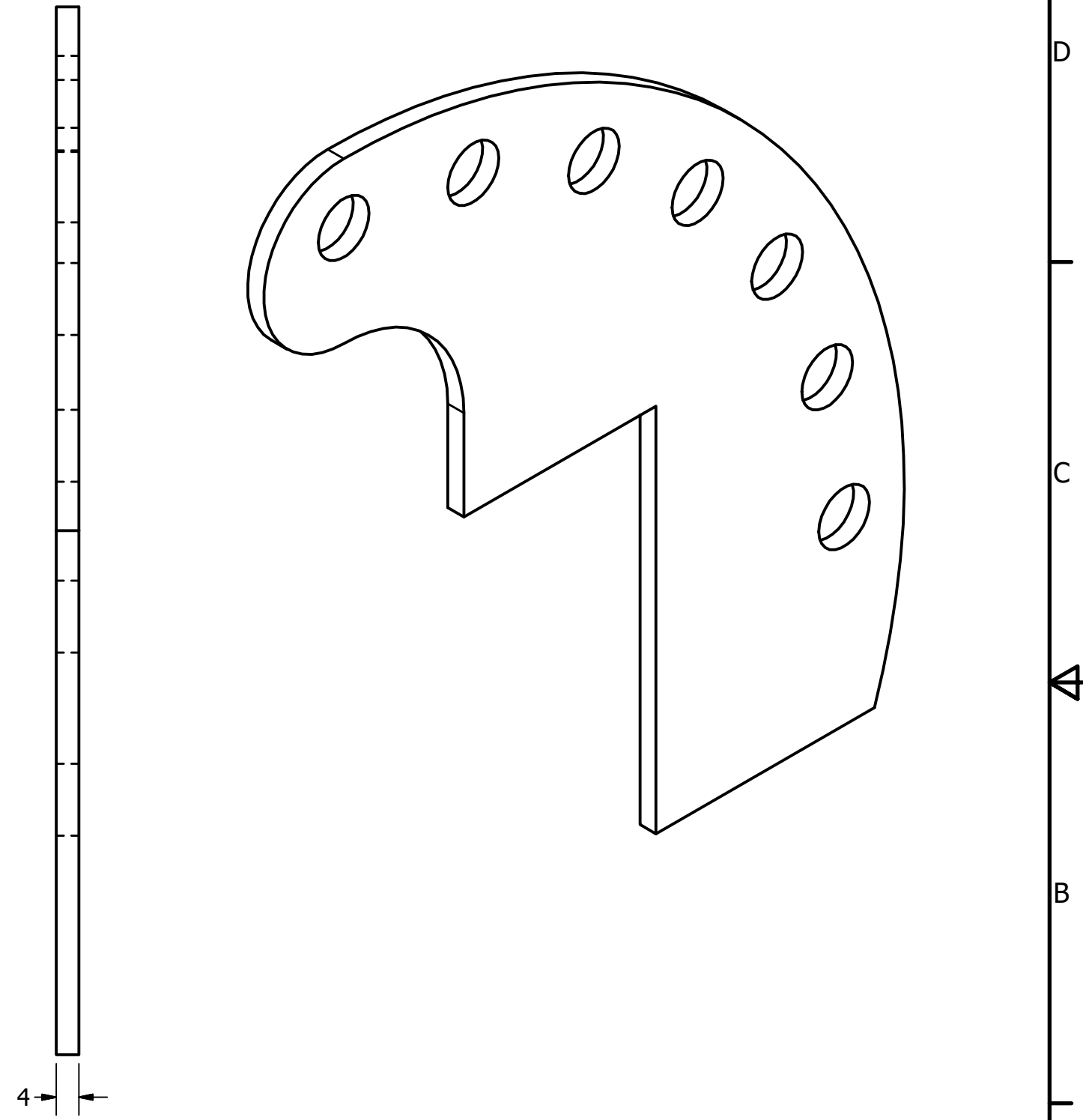
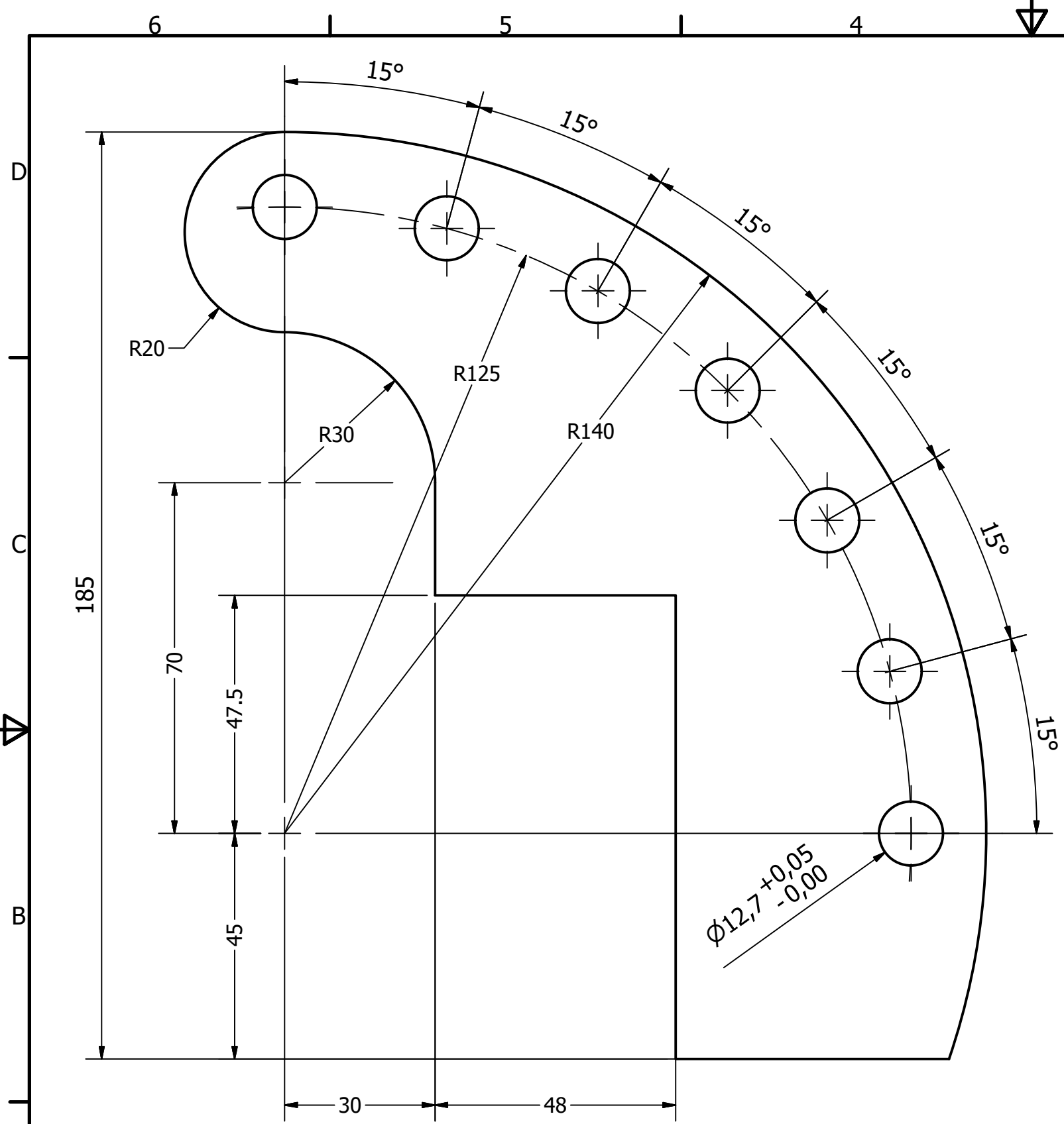
Figure 0-2 Recommended position of tripod and camera.

Appendix-B Machine drawings of fabricated parts



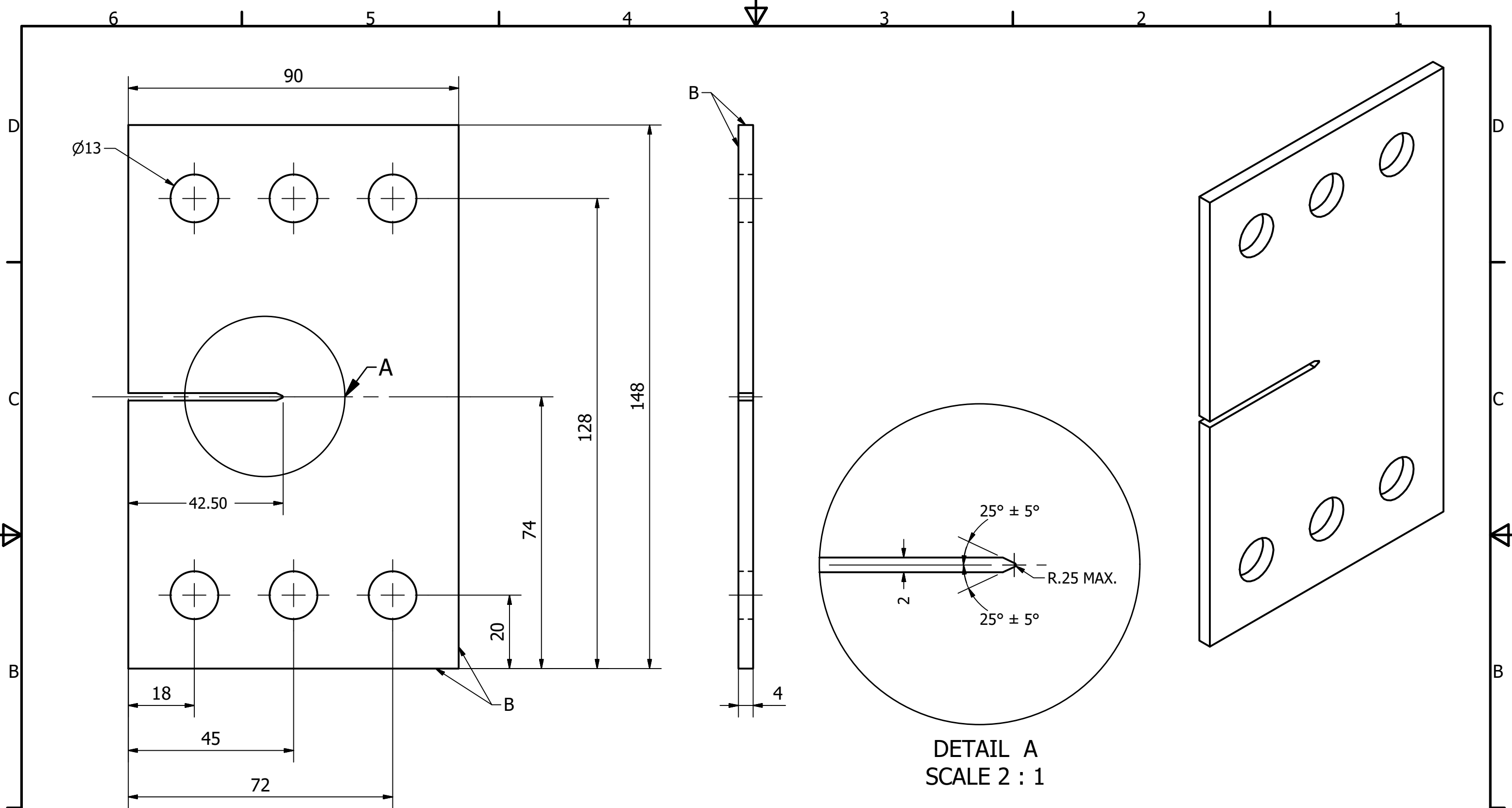
- Notes:
1. TOLERANCES ACCORDING TO NS-ISO 2768-1
 2. MATERIAL: EN S355
 3. QUANTITY: 4

| 1 | 20.03.2018 | ISSUED FOR FABRICATION | JR | - | - |
|---|------------|------------------------|-----------------------------------|------------|----------|
| Rev. | Date | Description | Prep. | Chk. | Appr. |
| Designed by Jonas Rydland | | | Title SIDE PLATE LOADING CLAMP | | |
|  | | | Scale 1 : 1 | Size A3 | |
| | | | Drawing no. JR2018-0001 | | Rev 1 |



- Notes:
1. TOLERANCES ACCORDING TO NS-ISO 2768-1
 2. MATERIAL: EN S355
 3. QUANTITY: 2


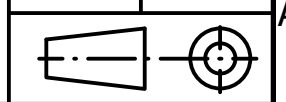
| 1 | 20.03.2018 | ISSUED FOR FABRICATION | JR | - | - |
|------------------------------|------------|------------------------|-------------------------------------|----------------|-------|
| Rev. | Date | Description | Prep. | Chk. | Appr. |
| Designed by Jonas Rydland | | | Title MIDDLE PLATE LOADING CLAMP | | |
| University of Stavanger | | | Scale 1 : 1 | Size A3 | |
| Drawing no. JR2018-0002 | | | Rev 1 | Sheet 1 / 1 | |

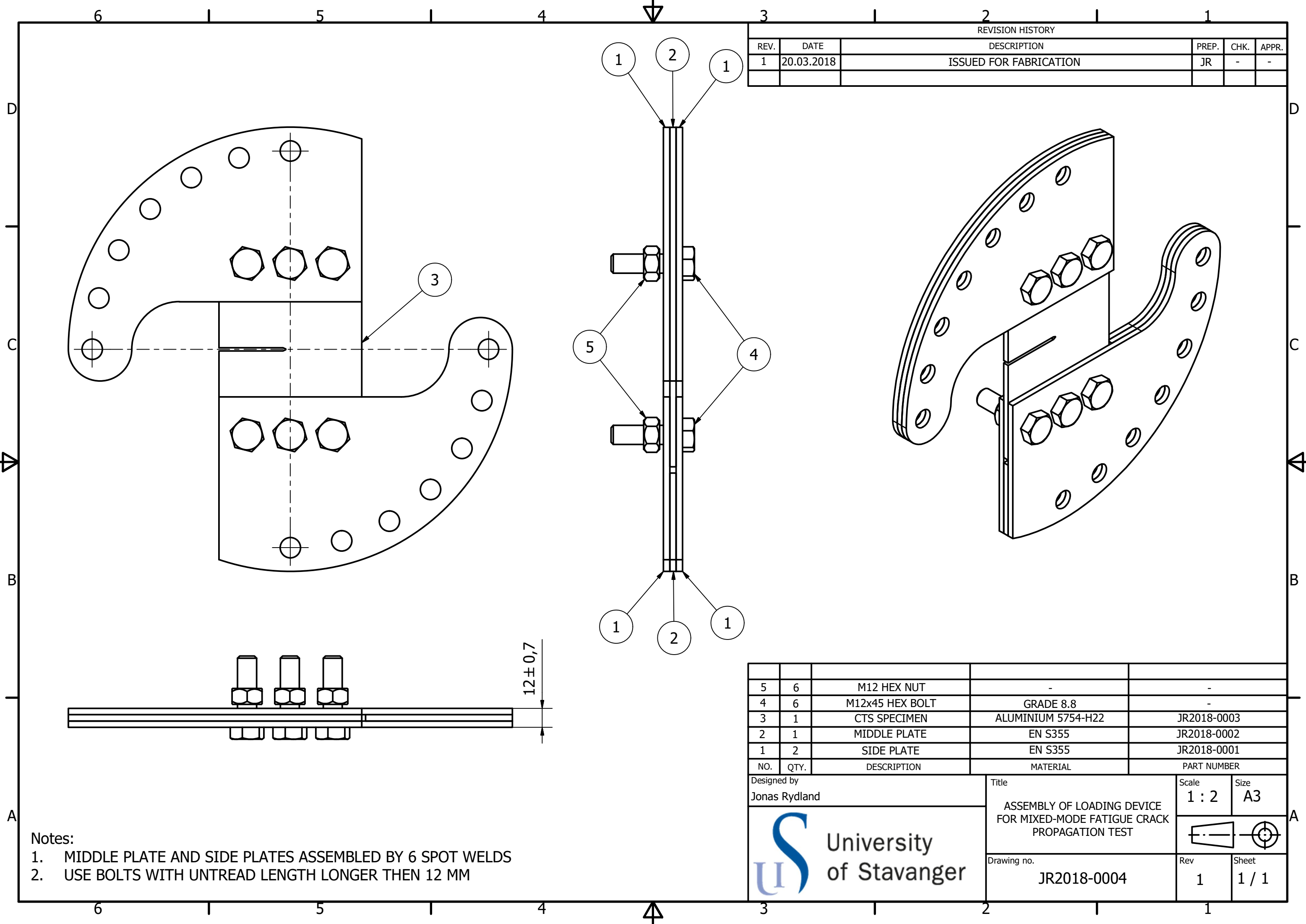


DETAIL A
SCALE 2 : 1

NOTES


1. SURFACES B TO BE PERPENDICULAR AND PARALLEL WITHIN ± 0.1 , TIR
2. TOLERANCES ACCORDING TO NS-ISO 2768-1
3. MATERIAL: ALUMINIUM ALLOY - 5754 H22
4. QUANTITY: 3
5. NOTCH TO BE MACHINED TO 41 MM
6. FINAL NOTCH LENGTH TO BE PREPARED BY SAWCUT TO 42.5 MM
7. MINIMUM FATIGUE PRECRACK: 2.5 mm

| 1 | 20.03.2018 | ISSUED FOR FABRICATION | JR | - | - |
|---|------------|------------------------|----------------------------|------|---|
| Rev. | Date | Description | Prep. | Chk. | Appr. |
| Designed by Jonas Rydland | | | Scale 1 : 1 | | Size A3 |
|  | | | Title CTS SPECIMEN | |  |
| | | | Drawing no. JR2018-0003 | | |



| REVISION HISTORY | | | | | |
|------------------|------------|------------------------|-------|------|-------|
| REV. | DATE | DESCRIPTION | PREP. | CHK. | APPR. |
| 1 | 20.03.2018 | ISSUED FOR FABRICATION | JR | - | - |

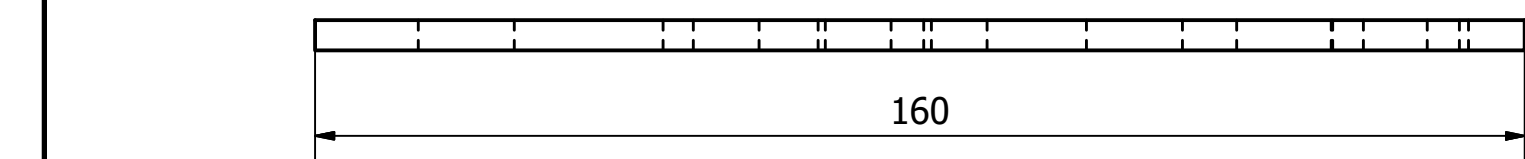
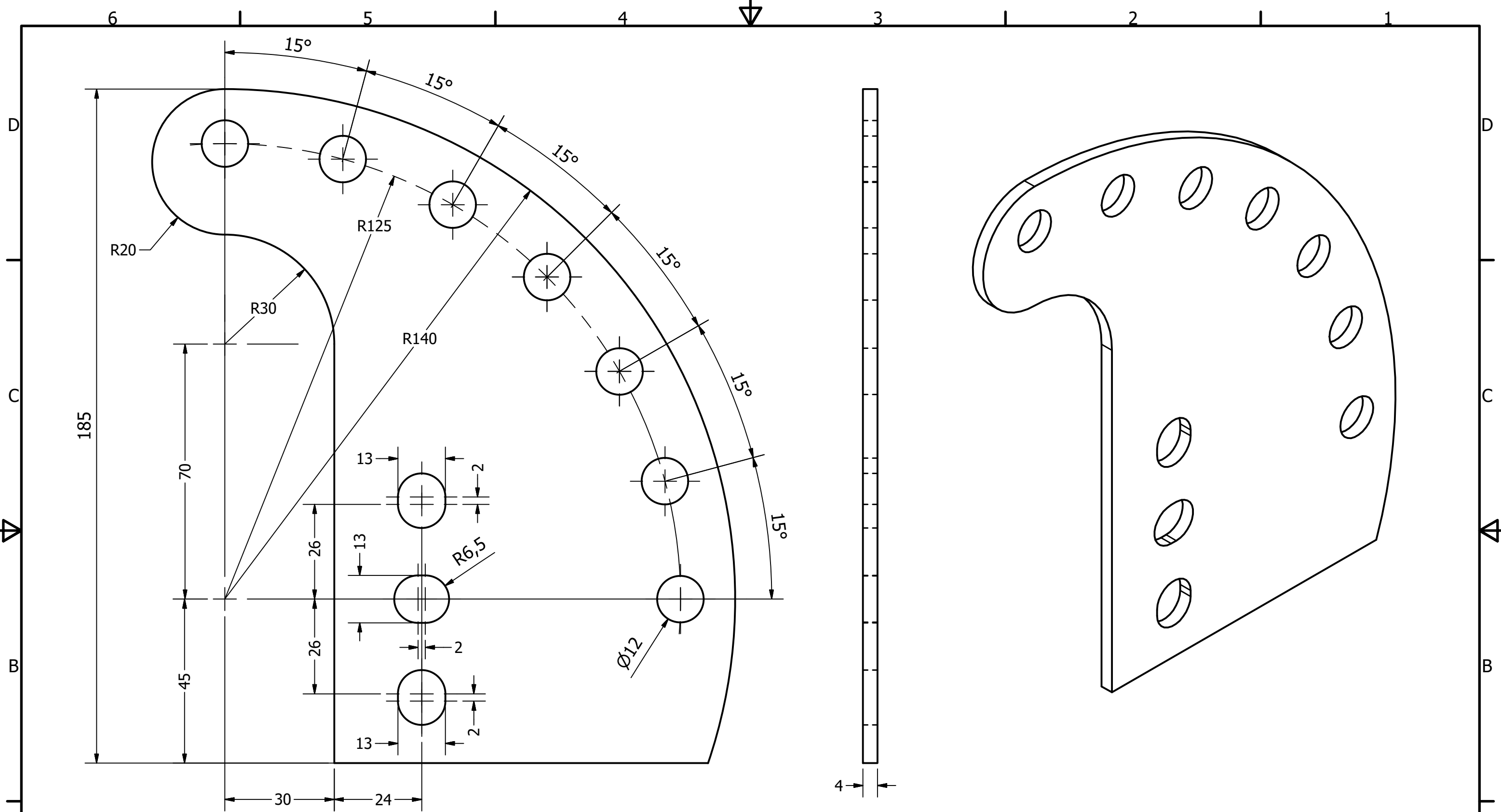
| NO. | QTY. | DESCRIPTION | MATERIAL | PART NUMBER |
|-----|------|-----------------|--------------------|-------------|
| 5 | 6 | M12 HEX NUT | - | - |
| 4 | 6 | M12x45 HEX BOLT | GRADE 8.8 | - |
| 3 | 1 | CTS SPECIMEN | ALUMINIUM 5754-H22 | JR2018-0003 |
| 2 | 1 | MIDDLE PLATE | EN S355 | JR2018-0002 |
| 1 | 2 | SIDE PLATE | EN S355 | JR2018-0001 |

| | | | |
|--|---|----------------|----------------|
| Designed by Jonas Rydland | Title ASSEMBLY OF LOADING DEVICE FOR MIXED-MODE FATIGUE CRACK PROPAGATION TEST | Scale 1 : 2 | Size A3 |
|  University of Stavanger | Drawing no. JR2018-0004 | Rev 1 | Sheet 1 / 1 |


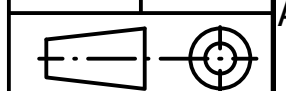
- Notes:
- MIDDLE PLATE AND SIDE PLATES ASSEMBLED BY 6 SPOT WELDS
 - USE BOLTS WITH UNTREAD LENGTH LONGER THEN 12 MM

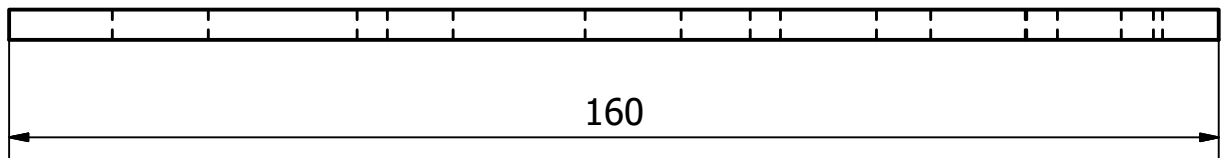
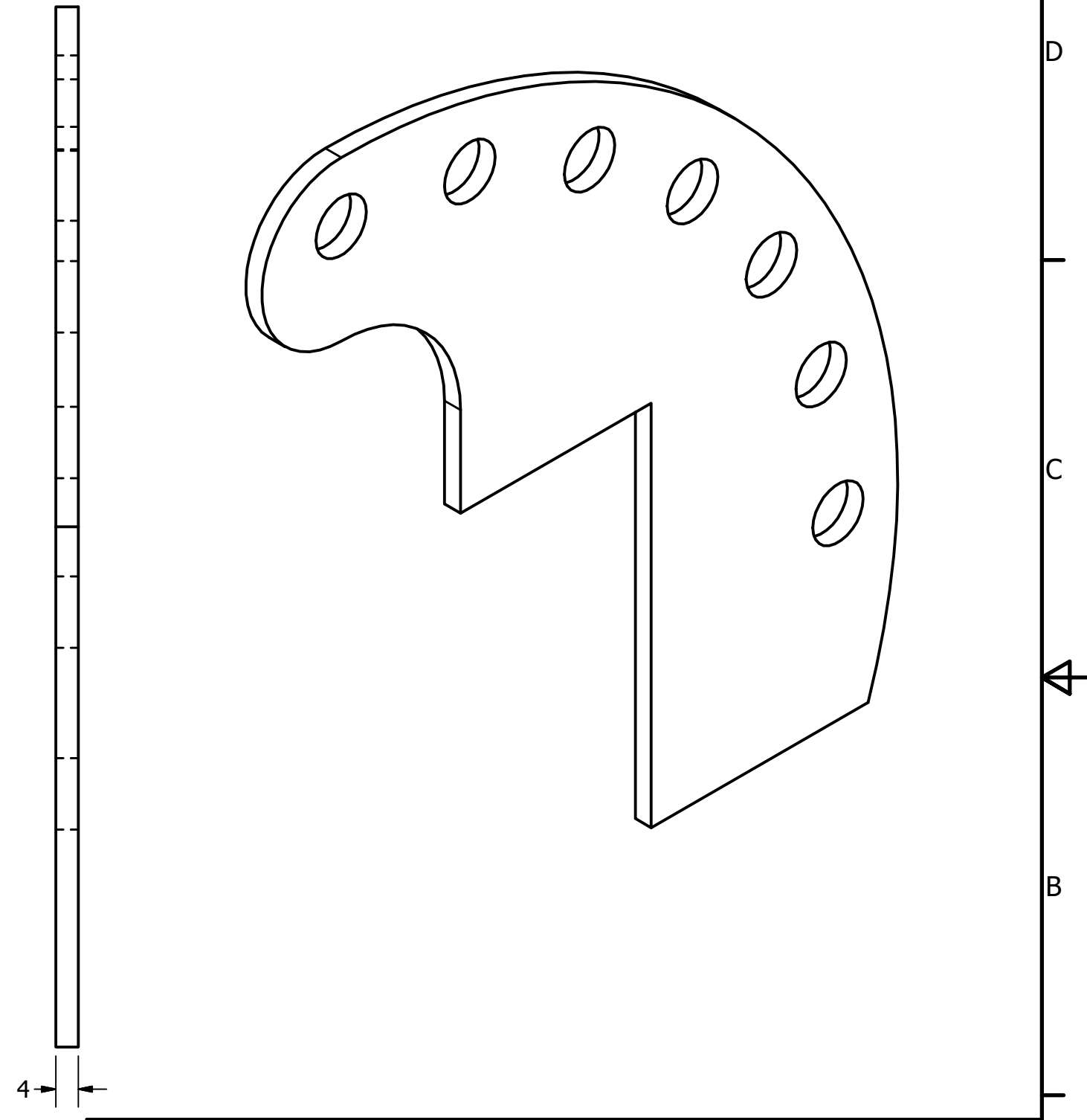
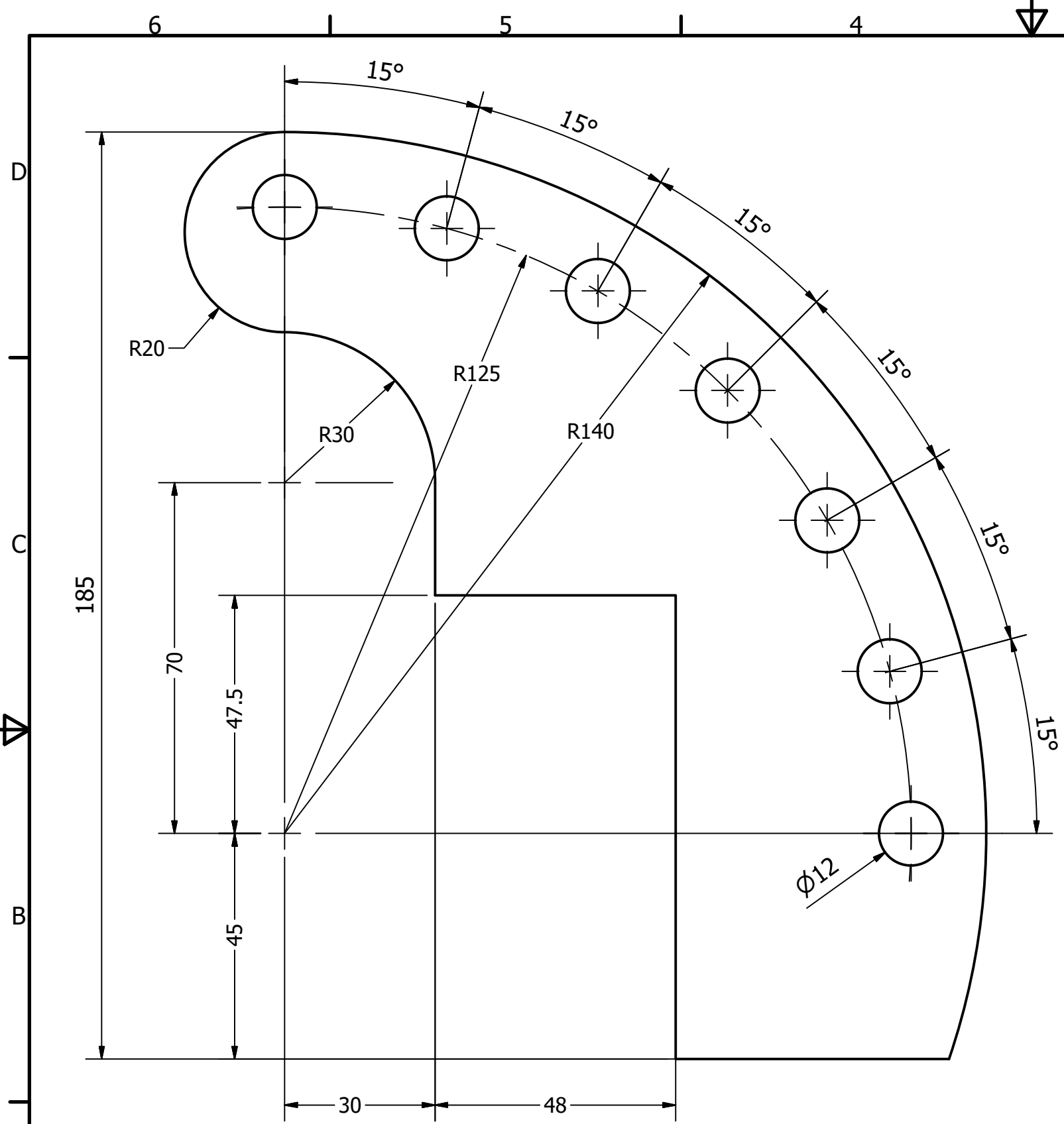
12±0,7

Appendix-C Revised machine drawings for improvement



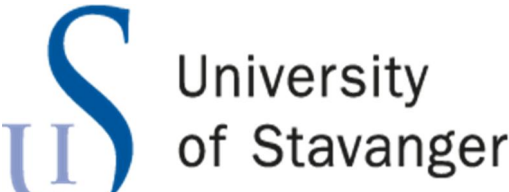
- Notes:
1. TOLERANCES ACCORDING TO NS-ISO 2768-1
 2. MATERIAL: EN S355
 3. QUANTITY: 4

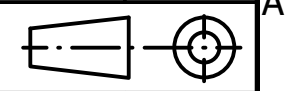
| 2 | 19.05.2018 | DIAMETER OF CIRCULAR HOLES CHANGED | JR | - | - |
|---|------------|------------------------------------|-----------------------------------|------|---|
| 1 | 20.03.2018 | ISSUED FOR FABRICATION | JR | - | - |
| Rev. | Date | Description | Prep. | Chk. | Appr. |
| Designed by Jonas Rydland | | | Scale 1 : 1 | | Size A3 |
|  | | | Title SIDE PLATE LOADING CLAMP | |  |
| | | | Drawing no. JR2018-0001 | | |

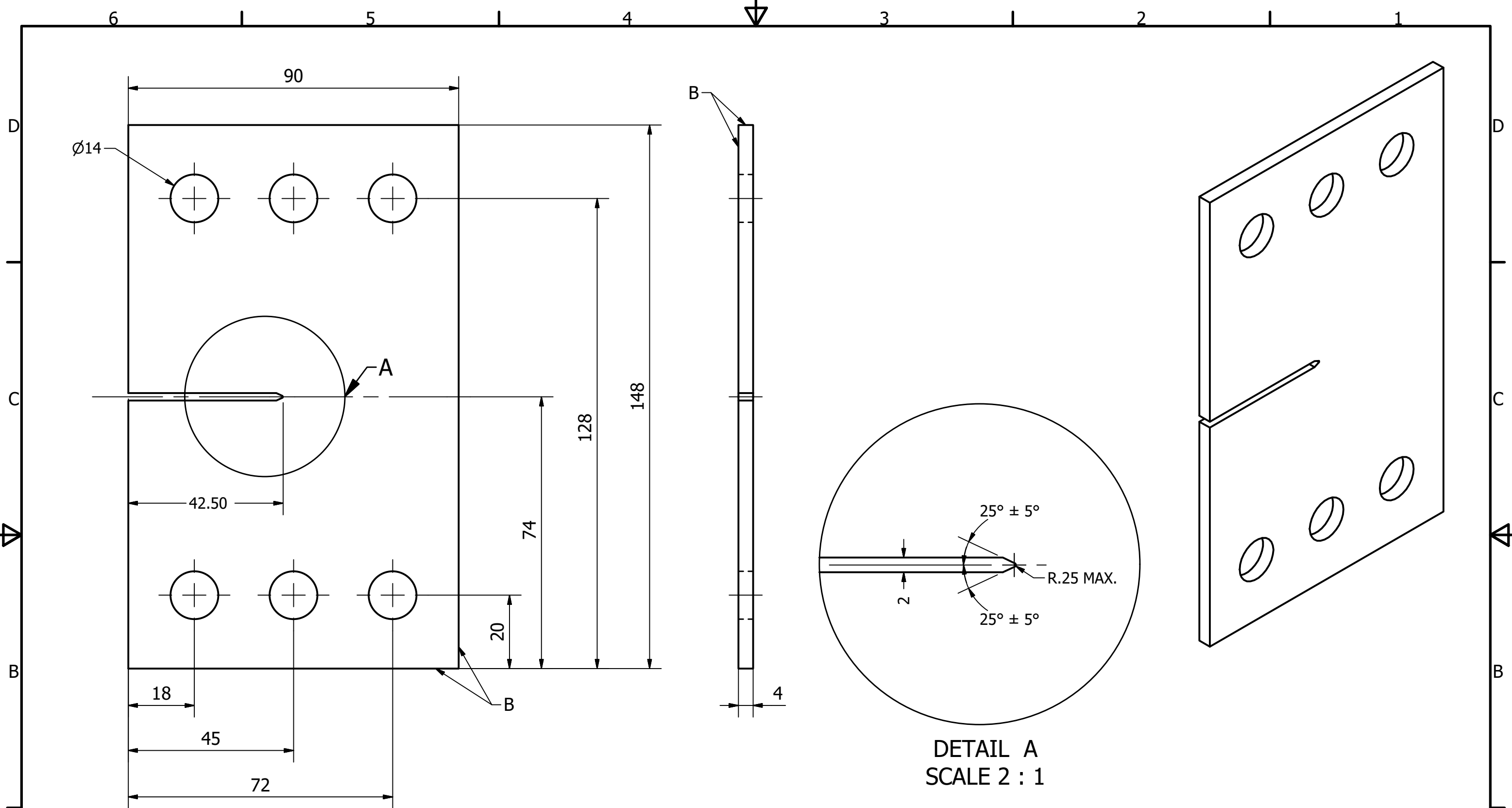


- Notes:
1. TOLERANCES ACCORDING TO NS-ISO 2768-1
 2. MATERIAL: EN S355
 3. QUANTITY: 2


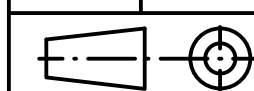
| Rev. | Date | Description | Prep. | Chk. | Appr. |
|------|------------|---------------------------|-------|------|-------|
| 2 | 19.05.2018 | DIAMETER OF HOLES CHANGED | JR | - | - |
| 1 | 20.03.2018 | ISSUED FOR FABRICATION | JR | - | - |

| | | | |
|---|-------------------------------------|----------------|----------------|
| Designed by Jonas Rydland | Title MIDDLE PLATE LOADING CLAMP | Scale 1 : 1 | Size A3 |
|  | Drawing no. JR2018-0002 | Rev 2 | Sheet 1 / 1 |

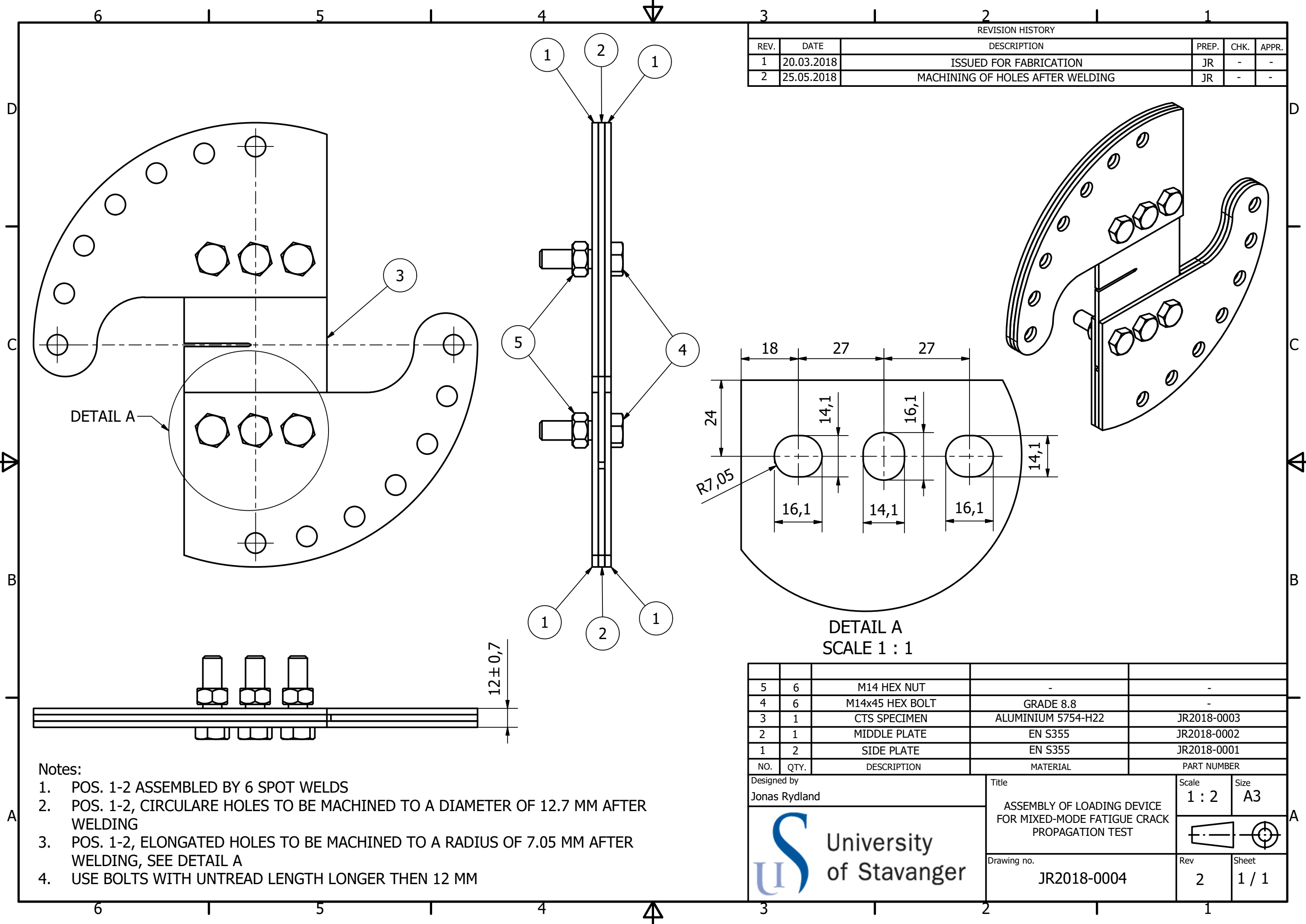




- NOTES**
1. SURFACES B TO BE PERPENDICULAR AND PARALLEL WITHIN ± 0.1 , TIR
 2. TOLERANCES ACCORDING TO NS-ISO 2768-1
 3. MATERIAL: ALUMINIUM ALLOY - 5754 H22
 4. QUANTITY: 3
 5. NOTCH TO BE MACHINED TO 41 MM
 6. FINAL NOTCH LENGTH TO BE PREPARED BY SAWCUT TO 42.5 MM
 7. MINIMUM FATIGUE PRECRACK: 2.5 mm


| 2 | 19.05.2018 | DIAMETER OF HOLES CHANGED | JR | - | - |
|---|------------|---------------------------|----------------------------|------|---|
| 1 | 20.03.2018 | ISSUED FOR FABRICATION | JR | - | - |
| Rev. | Date | Description | Prep. | Chk. | Appr. |
| Designed by Jonas Rydland | | | Scale 1 : 1 | | Size A3 |
|  | | | Title CTS SPECIMEN | |  |
| | | | Drawing no. JR2018-0003 | | |

| REVISION HISTORY | | | | | |
|------------------|------------|----------------------------------|-------|------|-------|
| REV. | DATE | DESCRIPTION | PREP. | CHK. | APPR. |
| 1 | 20.03.2018 | ISSUED FOR FABRICATION | JR | - | - |
| 2 | 25.05.2018 | MACHINING OF HOLES AFTER WELDING | JR | - | - |



| NO. | QTY. | DESCRIPTION | MATERIAL | PART NUMBER |
|-----|------|-----------------|--------------------|-------------|
| 5 | 6 | M14 HEX NUT | - | - |
| 4 | 6 | M14x45 HEX BOLT | GRADE 8.8 | - |
| 3 | 1 | CTS SPECIMEN | ALUMINIUM 5754-H22 | JR2018-0003 |
| 2 | 1 | MIDDLE PLATE | EN S355 | JR2018-0002 |
| 1 | 2 | SIDE PLATE | EN S355 | JR2018-0001 |

- Notes:
1. POS. 1-2 ASSEMBLED BY 6 SPOT WELDS
 2. POS. 1-2, CIRCULARE HOLES TO BE MACHINED TO A DIAMETER OF 12.7 MM AFTER WELDING
 3. POS. 1-2, ELONGATED HOLES TO BE MACHINED TO A RADIUS OF 7.05 MM AFTER WELDING, SEE DETAIL A
 4. USE BOLTS WITH UNTREAD LENGTH LONGER THEN 12 MM

| | | | |
|---|---|----------------|----------------|
| Designed by Jonas Rydland  | Title ASSEMBLY OF LOADING DEVICE FOR MIXED-MODE FATIGUE CRACK PROPAGATION TEST | Scale 1 : 2 | Size A3 |
| | Drawing no. JR2018-0004 | Rev 2 | Sheet 1 / 1 |

Appendix-D Material certification AL 5754-H22

| | | | | | | | | | | | |
|--|--|-------------------------------|----------------------|----------------------------|--|-----------------------------------|------------------------------------|-------|------------|------|------|
| Henan Mingtai Al. Industrial Co.,Ltd | | | | | | | | | | | |
| Mill certificate: (according to EN10204/3.1B) 工厂证书 (按照 EN 10204/3.1B) | | | | | | | | | | | |
| Issued Date : 签发日期 : | | | | Certificate No. 证书编号 | | | | | | | |
| MILL CERTIFICATE 工厂证书 | | | | | | | | | | | |
| 发票号 Invoice No. | H-MTALU161101 | 起运港 Loading Port: | Qingdao, China | 目的港: Destination Port: | FREDERICIA, DENMARK | | | | | | |
| 货物描述 Description of Goods | ALUMINUM SHEETS ALLOY 5754/H22 P.O. NO.:120339614 FOB QINGDAO, CHINA | | | | | | | | | | |
| 客户名称 Customer | 族铝可/Alumeco | 客户订单号 Customer order No. | 120339614 | Standard testing Ref. 检测标准 | Material Standard EN 485-2 物料性能标准 EN 485-2 Tolerance Standard EN 573-3 化学成分标准 EN EN 573-3 | | | | | | |
| 合金状态 Alloy&temper | EN AW-5754 | | | | | | | | | | |
| 物理性能 Mechanical properties | | | | | | | | | | | |
| 序 No. | 产品型号 Product No. | 客户料号 Customer No. | 合金状态 Alloy&temper | 项目Item | 抗拉强度 Tensile Strength(Mpa) | 屈服强度 RP0.2 Yield Strength(Mpa) | 断后延伸率 Elongation after fracture | | | | |
| 要求 Req. | | | | | 220-270 | Min130 | Min11 | | | | |
| 1 | D1611034 | 4.0*1000*2000 | EN AW-5754H22 | 结果 Result | 240 | 200 | 13 | | | | |
| 2 | D1611033 | 4.0*1500*3000 | EN AW-5754H22 | 结果 Result | 232 | 190 | 14 | | | | |
| 化学成分 Chemical composition | | | | | | | | | | | |
| 序 | 合金状态 Alloy&temper | 化学元素 Element | Si | Fe | Cu | Mn | Mg | Cr | Zn | Ti | Al |
| 要求 Req. | | | 0.4 | 0.4 | 0.10 | 0.50 | 2.6-3.6 | 0.3 | 0.2 | 0.15 | Rem. |
| 1 | 4.0*1000*2000 | 结果 Result | 0.048 | 0.32 | 0.01 | 0.13 | 2.985 | 0.076 | 0.014 | 0.02 | - |
| 2 | 4.0*1500*3000 | 结果 Result | 0.048 | 0.32 | 0.01 | 0.13 | 2.985 | 0.076 | 0.014 | 0.02 | - |
| 检测/ Inspected by | | Quality inspection department | 日期 /Date | 2016-11-24 | | 整批结果判定 Final conclusion | | | | | |
| 审核/ Checked by | | Quality inspection department | 日期/ Date | 2016-11-24 | | 合格/Pass (√) | | | 不合格/NG () | | |

0002823522
0002823524
0002823526
0002823527
0002823528
0002823529
0002823530
0002823531
0002823532

HENAN MINGTAI AL. INDUSTRIAL CO., LTD
河南明泰铝业股份有限公司

张磊